CARBON NANOTUBE MODIFIED POLYDIMETHYLSILOXANE – FROM PERCOLATION TO PIEZORESISTANCE

By

Cyrill Cattin

A thesis submitted to McGill University in partial fulfillment of the requirements of the degree of Doctor of Philosophy

Structures and Composite Materials Laboratory

Department of Mechanical Engineering

McGill University, Montreal, Canada

ABSTRACT

Transparent conductors and flexible sensors are essential components of modern technology. Doped metal oxides and conductive polymers are typically used as the functional materials. With the former being inherently brittle and increasingly expensive and the latter suffering from chemical instability and complex processing, it is widely accepted that further technological progress requires new materials. Carbon nanotube modified polymers show great promise for the development of components that simultaneously exhibit electrical conductivity, optical transparency, and or mechanical flexibility. The interest in carbon nanotube modified polymers is reflected in a substantial and ever increasing amount of research devoted to the development of exactly such materials. Progress over the past years has been considerable, yet fundamental problems remain to be explored; most notably, the nature of electron conduction through carbon nanotube modified polymers is not fully understood. In this work, electron conduction in carbon nanotube modified polymers is studied, focusing on the configurational characteristics of the particle network that underlie the electrical behaviour of the material.

Multiwalled carbon nanotube modified polydimethylsiloxane is used as a model material. Detailed analyses of electrical and rheological material properties provide the basis for the investigation of the interdependence between network configuration and electrical behaviour. It is shown that electron conduction in carbon nanotube modified

polymers is controlled by percolation, involves quantum mechanical tunnelling at carbon nanotube junctions, and primarily depends on the configuration of the particle network, which can be described by two parameters, namely the percolation threshold and the conductivity exponent. At particle mass fractions close to the percolation threshold the electrical behaviour of the material is dominated by the characteristics of individual electron-conducting paths, in which electron conduction is controlled by quantum mechanical tunnelling between adjacent but non-contacting particles; at higher particle mass fractions, despite quantum mechanical tunnelling events within the individual electron-conducting paths, the electrical behaviour of the material is dominated by the characteristics of the network as a whole, which can be viewed as a resistor network. It is found that the piezoresistive effect in electroconductive nanocomposites is rooted in a mechanical deformation induced change in the distribution of local conductances and it is shown that the conductivity exponent depends on the distribution of local conductances, and that the latter varies with network morphology. It is inferred that the prevalent assumption that percolation theory presupposes direct contact between adjacent particles within electron-conducting paths is incorrect, and that, instead, percolation theory assumes a particle network with constant local conductance. With regard to the use of carbon nanotube modified polymers as functional materials, it is shown that particle mass fraction together with processing can be adapted to optimize performance. Optimized percolation by means of external fields is studied in detail, and key parameters as well as the underlying microstructural changes within the particle network are identified.

ABRÉGÉ

Des conducteurs transparents et des capteurs flexibles sont des composantes indispensable de la technologie moderne. Des oxydes métalliques dopés et des polymères conducteurs sont typiquement utilisés en tant que matériaux fonctionnels. Le premier étant intrinsèquement fragile et de plus en plus cher et le dernier souffrant d'instabilité chimique et de fabrication complexe, il est généralement reconnu qu'un progrès technologique continu nécessite des nouveaux matériaux. Les polymères modifiés de nanotubes de carbone sont très prometteurs pour le développement de composants qui sont simultanément conducteur et transparent et ou flexible. L'intérêt porté aux polymères modifiés de nanotubes de carbone se traduit par un effort important et croissant en recherche scientifique consacrée à l'élaboration de tels matériaux. Le progrès au cours des dernières années a été considérable, mais des problèmes fondamentaux restent à être expliqué; en particulier, la nature de conduction par électrons n'est pas entièrement comprise. Dans ce travail, la conduction par électrons dans les polymères modifiés de nanotubes de carbone ainsi que les caractéristiques de la configuration du réseau de particules qui sous-tendent le comportement électrique du matériau sont étudiées.

Le polydiméthylsiloxane modifié de nanotubes de carbone à parois multiples est utilisé comme matériau modèle. Des analyses détaillées des propriétés électriques et rhéologiques du matériau constituent la base de l'analyse de l'interdépendance entre la configuration du réseau et le comportement électrique. Il est montré que la conduction

par électrons est contrôlée par percolation, consiste en l'effet tunnel au niveau des jonctions de nanotubes de carbone, et dépend principalement de la configuration du réseau des particules, qui peut être décrit par deux paramètres, à savoir le seuil de percolation et l'exposant de conductivité. Pour des concentrations proches du seuil de percolation le comportement électrique du matériau est dominé par les caractéristiques des trajets conductrices individuels, dans lesquels la conduction par électrons est contrôlé par l'effet tunnel; pour des concentration plus élevées, en dépit des effets quantiques au sein les trajets conductrices individuels, le comportement électrique du matériau est dominée par les caractéristiques du réseau dans son ensemble, qui peut être considéré comme un réseau de résistance. Il est constaté que la piézorésistance des nanocomposites conducteurs est dû à un changement dans la distribution des conductances locales induit par la déformation mécanique, et il est démontré que l'exposant de conductivité dépend de la distribution des conductances locales, et que celui-ci varie en fonction de la morphologie du réseau. Il en est déduit que l'hypothèse commune que la théorie de la percolation suppose un contact direct entre les particules adjacentes au sein des trajets conductrices individuels est incorrect, et qu'au lieu de cela la théorie de la percolation suppose un réseau de particules avec une conductance locale constante. En ce qui concerne l'utilisation des polymères modifiés de nanotubes de carbone en tant que matériaux fonctionnels, il est démontré que la concentration en particules ainsi que le traitement peuvent être adapté pour optimiser la performance du matériau. La percolation optimisée au moyen des champs externes est étudiée en détail, et les changements au niveau microstructure au sein du réseau ainsi que les paramètres clés sont identifiés.

ACKNOWLEDGMENTS

I am deeply grateful to Prof. Pascal Hubert, my doctoral thesis supervisor, for having given me the possibility to do this research, and for supporting it. The expert advice, patient guidance, and both professional and personal support he has provided throughout my time at McGill University were much appreciated. I would also like to thank Prof. Srikar Vengallatore and Prof. Eliot Fried for their time and input as members of the thesis advisory committee.

This work was made possible through financial support from McGill University, through the McGill Engineering Doctoral Award, and from the Canada Research Chairs Program, which is greatly acknowledged.

Many thanks go to Nicolas Brodusch and Tahereh Mousavand for help with SEM and TEM imaging, respectively, Prof. Bruce Lennox and Brendan Pietrobon for providing access to and technical assistance with the electrochemical workstation, Mostafa Yourdkhani for aid with the dispersion analysis, and Maximilien Debia and Wayne Wood for advice in regard to workplace safety.

I am very grateful to Prof. Larry Lessard and my peers at the Structures and Composite Materials Laboratory at McGill University for their invaluable support along the way and for providing an inspiring and cheerful working environment.

And last but not least, I would like to thank my family for helping me in countless ways and, especially, Monika for sharing in highs and lows.

TABLE OF CONTENTS

CHAPTER 1

Introduction

1.1 Presentation of the Problem

Over the past decades, transparent conductors and flexible sensors have become essential to modern technology, forming indispensable building blocks in numerous new applications, ranging from electrodes in solar cells to flat panel displays, and from flexible touch screens to structural health monitoring [1-4]. Nowadays, however, continued technological progress is hindered due to limited material availability and functionality. Tin-doped indium oxide, for example, it the most commonly used material for transparent conductors, but the cost of indium is rising steadily, and tin-doped indium oxide is inherently brittle, which is a deficiency of doped metal oxides in general [5-7]. Flexible sensors, on the other hand, are typically not made from a single material, but rather by integrating electrically active elements on flexible substrates, which is why they suffer from multistep processing and problems related to material integration [3, 4, 8].

Carbon nanotube modified polymers have the potential to provide a solution to this problem and to further technological progress in areas where transparent and or flexible electroconductive materials are key components. Modifying polymers with carbon nanotubes allows for the design of electroconductive functional nanocomposites where

electron flow through the material is implemented via the formation of an electrically conducting particle network throughout an electrically non-conducting polymer matrix. Amongst nanoparticles in general, carbon nanotubes stand out due to their excellent electrical properties and high aspect ratios, enabling a major improvement in electrical conductivity at small particle mass fractions, with a minimal impairment of other material properties, namely optical transparency and mechanical flexibility. In comparison to intrinsically conducting polymers (i.e., conjugated polymers where electrical conductivity is the result of electron delocalization) electroconductive nanocomposites typically exhibit superior chemical stability and better processability [7], and, more importantly, material selection is not limited to conjugated polymers, thus enabling their use in a wider range of applications.

The interest in carbon nanotube modified polymers as a transparent and or flexible electroconductive material is reflected in a considerable and ever increasing amount of research devoted to the development of exactly such materials. On the one hand, research has focused on characterization and selective production of carbon nanotubes. Progress in this field has been immense, starting in 1991 with the discovery of carbon nanotubes [9], and peaking out in 2013 with the fabrication of a computer built entirely from carbon nanotube field-effect transistors, which runs an operating system that is capable of multitasking [10, 11]. As a result, both physical and chemical properties of carbon nanotubes are well understood. On the other hand, research has focused on the integration of carbon nanotubes with polymers and the design of new materials exhibiting electrical conductivity combined with optical transparency and or mechanical flexibility. Progress

in this field has also been considerable leading to the development of transparent conducting films based on carbon nanotube modified polymer [12] or carbon nanotube film based flexible touch panels [13]. As a result, much has been learned about processing of electroconductive nanocomposites.

Between the above two research foci, however, there is a lack of literature and fundamental problems remain to be explored. Most notably, the nature of electron conduction through carbon nanotube modified polymers is not yet fully understood. It is well established that, on the one hand, the evolution of electrical conductivity with particle mass fraction is characteristic of percolation and thus describable by a percolation threshold and a conductivity exponent, and that, on the other hand, the electrical properties of the material depend on the configuration of the electron conducting particle network. It has further been shown that the latter can be optimized to bring about higher conductivity values for a given particle mass fraction. It is however unclear what microstructural changes cause such an increase in electrical conductivity, and, more importantly, it is unknown to date how the conductivity exponent is affected by network optimization. As to the development of a material that exhibits high electrical conductivity and high optical transparency simultaneously, for example, this is of significance as low conductivity exponents are essential for such materials [14]. It has also been reported that carbon nanotube modified polymers are piezoresistive materials; however, while some systems exhibit a positive interdependence between electrical resistance and compressive strain, for other systems this interdependence is negative. These seemingly conflicting results have left the research community puzzled up to now

as current knowledge fails at providing a valid explanation. A successful application of carbon nanotube modified polymers as flexible sensors requires an understanding of the strain induced configurational changes within the particle network, which presumably form the basis of the piezoresistive effect.

The thesis in hand addresses these problems. Both for the purposes of basic research and in order to further the applicability of carbon nanotube modified polymers as functional materials, it is of interest to attempt to understand the nature of electron conduction and its dependence on network configuration in more detail.

1.2 Thesis Objectives

The aim of this thesis is to investigate electron conduction in carbon nanotube modified polymers and its dependence on the configuration of the particle network. Multiwalled carbon nanotube modified polydimethylsiloxane is used as a model material. A detailed analysis of the electrical properties of the system studied shall provide the basis for the subsequent investigations into piezoresistance, network formation and optimized percolation. Furthermore the thesis is aiming at developing a clear picture of the microstructural changes within the particle network that underlie both the electric response to mechanical deformation and the changes in electrical behaviour due to network optimization.

1.3 Thesis Organisation

CHAPTER 2 first clearly defines the area of interest of this thesis, then reviews current knowledge of structural characteristics and intrinsic properties of CNTs, as well

as of the main physical properties of CNT – polymer nanocomposites, and then introduces research on electrical properties of CNT modified polymers.

CHAPTER 3 presents a detailed analysis of both the alternating and direct current electrical properties of the model material (i.e., multiwalled carbon nanotube modified polydimethylsiloxane), and CHAPTER 4 then studies the electric response to mechanical deformation of the material. Thereby, dominant conduction mechanisms are identified and the electrical behaviour of carbon nanotube modified polymers is related to the configuration of the particle network.

CHAPTER 5 addresses the problem of positive vs. negative piezoresistance in electroconductive nanocomposites with high aspect ratio particles. A percolation theory based model relating the variation in electrical resistance to compressive strain is developed and applied to the piezoresistance characterization of the model material, as well as to relevant data from the literature on carbon nanotube, graphene, and high structure carbon black based electroconductive nanocomposites. It is shown why current theories fail at providing a general description for the experimental findings, and the electric response to compressive and tensile deformation of both high aspect ratio particle and low aspect ratio particle based electroconductive nanocomposites is discussed.

CHAPTER 6 then looks at network formation and optimized percolation in multiwalled carbon nanotube modified polydimethylsiloxane. The rheological properties of the material prior to polymerization are analyzed in detail, network optimization by means of an electric field is studied and it is examined in what way this affects the conductivity exponent as well as what configurational changes form the basis for the

increase in electrical conductivity, and it is also studied how the electrical conductivity evolves during polymerization of the elastomeric matrix as well as how this depends on particle mass fraction.

In Chapters 3 to 6 an effort is made to identify to what extend the results pertain specifically to the system studied in this work (i.e., multiwalled carbon nanotube modified polydimethylsiloxane), and what results are applicable to carbon nanotube modified polymers in general. Finally, general conclusions, original contributions, and suggestions for future work are presented in CHAPTER 7.

CHAPTER 2

Review of Scientific Literature

2.1 Area of Interest

The first scientific study on carbon nanotube (CNT) modified polymers dates back to 1994 [15], i.e. soon after the discovery of CNTs [9] and the first reports on their excellent and largely unprecedented intrinsic properties [16-19]. As indicated in Chapter 1, research efforts since have been considerable and are ever increasing. Fundamental and applied research on CNT – polymer nanocomposites are often closely entangled and the breadth of research is enormous, encompassing many scientific disciplines ranging from physics to chemistry to materials science and engineering. Progress in various research areas is summarized in several review articles [20-30] and textbooks [31-36].

The area of interest of this thesis is electron conduction in bulk CNT modified polymers, i.e. electrical conductivity in a material in which the electrically conducting CNTs form a three-dimensional and macroscopically uniform network throughout an electrically non-conducting polymer matrix, as is outlined in Figure 2.1. In this Chapter relevant scientific literature is reviewed as follows: first, structural characteristics and intrinsic properties of CNTs are presented, second, mechanical and thermal properties as well as processing of CNT modified polymers are discussed, and, third, research on

electrical properties of CNT modified polymers is introduced. Each section concentrates on the most relevant aspects, but scientific references are given for more in-depth information. Also, literature specific to the subjects of Chapters 3 to 6 is further reviewed at the beginning of each chapter.

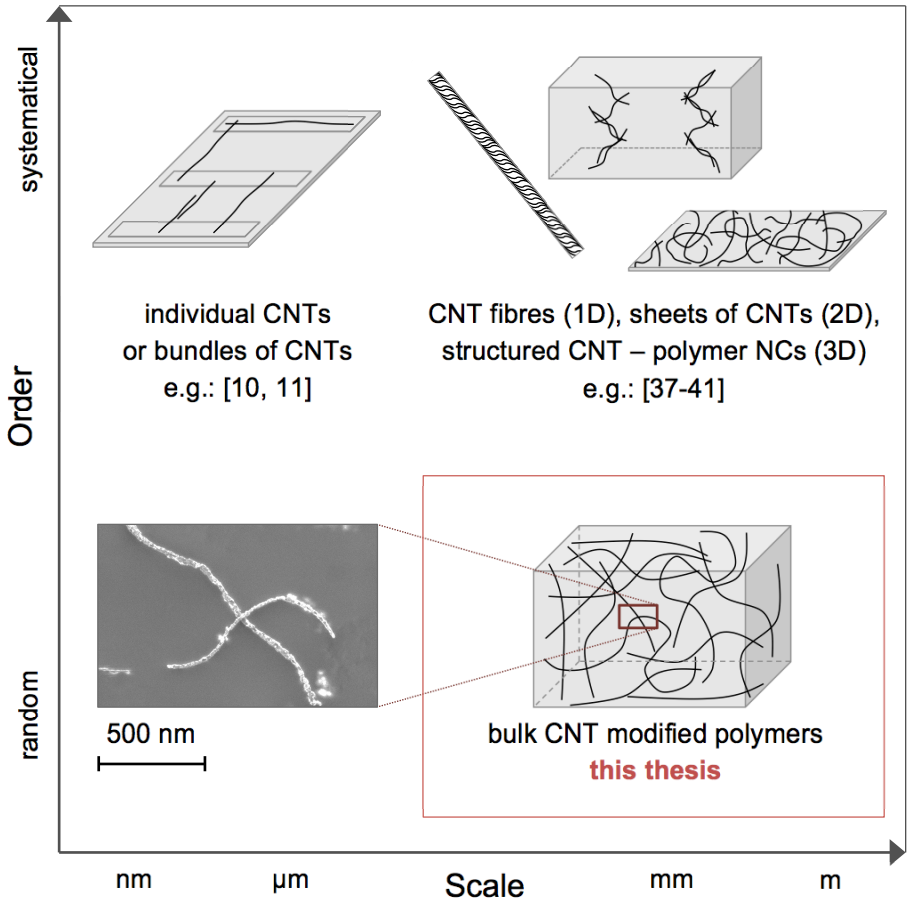

Figure 2.1. Pictorial illustration of research on CNT – polymer nanocomposites (NCs), ranging from controlled placements of CNTs on polymeric substrates at a nanoscopic scale, to random dispersions of CNTs in polymeric matrices at a macroscopic scale. This thesis looks at electron conduction in bulk CNT modified polymers (three-dimensional and macroscopically uniform CNT network throughout polymer matrix).

2.2 Carbon Nanotubes

CNTs are seamless cylinders of one or more layers of graphene. In the former case the carbon structure is called single-walled carbon nanotube (SWCNT) whereas in the latter case it is denoted multi-walled carbon nanotube (MWCNT) [31]. The cylinder length can vary from less than 100 nm to a few centimetres, while the diameters of SWCNTs and MWCNTs typically range from 0.8 to 2 nm and from 5 to 20 nm, respectively [30]. CNTs thus typically exhibit very high aspect ratios. Pristine CNTs have all carbon atoms bonded in a hexagonal lattice, except at their ends where CNTs can be open or capped; defects typical in mass-produced CNTs, however, introduce pentagons, heptagons, and other imperfections in the CNTs sidewalls, which is generally detrimental to their intrinsic properties [30, 31].

Owing to this particular atomic structure, CNTs exhibit outstanding electrical, mechanical and thermal properties. Depending on the orientation of the graphene layer with respect to the cylinder axis, the so-called chirality of CNTs, individual layers forming the CNT sidewalls can be metallic or semiconducting [31]. MWCNTs, the type of CNTs used in this work, are typically metallic [30], can exhibit electrical conductivities in excess of 10^7 S/m [42-44], and can carry currents of up to 10^9 – 10^{10} A/cm^2 [43]. Due to the one-dimensional nature of CNTs, electrons can travel through the material without scattering, which results in ballistic transport and minimal Joule heating [23]. In comparison, the best metal conductors such as silver, cooper or gold, exhibit similar electrical conductivities, but much smaller specific current carrying capacities. In addition, room temperature thermal conductivities higher than 3000 W/m.K have been

measured on individual MWCNTs [45], which exceeds the thermal conductivity of diamond, and, when considering the transvers section of the CNT sidewalls only, individual MWCNTs can exhibit an elastic modulus of up to 1 TPa, together with a tensile strength of 100 GPa [30, 31, 46], which is unparalleled. For more in-depth information about the science of CNTs, Reference [31] is recommended.

From a historical viewpoint it is interesting to note that there is some debate about who should be credited with discovering CNTs [47, 48]. TEM images published by Iijima in 1991 [9] are generally considered the first report of MWCNTs, and there is no doubt that this work is responsible for a tremendous increase in CNT related research activities. However, TEM evidences of nano-sized tubular carbon structures had already been reported before; according to [48] for the first time in 1952 by Radushkevich and Lukyanovich [49]. It has been conjectured that the uncertainty surrounding this question might explain why no Nobel Prize has yet been awarded in this area of research [31].

2.3 Bulk CNT – Polymer Nanocomposites

The most common approach to exploiting the excellent intrinsic properties of CNTs is by incorporating these nanoscopic particles into a macroscopic matrix. Bulk CNT – polymer nanocomposites are obtained by mixing CNTs with a polymer, which theoretically allows for combining properties of the two materials; e.g., the tensile strength of CNTs with the specific weight of polymers for use in lightweight structures, or the electrical conductivity of CNTs with the optical transparency and or the mechanical flexibility of polymers for use as electroconductive functional materials.

2.3.1 Mechanical properties of bulk CNT – polymer nanocomposites

The mechanical reinforcement of polymers by means of CNT addition is an area of research that has received a lot of attention, particularly in the early days of CNT – polymer nanocomposites research. As to the elastic properties, a parameter that is typically used to evaluate the degree of reinforcement is the particle volume fraction, p_v, dependent rate of increase of Young's modulus, Y, i.e. dY/dp_v [23, 50]. The most common theories for modelling mechanical properties of fibre based composites, which have also been applied to nanocomposites, i.e. the rule of mixtures and the Halpin–Tsai equations, both predict maximum dY/dp_v values of around 1 TPa [23]. The best results reported in literature are in this range [23, 51-53]; for the vast majority of studies, however, reported data give much lower maximum dY/dp_v values, and for many systems $dY/dp_v < 10$ GPa [23]. From the elastic moduli data compiled in [23] and [54] for more than one hundred different CNT – polymer systems, it becomes apparent that, on average, CNT addition to polymers increases the elastic modulus by a factor smaller than 2, which is low considering the orders of magnitude difference between the elastic moduli of the two constituent materials.

The reported strength properties of CNT modified polymers resemble the elastic properties in the sense that they are rather low compared with expectations from the intrinsic properties of CNTs (cf. Section 2.2), and also rather low compared to continuous carbon fibre reinforced polymers [55]. Just as for the elastic properties, reported strength properties of CNT – polymer nanocomposites tend to be widely scattered. On the one hand, it has been reported that the addition of 10 wt.% of MWCNT to natural rubber

increases the ultimate tensile strength from 1 MPa to around 7 MPa [56], yet, on the other hand, it was found that the addition of 9 wt.% of MWCNT to poly(styrene-co-butyl acrylate) actually decreases the ultimate tensile strength from about 35 MPa to 15 MPa [57]. On average over more than one hundred different systems [54], CNT addition to polymers increases strength by a factor of around 1.7, which is low in light of the fact that the strength properties of the reinforcing CNTs and the polymeric matrix differ by a factor of typically more than 1000.

Besides the elastic and strength properties, other mechanical properties of bulk CNT – polymer nanocomposites have also been studied, such as fracture toughness [58, 59] and hardness [60, 61]. Generally, CNT addition to polymers enhances the respective property, but to a lower degree than expected. For more information about mechanical properties of bulk CNT – polymer nanocomposites, References [23, 31, 54] are recommended.

2.3.2 CNT polymer interaction, dispersion, and processing

Interfacial shear strength and dispersion issues are believed to be the two main reasons for why the full potential of CNTs has not yet been reached with regard to mechanical reinforcement of polymeric matrices. Mechanical reinforcement requires an efficient load transfer of the external stresses applied to a CNT – polymer nanocomposite as a whole to the CNT network. On the one hand this depends on how well the two constituent materials are bonded, i.e. the interfacial properties. It is known that the latter depend on the chemistry of the system and on the nature of polymer morphology at the interface [23]; however, more work is needed to fully understand and improve CNT

polymer interfacial interactions. In this context, considerable research efforts are currently being devoted to improving the latter through both non-covalent and covalent interaction techniques [27], with CNT functionalization for chemical bonding of the reinforcing particles to the polymeric matrix receiving much attention [31, 62, 63]. On the other hand, efficient load transfer to the CNT network requires a uniform dispersion of the reinforcing particles to the level of individual CNTs being coated with polymer [23]. However, CNTs are highly flexible through bending and buckling [29] and naturally exhibit a large specific surface area, which, in combination with their high aspect ratio, leads to a strong tendency for CNTs to stick together and aggregate. It is difficult to disintegrate aggregates to the level of individual CNTs, and aggregate properties are generally inferior to those of individual CNTs [23]; therefore, CNTs in bulk CNT modified polymers predominantly stay in the form of aggregate, which thus lessens the reinforcing effect.

Aggregate disaggregation and CNT dispersion depends on the characteristics of the two constituent materials as well as on material processing. The most commonly used processing techniques are dry mixing, melt processing, solution mixing by means of a suitable solvent, in-situ polymerization, and variations thereof [23, 54, 64]. The choice of processing method is naturally narrowed by the type of the polymer; e.g., melt processing requires the matrix material to be thermoplastic, and solution mixing is limited to soluble polymers. With regard to CNT dispersion and aggregate disaggregation, solution mixing and in-situ polymerization generally give better results than dry mixing and melt processing; the latter, on the other hand, are simpler methods, which are more compatible

with standard industrial techniques. Given that the characteristics of the CNT network, and ultimately the material properties, depend on material processing, considerable research efforts are currently being devoted to improving CNT dispersion and aggregate disaggregation, the most popular routes being CNT functionalization [62] and the use of external fields (cf. Chapter 6). For more information about processing and interactions in CNT – polymer nanocomposites, References [23, 27, 54] are recommended.

2.3.3 Thermal properties of bulk CNT – polymer nanocomposites

The thermal conductivities of standard polymers roughly vary from 0.2 W/m.K for amorphous polymers to 0.5 W/m.K for highly crystalline polymers [65, 66]. CNT addition to polymers can increase the thermal conductivity by about one order of magnitude; e.g., polymethylmethacrylat modified with 4 wt.% of MWCNTs exhibits a thermal conductivity of up to 3.44 W/m.K [67]. Although significant, this increase is low compared with expectations from the intrinsic thermal conductivity of CNTs (cf. Section 2.2). A large thermal resistance at CNT to polymer interfaces has been identified as the primary issue [66]. The latter is believed to be due to poor chemical bonding between the two constituent materials, and to phonon mismatch, resulting in severe phonon scattering at the interface and to a drastic reduction of the interfacial thermal transport properties. In addition, CNT to CNT interfaces also exhibit considerable thermal resistances; the thermal conductivities of MWCNT films, for example, have been reported to be about 15 W/m.K [68] to 25 W/m.K [69], which is two orders of magnitude lower than the intrinsic

thermal conductivity of individual MWCNTs. For more information about thermal properties of bulk CNT – polymer nanocomposites, Reference [66] is recommended.

The mechanical, thermal and electrical (cf. Section 2.4) properties of CNT modified polymers are by far the most studied ones, it should however be noted that other properties, such as optical [70-72], fire-retardant [73], and tribological properties [74, 75], are also being investigated. In this context it should further be noted that, in order to take advantage of their outstanding intrinsic properties, CNTs are not only being added to polymers, but also to metallic [76], ceramic [77], or cementitious [78] matrices.

2.4 Electrical Properties of Bulk CNT – Polymer Nanocomposites

Given the above-presented discrepancies between theoretical expectations and experimental findings, reasonable doubt has to be entertained with regard to the use of CNTs as a major constituent in composite materials for mechanical or thermal applications. The situation is very unlike though with respect to electrical applications, as the requirements for the CNT network are significantly different: first, in contrast to mechanical reinforcement, electrical enhancement does not require strong CNT polymer interfacial interactions, nor a uniform dispersion of the electrically conducting particles to the level of individual CNTs, and, second, significant differences apply between the thermal and electrical properties as the CNT to polymer conductivity ratio is several orders of magnitude higher for electrical conductivity, and the conductivity is not of phononic type but of electronic type instead.

As indicated before, CNT – polymer nanocomposites are electroconductive because of the CNTs forming an electron-conducting network throughout a polymer matrix, which typically is electrically insulating. As introduced in Sections 2.2 and 2.3.2, CNTs exhibit unparalleled specific electrical conductivity and current carrying capacity values, have very high aspect ratios, are of nanoscopic size, and are mechanically flexible. The combination of these four factors makes CNTs the prime filler material and stand out in comparison to other candidates, such as carbon black or metallic nanofibres. They enable a major improvement in electrical conductivity at small particle mass fractions, without significant compromises on other properties of the polymeric matrix, and make CNT – polymer nanocomposites an interesting functional material for a wide range of applications where polymers are preferred to metals or ceramics, but where electrical conductivity is a required material property; e.g., flexible tactile sensors [8], low-resistance high-transparency films [12], flexible electro-chromic films [79], or transparent and or flexible electric heating elements [80].

The potential of CNT – polymer nanocomposites is reflected in a steadily high number of patents issued each year, and an annually increasing number of scientific publications, as is shown in Figure 2.2. The potential is also reflected in an annually increasing CNT production capacity (cf. inset in Figure 2.2). The breadth of different CNT – polymer systems that have been looked at is immense. The evolution of the electrical conductivity of CNT modified polymers with particle mass fraction is of similar type for all systems. The electrical conductivity typically remains at the level of the polymer matrix up to a critical mass fraction, at which the material exhibits a sudden

transition from electrically insulating to conducting. Above that critical point, the electrical conductivity then increases with particle mass fraction, with a progressively decreasing improvement in electrical conductivity per unit particle mass fraction (cf. Figure 3.11). The sudden transition from electrically insulating to conducting is typically described by percolation theory. The latter will be introduced in Chapter 3.4.3, and its application to electron conduction in CNT modified polymers will be a recurrent topic throughout this thesis.

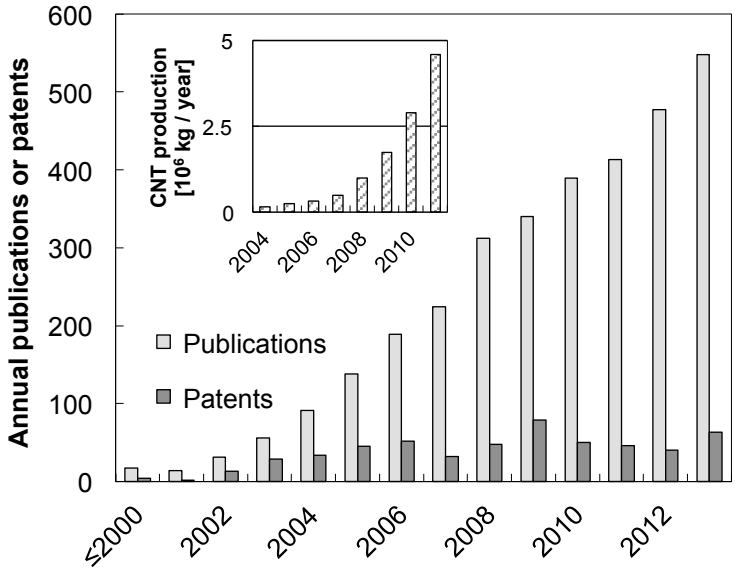

Figure 2.2. Annual scientific publications and patents, according to the result analysis tool of Elsevier's bibliographic database Scopus, with the words 'carbon nanotube', 'polymer', and 'electrical' appearing altogether in article title, keywords, and or abstract. Inset: Annual CNT production capacity, taken from [30], where it was estimated based on a survey among thirty manufacturers of CNTs.

Just as for the mechanical properties, reported electrical properties of CNT – polymer nanocomposites tend to be widely scattered (cf. Figures 6.1 and 6.2), and just as for other material properties of CNT – polymer nanocomposites this is a consequence of the fact that the electrical properties depend on the characteristics of the particle network, which in turn depend not only on the characteristics of the constituent materials but primarily also on material processing (cf. Section 2.3.2). For epoxy resin modified with 1 wt.% of MWCNT, for example, reported electrical conductivity values vary from less than 10^{-10} S/m [81] to 1 S/m [82], and the corresponding minimum particle mass fraction needed to form an electron-conducting MWCNT network throughout the epoxy matrix range from 0.000025 to more than 0.035. For MWCNT modified polycarbonate, on the other hand, some studies observed a transition from electrically insulating to conducting at particle mass fractions that had no significant influence of the viscoelastic properties of the material [83, 84], whereas other studies found both the viscous and the elastic portion of the viscoelastic behaviour of the material to increase significantly at particle mass fractions below the insulator to conductor transition [85, 86]. In addition, in some cases published results are mutually contradicting; the electric response to uniaxial compression of MWCNT modified polydimethylsiloxane, for instance, has been reported to be positive in some studies [87, 88], but to be negative in others [89].

This breadth of reported results, and in particular the apparent contradictions, present major obstacles with regard to an understanding of electron conduction in CNT modified polymers and its dependence on the configuration of the CNT network. Against this background, the main issues, namely nonuniversal percolation, positive vs. negative

piezoresistance, as well as network formation and optimization, will be addresses one by one in Chapters 3 through 6, where relevant scientific literature is reviewed in more detail.

CHAPTER 3

Measurement and Analysis of Electrical Properties of MWCNT – PDMS Nanocomposites

Parts published in Materials Research Society Symposium Proceedings – MRS Proceedings 2012, 1410. DOI: 10.1557/opl.2012.856.

3.1 Introduction

The addition of small quantities of CNTs to electrically non-conducting polymers can transform the latter into electrically conducting ones, without significant compromises on other material properties, which makes CNT – polymer nanocomposites an interesting candidate for a wide range of applications where polymers are preferred to metals or ceramics, but where electrical conductivity is a requirement (cf. Chapter 2). The interest in the electrical properties of CNT – polymer nanocomposites is reflected in a high number of scientific articles published each year: according to the result analysis tool of Elsevier's bibliographic database Scopus, more than one scientific publication per day has become available over the course of this dissertation research, where the words 'carbon nanotube', 'polymer', and 'electrical' appear altogether in article title, keywords, and or abstract (cf. Figure 2.2).

The majority of these publications look at the electrical properties of CNT modified thermoplastic and thermosetting polymers, cf. [83, 84, 86, 90-128] and [81, 82, 129-155],

respectively, with polystyrene and epoxy resin being among the most used matrix materials. In comparison, studies where the matrix is an elastomeric polymer are rather scarce; when it comes to CNT modified polydimethylsiloxane (PDMS), for example, the material system studied here, only a handful articles look specifically at electrical characteristics, cf. [80, 88, 156-161].

The electrical properties of CNT modified polymers depend essentially on the configuration of the percolated particle network (i.e., number of electron-conducting paths, average number of CNT to CNT electrical contacts within the electron-conducting paths, etc.), which in turn depends on the characteristics of the constituent materials (i.e., particle aspect ratio and curvature, polymer viscosity, etc.) and material processing (i.e. degree of particle deagglomeration, homogeneity of dispersion, etc.). In this regard, type and production method of the CNTs are typically less important than the type of the polymer and the technique used to produce the nanocomposites [26]. However, even though in most of the above-cited work on CNT modified PDMS the same technique was used to produce the nanocomposites, the electrical properties vary considerably: reported electrical conductivities at a CNT weight fraction of 0.01, for example, vary from less than 10^{-10} S/m [159] to 10^{-1} S/m [80], and the corresponding minimum particle mass fraction needed to form an electron-conducting CNT network throughout the PDMS matrix vary between 0.0027 and 0.0175. Consequently, even for a same class of nanocomposites, reported data on electrical properties are not generally applicable, and a study of electron conduction and network formation in CNT modified polymers, as it is the objective of this work, therefore requires an electrical analysis of the system at hand.

3.2 Research Objectives

The aim of this chapter is to measure and analyse electrical properties of CNT modified PDMS, and therewith to gain insight into electron conduction in such nanocomposites. First, the electrical conductivity of a CNT network without PDMS matrix is analysed. Second, the electrical conductivity of CNT modified PDMS is studied as a function of CNT mass fraction, and it is evaluated to what extend the result depends on the specifics of the measuring technique. Third, electron conduction through the percolated particle network is addressed by both alternating current and direct current experiments.

3.3 Materials and Methods

The materials used in this study were MWCNTs and PDMS. The electrical conductivity of MWCNT modified PDMS as a function of MWCNT mass fraction was evaluated according to a standard testing method using two different electrode systems, namely a resistivity test fixture with conductive rubber pad electrodes and an electric circuit using conductive silver paint electrodes. In addition, both alternating current (AC) and direct current (DC) electrical properties were analyzed and a new measuring technique was developed to determine the electrical conductivity of a MWCNT network without PDMS.

3.3.1 Materials

PDMS (Gelest OE41) was purchased from Gelest, Inc. and MWCNTs (Baytubes C 150 P) were obtained from Bayer MaterialScience LLC.

Gelest OE41 is an addition cure, filler-free, two-part, pure silicon elastomer, that was selected for its low viscosity of the catalyzed mix (1.75 – 2.5 Pa.s), its long pot-life at room temperature (18 h at 25 °C) and its moderate cure temperature (e.g., cure at 55 °C for 4 h). Because it is an addition cure system, no byproducts are formed, which enables fabrication of test samples with good dimensional stability. The base polymer (vinyl-terminated polydimethylsiloxane and vinyl-modified Q silica resin) and the curing agent (methylhydrosiloxane–dimethylsiloxane copolymer) react via platinum catalyzed hydrosilylation. Both the reacting groups and the bond forming chemistry are schematically illustrated in Figure 3.1.

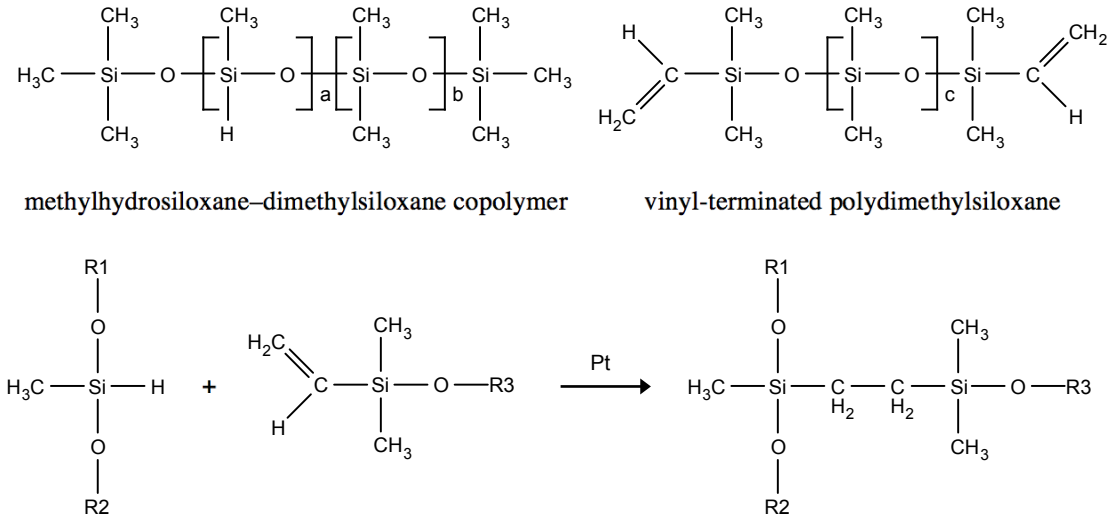

Figure 3.1. Schematic illustrating the reacting groups and the platinum catalyzed hydrosilylation of methylhydrosiloxane–dimethylsiloxane copolymer with vinyl-terminated polydimethylsiloxane.

Baytubes are agglomerates of MWCNTs, with a loose agglomerate size in the range of 0.1 to 1 mm. As specified by the manufacturer, the CNTs were grown by chemical vapour deposition, have a narrow diameter distribution with inner and outer diameters of around 4 nm and 13 nm respectively, and an average length of above 1 μm. Due to breakup of MWCNTs during material processing, the CNTs dispersed in the PDMS matrix were shorter, and varied in length between 200 nm and 1 μm. Transmission electron microscope (TEM) images of individual MWCNTs are shown in Figure 3.2. Figure 3.3 shows scanning electron microscope (SEM) images of MWCNTs, showing both large agglomerates of MWCNTs and individual MWCNTs. The electron-microscopical study qualitatively confirmed the geometrical information provided by the manufacturer, and, more importantly, revealed good quality MWCNT samples with little impurities and no free amorphous carbon.

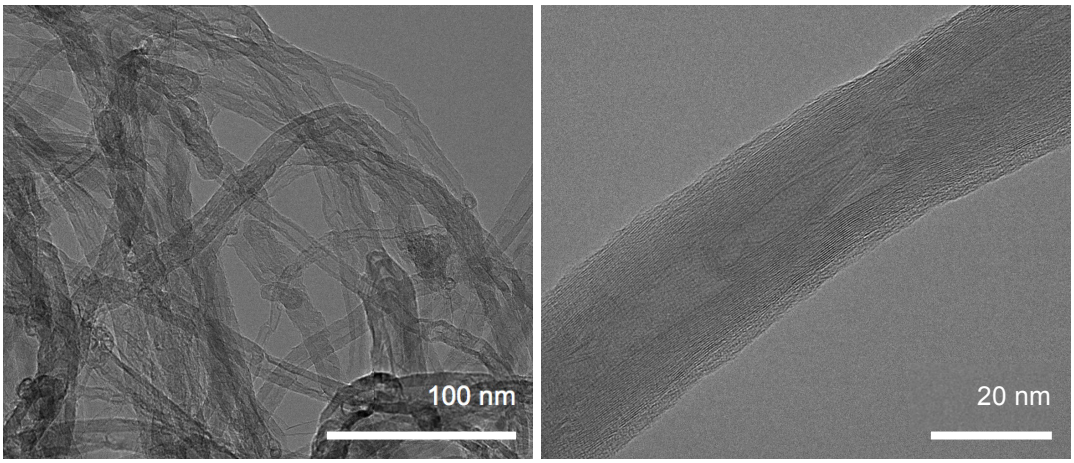

Figure 3.2. TEM images of Baytubes C 150 P, obtained using a Philips CM-200 microscope operating at 200 kV. The samples were prepared by dropping a MWCNT in isopropanol suspension onto 400-mesh carbon-coated copper grids, and evaporating the solvent. The images were not enhanced and are shown as recorded (raw data).

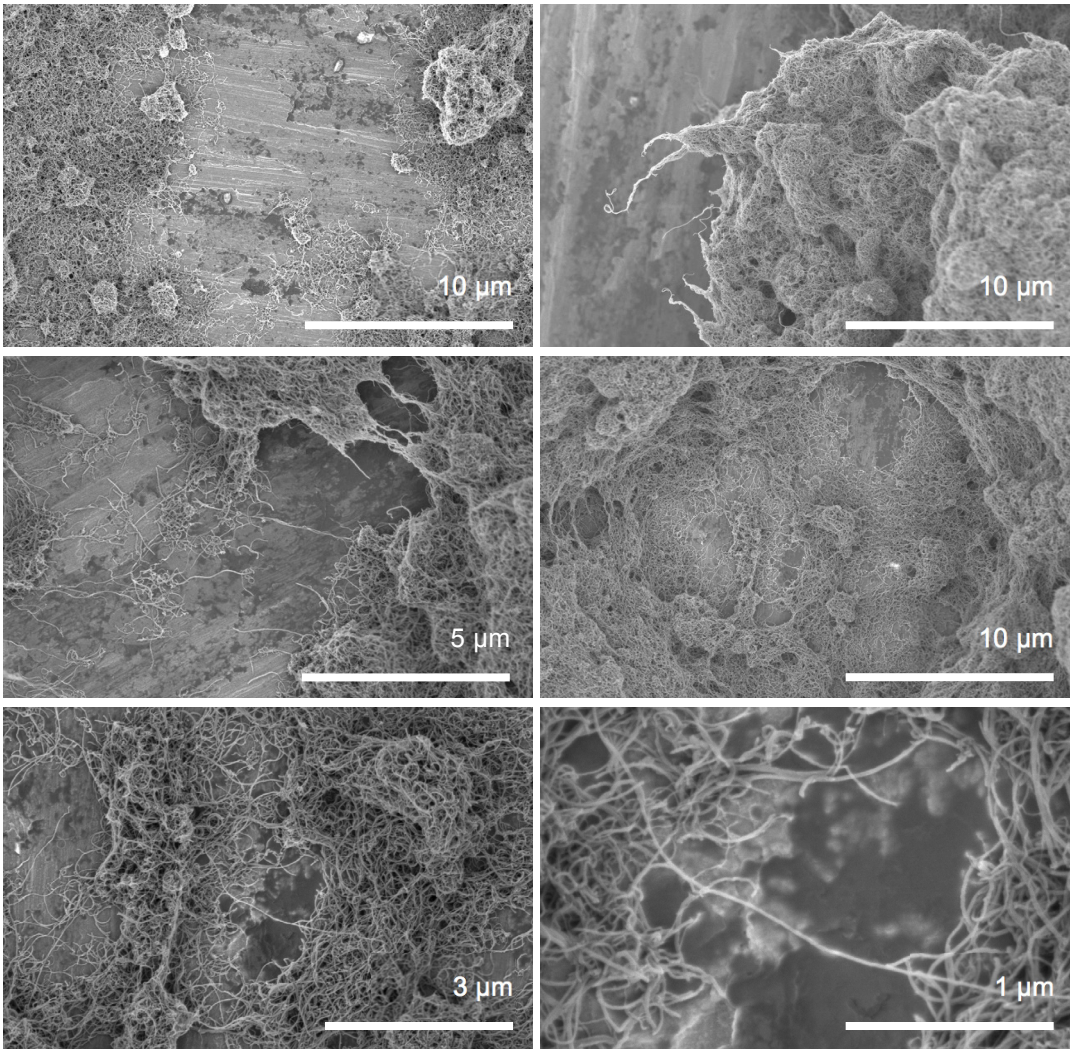

Figure 3.3. SEM images of Baytubes C 150 P, recorded on a Hitachi SU-8000 cold-field emission scanning electron microscope, using an accelerating voltage of 1.0 kV and a working distance of 7.6 mm. Secondary electrons (SE) were collected with two through-the-lens detectors and a conventional SE detector located in the specimen chamber. Sample preparation involved dropping a MWCNT in isopropanol suspension onto a SEM sample holder, and evaporating the solvent. The images were not enhanced and are shown as recorded (raw data).

3.3.2 Sample preparation

Toluene, purchased from Sigma-Aldrich Canada Corp., was used as an organic solvent to facilitate MWCNT deagglomeration and mixing of the constituent materials. For each concentration the desired amount of MWCNTs was first dispersed in toluene for 90 min, using an ultrasonic bath (Model 2510, Branson Ultrasonics Corp.), and then added to the PDMS base polymer and the PDMS curing agent, such that the MWCNT/toluene to PDMS weight ratio was 1:3. Subsequently the mixture was shear-mixed for 5 min, using a disperser (T 10 basic Ultra-Turrax, IKA Works, Inc.) rotating at 940 rad/s, degassed in low vacuum, and toluene was evaporated in an air-circulating oven at 40 °C. Degassing and evaporation times were 30 min each. The variability in MWCNT mass fraction was estimated to be < 10 %. Pictures and optical microscopy (OM) images of MWCNT in PDMS suspensions are given in Figure 3.4 and Figure 3.5, respectively.

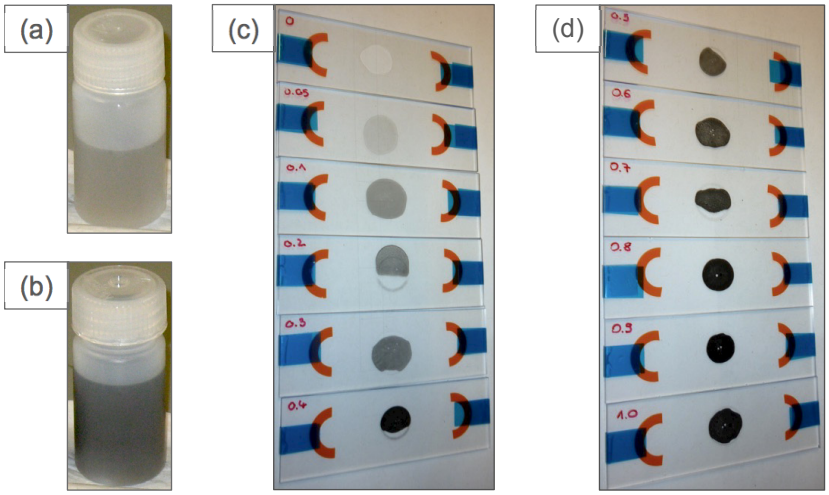

Figure 3.4. Pictures of MWCNT in PDMS suspensions, after degassing and solvent evaporation, but prior to thermal curing. (a + b) as prepared, and (c + d) small droplets squeezed between two glass slides, with increasing MWCNT mass fraction from top to bottom: from 0 to 0.004 in (c), and from 0.005 to 0.01 in (d).

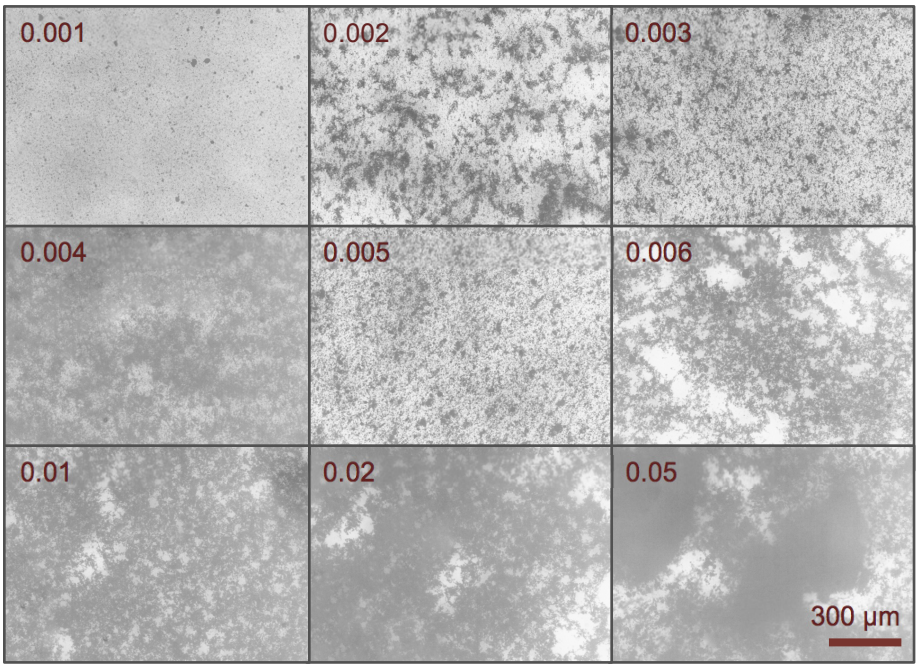

Figure 3.5. OM images of MWCNT in PDMS suspensions, after degassing and solvent evaporation, but prior to thermal curing. The images were recorded on a Nikon Microscope and the labels indicate particle mass fractions.

Dry MWCNTs were handled inside a glove box with attached vacuum chamber for material transport and air cleaning. The glove box was part of a working practice to minimize/eliminate potential health, safety, and environmental risks associated with the handling of dry CNTs in laboratory research. Both the glove box set-up and the working practice are presented in Appendix A.

Thin film samples with concentrations varying from 0 wt.% to 5.0 wt.% were manufactured by solution casting onto release film covered glass substrates, followed by thermal curing in an air-circulating oven. The samples were 10 cm in diameter and varied in thickness from 0.4 to 1 mm. Electron-microscopical images of cured 1 wt.% MWCNT – PDMS nanocomposite thin films are shown in Figure 3.6; the SEM and TEM images

indicate a percolated CNT network, with interconnected CNTs and or CNT agglomerates. Figure 3.7 shows three film samples with MWCNT mass fractions of 0, 0.001, and 0.01.

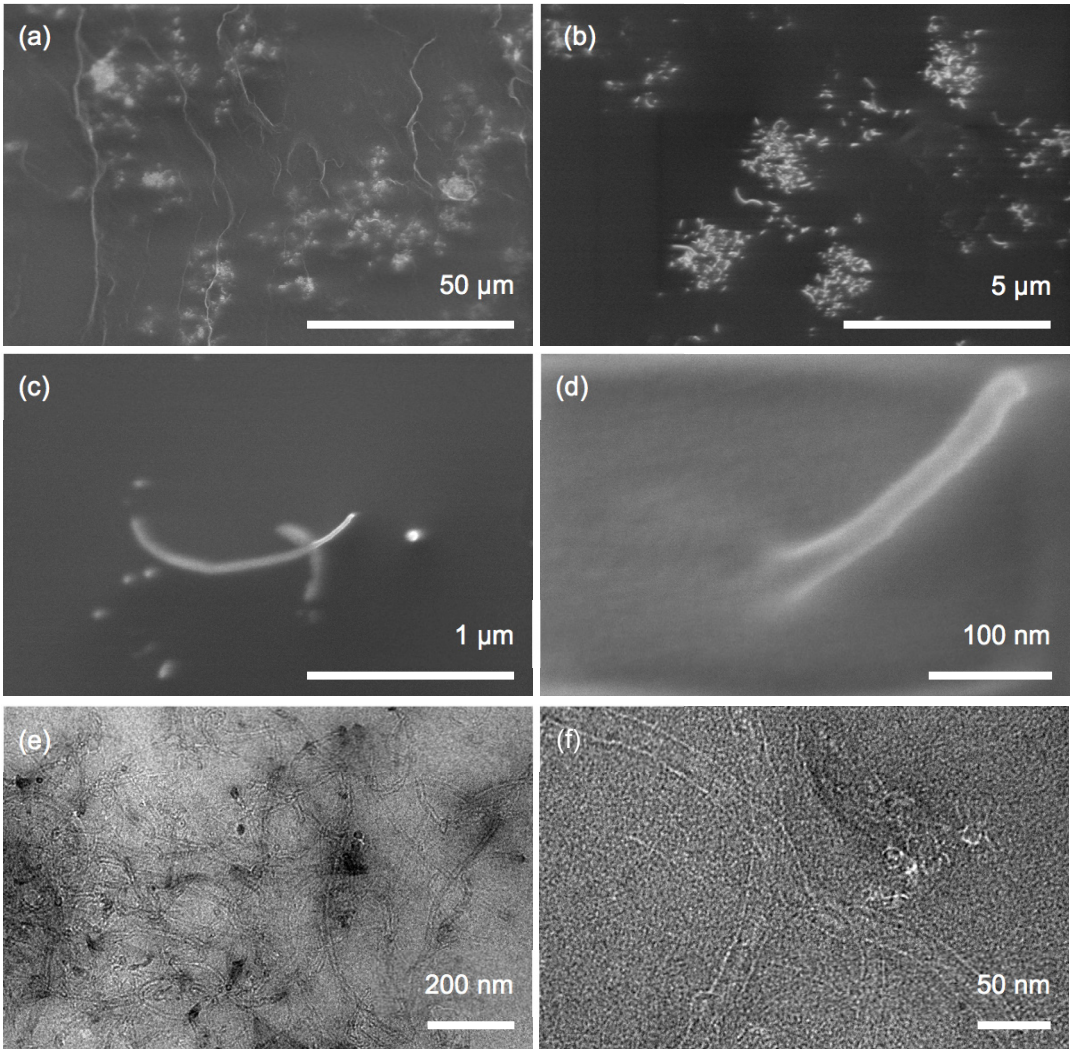

Figure 3.7. SEM (a - d) and TEM (e + f) images of 1 wt.% MWCNT – PDMS nanocomposite thin film samples. The SEM image was recorded on a Hitachi SU-8000 cold-field emission scanning electron microscope, using an accelerating voltage of 0.5 kV and a working distance of 7.1 mm. The TEM image was obtained using a Philips CM-200 microscope operating at 200 kV. Images are shown as recorded (raw data).

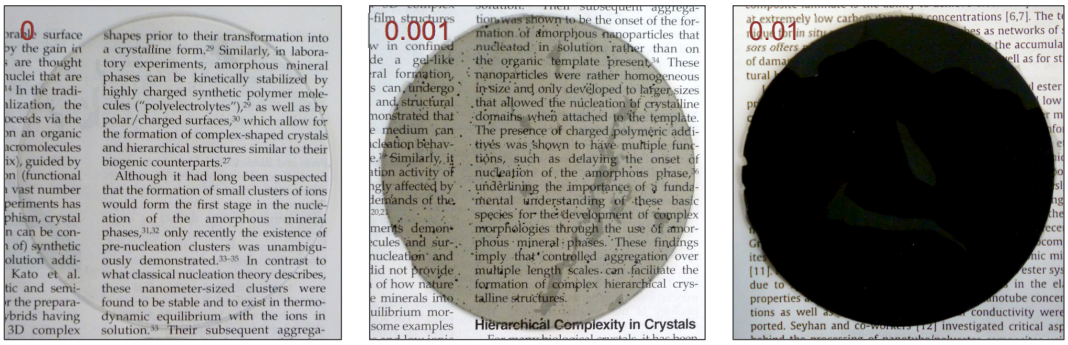

Figure 3.6. Pictures of thin film samples with varying MWCNT concentration produced by solution casting and thermal curing, and used for electrical characterization. The labels indicate particle mass fraction.

3.3.3 Electrical characterization

A picture and a schematic representation of the set-up used to measure the electrical conductivity of a dry MWCNT network without PDMS are given in Figure 3.8. Baytubes C 150 P were filled into a plastic tube with inner diameter of 4.7 mm, which was closed on both sides by movable flat-headed plastic pistons. The network was contacted by silver paint electrodes (high purity silver paint, SPI Supplies / Structure Probe, Inc.), which were applied onto the pistons and contacted by insulated copper wires. A DC power supply (Model ABC 40-0.5, KEPCO Inc.) was used to apply an electric potential difference, ΔV, which was gauged by means of a digital multimeter (Model 73 Series II, Fluke Corp.) and is indicated in the legend of the Figure 3.10. The electric current, I, was measured with the same type of digital multimeter, and the electrical conductivity, σ, was calculated according to :

$$\sigma = \frac{1}{\rho} = \frac{l}{RA} = \frac{l\,I}{\Delta V A}\,, \tag{3.1}$$

where ρ is the electrical resistivity of the material, R is the electrical resistance of the sample, l is the electrode spacing, and A is the area of the electrodes. All measurements were taken at room temperature.

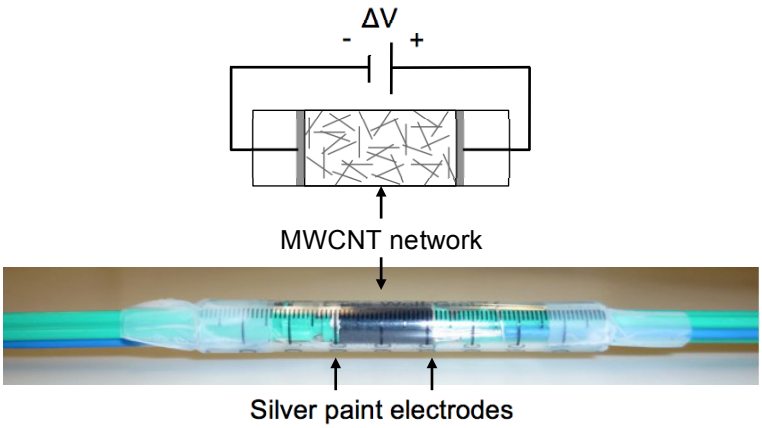

Figure 3.8. Picture (bottom) and schematic representation (top) of set-up used to measure the electrical conductivity of a dry MWCNT network.

The DC electrical volume conductivity of MWCNT modified PDMS was obtained according to ASTM D257, using a high resistance meter (Model 6517A, Keithley Instruments, Inc.) and a resistivity test fixture with conductive rubber pad electrodes (Model 8009, Keithley Instruments, Inc.). An electric potential difference of 10 V was applied, and the electrical conductivity was calculated from the measured electrical resistance using Equation 3.1. The DC electrical volume conductivity was also measured by means of an electronic circuit where electrical contact with the sample is made by conductive silver paint. Circular silver paint electrodes of uniform size and shape were applied on both sides of 4 cm wide disc samples, which were cut from thin films produced by solution casting. The electrodes were contacted by Kapton insulated, silver

plated copper wires, the resistance was obtained using the high resistance meter with an electric potential difference of 10 V, and the electrical conductivity was calculated from the electrical resistance using Equation 3.1. A photo of disc samples with contacted silver paint electrodes is given in Figure 3.9.

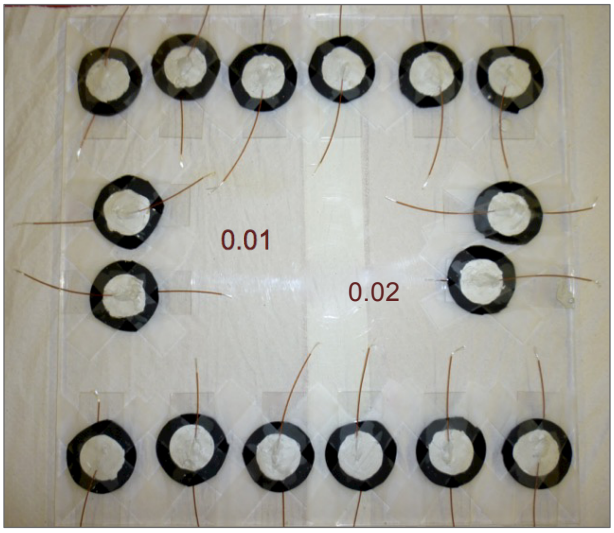

Figure 3.9. Picture of samples used to measure the electrical conductivity of MWCNT modified PDMS. The disc samples were 4 cm in diameter and the circular electrodes were of uniform size and shape. The labels indicate particle mass fraction.

For both DC measuring techniques the test – retest variability on one and the same sample was < 18 % at $p < p_c$ and < 5 % at $p > p_c$, with p being the particle mass fraction and p_c being the percolation threshold, i.e. the minimum particle mass fraction needed to form an electron-conducting MWCNT network throughout the PDMS matrix (cf. Section 3.4.3). The test – retest variability on different samples of the same particle mass fraction was < 40 %. Given this seemingly large variability it should be noted that, above p_c,

subsequent σ values (e.g. σ measured at p = 0.01 and σ measured at p = 0.02) differ by a factor of 5 in average. It should also be noted that the test – retest variability decreases rapidly as the MWCNT mass fraction increases, which is likely related to the number of electron-conducting paths within the particle network. The latter increases with increasing particle mass fraction; the smaller that number of paths, the bigger the influence of small differences between MWCNT networks in different samples, and vice versa. Standard deviations in both particle mass fraction and electrical conductivity are shown in Figure 3.12. All measurements were taken at room temperature.

The AC electrical conductivity, σ_{AC}, was obtained on disc samples with silver paint electrodes (cf. Figure 3.9), using an electrochemical workstation (Model 760C, CH Instruments). All measurements were performed at an electric potential difference of 2.4 V with superimposed AC amplitude of 0.4 V, and the frequency was scanned from 1 Hz to 10'000 Hz, with a quiet time of 2 s. Above 100 Hz, both current and electric potential were measured in order to calculate the impedance, Z_{AC}, and 12 frequency components per decade were measured. Below 100 Hz, only the current was measured and the applied electric potential was assumed to have no extra phase shift and to be accurate. σ_{AC} was obtained by:

$$\sigma_{AC} = \frac{l}{Z_{AC}A} = \frac{Y_{AC}l}{A}\,, \tag{3.2}$$

where Y_{AC} is the admittance, l is the electrode spacing, and A is the area of the electrodes. The test – retest variability on different samples of the same particle mass fraction was <

60 %, and as for the DC characterization, the test – retest variability decreased rapidly with increasing MWCNT mass fraction. Measurements were taken at room temperature

The current-voltage (IV) behaviour was analyzed using disc samples with silver paint electrodes (cf. Figure 3.9) and the high resistance meter, with an electric potential difference that varied between 0.5 V and 32 V. Measurements were taken at room temperature.

The temperature dependence of the electrical conductivity was obtained on disc samples with silver paint electrodes (cf. Figure 3.9), at an electric potential difference of 2 V, with the samples being heated in an air-circulating oven and the temperature being measured on the samples directly.

3.4 Results and Discussion

To evaluate the potential of MWCNT addition to PDMS as regards the electrical conductivity of such nanocomposites, it is helpful to also analyse the electrical conductivity of a dry network of Baytubes C 150 P, the MWCNTs used in this work, without PDMS.

3.4.1 Electrical conductivity of MWCNT network without PDMS

As described in Section 3.3.3 the electrical conductivity of a network of MWCNTs without PDMS was measured by filling the particles into a plastic tube, which was closed on both sides by movable electrodes. Figure 3.10 shows the evolution of the electrical conductivity with electrode spacing.

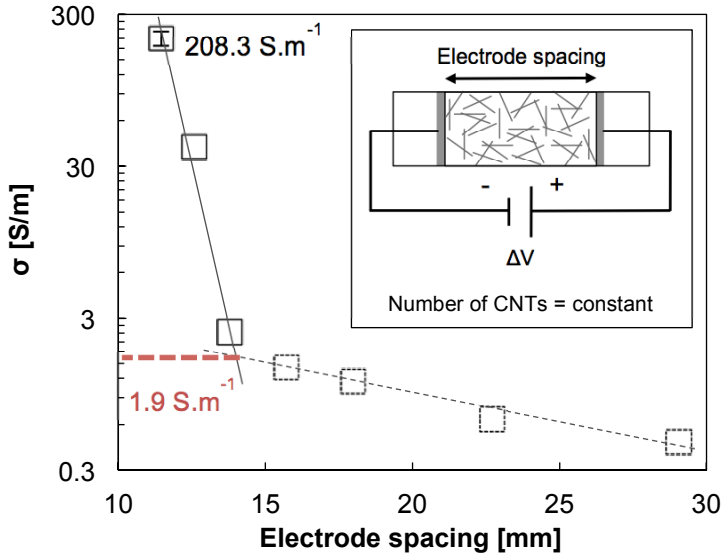

Figure 3.10. Electrical conductivity of a dry network of Baytubes C 150P as a function of electrode spacing. The inset shows a schematic of the experimental set-up. The vertical error bars at an electrode spacing of 11.5 mm give the standard deviation over measurements taken at 0.25 V, 0.5 V, 1 V and 2 V. All other measurements have been taken at 2 V.

At an electrode spacing of 29 mm, the CNTs form an electron-conducting network connecting the two electrodes, the test volume, however, is not completely filled by the loose CNT network. As the electrode spacing is reduced, so is the test volume between the electrodes, and the geometry of the CNT network is changed to shorter length and larger transverse section. As a consequence, the electron-conducting paths become shorter and more electron-conducting paths are formed, which leads to a reduction in electrical resistance and thus to an increase in electrical conductivity. It should be noted that as long as the volume occupied by the CNT network is smaller than the test volume, the electrical conductivity of the CNT network, as calculated by Equation 3.1, is

underestimated because the actual electrode area in contact with the CNT network is smaller than A, which is the area of the entire electrode. For the case presented in Figure 3.10, it appears that the ratio of volume occupied by the CNT network to test volume becomes unity at an electrode spacing of 14 mm. As the electrode spacing is further reduced, the change in electrical conductivity with electrode spacing becomes more pronounced. In this region, the CNT network is compressed. First, because CNTs are flexible through bending and buckling [29] this likely leads to an increasing number of CNT to CNT electrical contacts and therewith to the formation of additional electron-conducting paths. Second, the intertube electron transfer at CNT to CNT junctions increases if compressive pressure is applied to the junction [162]. Both processes lead to an increase in σ.

From the above it follows that the electrical conductivity of a loose network of Baytubes C 150P can be estimated to be $\sigma \approx 2$ S/m, which can be considered as the maximum electrical conductivity, σ_{max}, that can theoretically be obtained in Baytubes C 150P modified PDMS nanocomposites produced by the technique described in Section 3.3.2. The highest values reported in literature for the electrical conductivity of dry MWCNT networks are two to three orders of magnitude higher, i.e. 300 to 4'400 S/m [163, 164], depending on the degree of porosity, the quantity and quality of metallic CNTs within the network, as well as sample geometry and measuring technique. It should however be noted that these values are not directly comparable to the value found in this work, as they have been obtained on thin films (130 to 200 μm thick) produced by a filtration method. Thin MWCNT films typically exhibit a relatively high anisotropy in in

plane to perpendicular electrical conductivity due to CNT alignment during filtration [164], and are thus not comparable to more isotropic MWCNT networks formed in bulk CNT – polymer nanocomposites. In this context it is interesting to note that the majority of the maximum electrical conductivity values reported in literature for bulk CNT – polymer nanocomposites are $\sigma_{max} \leq 2$ S/m (cf. Figure 6.1).

In comparison to the electrical conductivity of individual MWCNTs, which can be as high as 10^7 S/m [42, 43], MWCNT networks are orders of magnitude less conductive. This difference in electrical conductivity between individual MWCNTs on the one hand, and MWCNT networks on the other hand, is due to the fact that electron transport in MWCNT networks is limited by the intertube electron transfer at CNT to CNT junctions, with junction resistances in the kΩ to MΩ range [44, 165].

3.4.2 Electrical conductivity of MWCNT modified PDMS

The evolution of the electrical conductivity of MWCNT – PDMS nanocomposites with particle mass fraction is shown in Figure 3.11. Up to a particle mass fraction of 0.003, the addition of MWCNTs has no effect on σ, which remains at the level of non-modified PDMS, i.e. at around 3×10^{-13} S/m. As the particle mass fraction is increased from 0.003 to 0.004, σ increases by seven orders of magnitude and the material exhibits a sudden transition from electrically insulating to conducting with $\sigma > 10^{-6}$ S/m. At $p > 0.004$, σ further increases with particle mass fraction, reaching $\sigma \approx 10^{-2}$ S/m at $p = 0.05$; the higher p, however, the lower the incremental increase in electrical conductivity with particle mass fraction.

Sudden transitions from one behaviour to another, e.g. from electrically insulating to electrically conducting, are typically described by percolation theory, which is a widely studied and ever evolving field that has been covered by several books and book chapters [166-168], and has first been applied to CNT modified polymers by Coleman et al. [90]. In the next section it is applied to the MWCNT – PDMS system studied here.

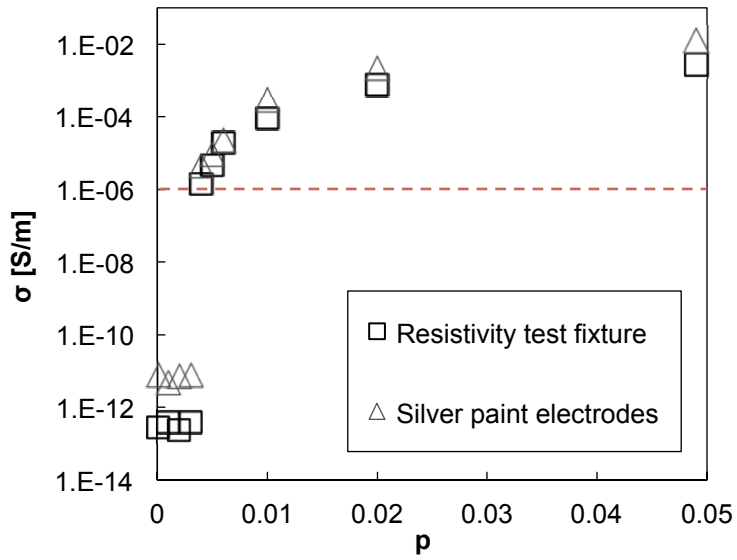

Figure 3.11. Semilogarithmic plot of change in electrical conductivity with MWCNT mass fraction, measured according to ASTM D257 with two different electrode systems (cf. Chapter 3.3.3). Standard deviations in both particle mass fraction and electrical conductivity are shown in Figure 3.12. The dotted line indicates the insulator to semiconductor transition.

3.4.3 Electrical percolation in MWCNT modified PDMS

For suspensions of electrically conducting particles in an electrically insulating matrix, percolation theory defines the minimum particle mass fraction needed to form an

electron-conducting network throughout the insulating matrix as the so-called percolation threshold and describes the evolution of electrical conductivity with particle mass fraction by a power-law behaviour:

$$\sigma \propto (p - p_c)^t \ , \tag{3.3}$$

where t is the so-called conductivity exponent. Equation 3.3 applies to particle mass fractions above but close to the percolation threshold, i.e. when $p > p_c$ and $(p - p_c)$ is small. Percolation in MWCNT modified PDMS is schematically shown in Figure 3.12. At $p < p_c$, the particle mass fraction is too small to have an effect on the electrical conductivity of the material, which is schematically shown in Figure 3.12 (a) and indicated by the dotted vertical line in Figure 3.12 (d); although the particles added to the system do form local networks, no electron-conducting path is formed that spans the entire sample. As the particle mass fraction is increased to p_c, a first electron-conducting path throughout the entire sample is formed and the material is no longer electrically insulating, cf. Figure 3.12 (b) and full vertical line in Figure 3.12 (d). At $p > p_c$, the number of electron-conducting paths increases with particle mass fraction and so does the electrical conductivity of the material, as is schematically shown in Figure 3.12 (c) and indicated by the dashed vertical line in Figure 3.12 (d).

The particle mass fraction at which an electron-conducting network throughout the insulating matrix starts being formed can be obtained by fitting Equation 3.3 to experimental data. In the inset of Figure 3.12 (d) this is done by means of a logarithmic plot of σ vs. $(p - p_c)$, where p_c was incrementally varied until the best linear fit of Equation 3.3 to the experimental data was obtained.

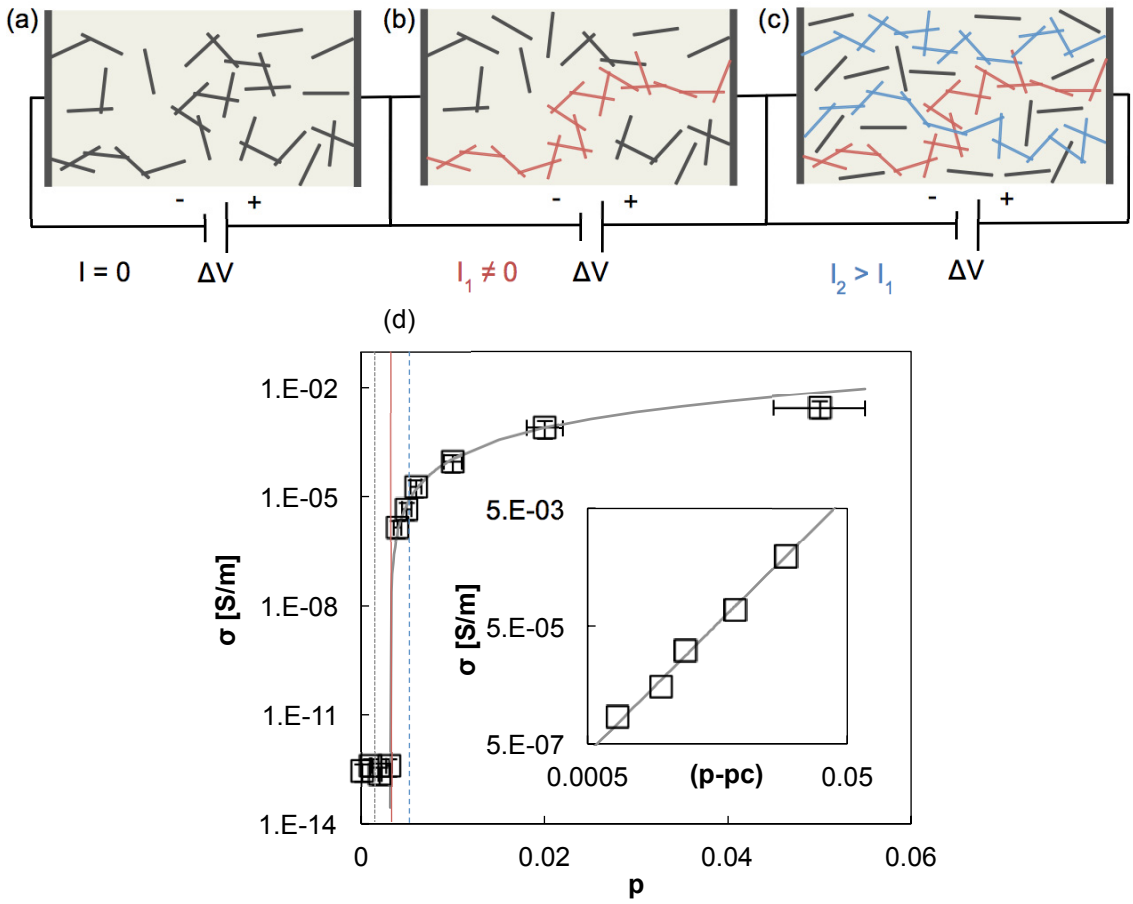

Figure 3.12. (a – c) Schematic of electrical percolation in CNT modified polymers, showing the formation of a first electron-conducting path at $p = p_c$. (d) Semilogarithmic plot of measured (ASTM D257 with resistivity test fixture, empty symbols) and calculated (Equation 3.3, solid line) change in electrical conductivity with MWCNT mass fraction. Error bars indicate standard deviations in both particle mass fraction and electrical conductivity. Inset: logarithmic plot of σ vs. $(p - p_c)$ showing the best fit of Equation 3.3 to the experimental data.

The so obtained electrical percolation parameters p_c and t are specified in Table 3.1, together with the proportionality constant, σ_x, which was also obtained through the fitting procedure and which was used to fit Equation 3.3 to the semilogarithmic plot of σ vs. p

(cf. solid line in Figure 3.12). Also given in Table 3.1 is the coefficient of determination, R^2, for the fitting of Equation 3.3 to the experimental data. For the data shown in Figure 3.12, $R^2 = 0.99332$, which shows that the evolution of electrical conductivity with particle mass fraction in MWCNT modified PDMS is indeed well described by percolation theory.

Table 3.1. Electrical percolation parameters p_c and t, proportionality constant σ_x, and coefficient of determination, R^2, for the fit of Equation 3.3 to the experimental data.

Electrode system	p_c	t	σ_x [S/m]	R^2
Resistivity test fixture	0.00305	2.22	5.66	0.99332
Silver paint electrodes	0.00313	2.20	14.16	0.97273

As outlined in Section 3.1, reported p_c values for MWCNT modified PDMS range from 0.0027 [80] to 0.0175 [159]. An exception is the work published by Kwon et al. [88], who report a percolation threshold of 0.00045. The MWCNTs used in their work are characterized by an extremely high aspect ratio, i.e. 2600 to 7400, which can explain the low percolation threshold, as the latter is assumed to be inversely proportional to the particle aspect ratio [26, 169]. It should however be noted that the electrical recordings were obtained on thin samples with an electrode spacing to CNT length ratio of just about 5, which is why their result likely do not characterize bulk MWCNT – PDMS nanocomposites and therefore can not be compared to the p_c values found here nor the ones cited. A percolation threshold of around 0.003 (cf. Table 3.1) is at the lower end of the range of values reported for MWCNT modified PDMS, and is comparable with the majority of results reported for CNT modified polymers in general (cf. Figure 6.1). In

their review of electrical percolation in CNT modified polymers, Bauhofer et al. [26] found that with optimized dispersion methods a percolation threshold of 0.001 might be obtainable for most CNT – polymer nanocomposite. The slightly higher percolation threshold found in this work can be explained by the fact that sample manufacturing was not optimized in terms of low percolation threshold and high electrical conductivity, but rather in terms of repeatability, as this was key for the investigation of both electron conduction and network formation.

Percolation theory predicts the conductivity exponent to be universal, i.e., to not dependent upon the nature of the particles and or the configuration of the particle network, but to solely dependent on the network dimensionality, such that t = 1.3 for any two-dimensional network, and t = 2 for any three-dimensional network [166, 167]. From Figure 3.12 (d) and Table 3.1 it appears that the MWCNT – PDMS system studied here is characterized by a nonuniversal conductivity exponent. It is interesting to note that this is actually true for most CNT modified polymers (cf. Figure 6.2 and [26, 170]). The origin of this nonuniversality will be introduced in the next section and the discrepancy between theory and experimental data will be discussed in detail in Chapter 6.

With regard to the value of the proportionality constant (σ_x = 5.66 S/m, cf. Table 3.1), which can be considered as a theoretical estimation of σ_{max}, it is interesting to note that it is very close to the electrical conductivity value of a non-compressed MWCNT network without PDMS ($\sigma \approx 2$ S/m, cf. Figure 3.10). Such a comparison however has to be made with caution, keeping in mind that percolation theory is thought to be applicable when $p > p_c$ and $(p - p_c)$ is small.

3.4.4 Quantum mechanical tunnelling

Percolation theory assumes direct contact between adjacent particles within the electron-conducting particle network. Electron-flow between adjacent CNTs, however, does not require physical contact between the particles, but, as long as the interparticle separation is small enough, is also possible through a quantum mechanical effect called tunnelling, as is schematically shown in Figure 3.13.

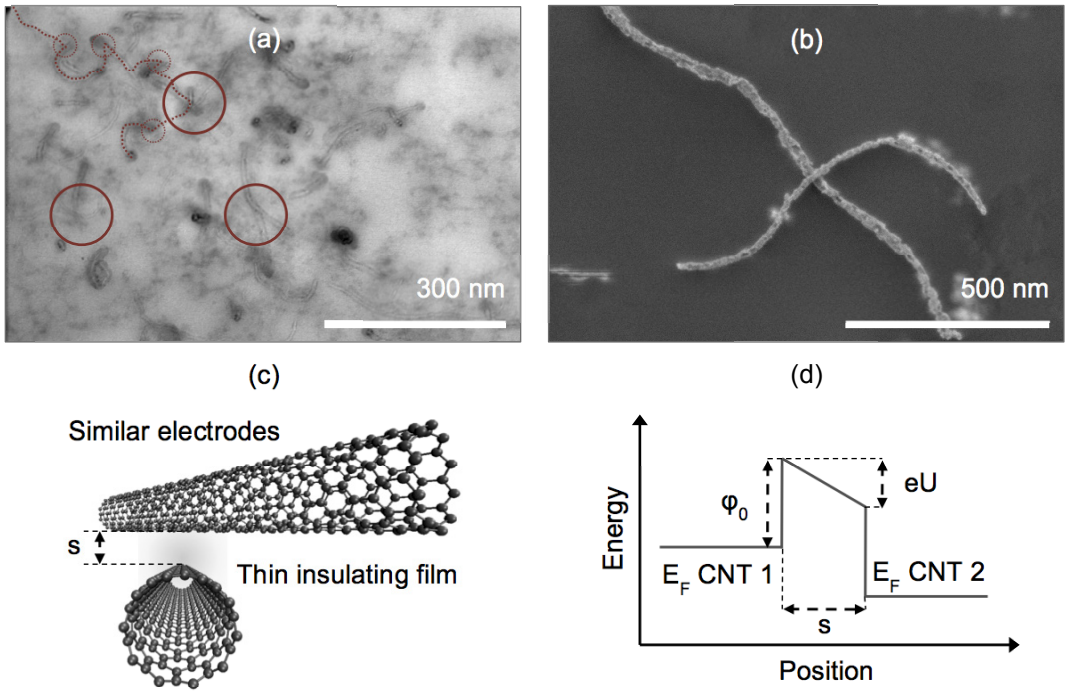

Figure 3.13. (a) Scanning TEM image of 1 wt.% MWCNT modified PDMS. The full and dotted circles highlight CNT to CNT junctions and the dotted line indicates part of an electron-conducting path. (b) SEM image of crossing CNTs. (c + d) Pictorial illustration of quantum mechanical tunnelling in CNT modified polymers, showing crossing CNTs separated by a thin insulating film (c), and the rectangular potential barrier in the insulating film between the two similar electrodes when a voltage is applied between them. E_F is the Fermi level of the electrode and e the elementary charge; the other symbols are defined in the text.

For two electrodes separated by a thin insulating film the equilibrium conditions require the top of the energy gap of the insulator to be positioned above the Fermi level of the electrodes [171]. Thereby the insulating film introduces a potential barrier between the electrodes. This potential barrier impedes electron flow between the electrodes, the impediment, however, is not necessarily infinitely large. The degree to which electron flow is impeded depends on the specifics of the junction and is best described by a generalized expression for quantum mechanical tunnelling between similar electrodes separated by a thin insulating film as developed by Simmons [94]. Assuming that the thickness, s, of the insulating film in the contact area is uniform and that the variation of barrier height along the thickness can be neglected, the current density, J, penetrating the insulating film can then be expressed as:

$$J = \frac{6.2\times10^{10}}{(\Delta s)^2}\left[\varphi e^{-1.025\Delta s\sqrt{\varphi}} - (\varphi + U)e^{-1.025\Delta s\sqrt{\varphi+U}}\right], \tag{3.4}$$

with

$$\varphi = \varphi_0 - \left(\frac{U}{2s}\right)(s_1 + s_2) - \frac{5.75}{\varepsilon_r \Delta s} ln\left(\frac{s_2(s-s_1)}{s_1(s-s_2)}\right), \tag{3.4.1}$$

$$s_1 = \frac{6}{\varepsilon_r \varphi_0}, \tag{3.4.2}$$

$$s_2 = s\left[1 - \frac{36}{3\varphi_0\varepsilon_r s + 20 - 2U\varepsilon_r s}\right] + \frac{6}{\varepsilon_r \varphi_0}, \tag{3.4.3}$$

and

$$\Delta s = s_2 - s_1, \tag{3.4.4}$$

where J is given in [A/cm^2], s is taken in [Å], U is the voltage across the thin insulating film in [V], φ is the mean barrier height in [V], φ_0 is the height of the rectangular barrier

in [V], s_1 and s_2 are the limits of the barrier at the Fermi level in [Å], and ε_r is the relative permittivity of the insulating film material. The more the potential barrier impedes electron flow, the smaller J; hence, the higher the junction resistance.

In literature there is a relatively large body of evidence that indicates that electron conduction in CNT modified polymers in general, and in MWCNT modified PDMS in particular, is indeed dominated by quantum mechanical tunnelling. Frist, as regards p_c and σ_{max}, the type of the particles is found to be less important than the type of the polymer [26]. If adjacent CNTs within the electron-conducting network would all be in direct contact, the opposite would be true, as in this case it should not matter what type of polymer holds the CNT network. From Equation 3.4 it can be derived that if electron conduction is dominated by tunnelling, the type of polymer does play a role as J depends on the relative permittivity of the insulating film material. Second, CNT modified polymers typically exhibit a non-linear IV behaviour (cf. Section 3.4.5 and [80, 158, 172]), which shows that electron transport in CNT modified polymers does not obey Ohm's law. Third, the electrical conductivity of CNT modified polymers typically increases with temperature (cf. Section 3.4.5 and [149, 157]) indicating semiconducting material characteristics.

As regards the nonuniversal conductivity exponent found for the MWCNT modified PDMS studied here (cf. Table 3.1), Balberg [173] identified quantum mechanical tunnelling between adjacent but non-contacting particles within the electron-conducting network as the potential origin of this nonuniversality.

3.4.5 AC and DC electrical characteristics

Figure 3.14 shows the frequency dependence of the electrical conductivity of MWCNT modified PDMS. At $p < p_c$, the electrical conductivity is frequency dependent over the entire range studied and increases with increasing frequency. At $p > p_c$, on the other hand, the MWCNT – PDMS nanocomposites exhibit a frequency independent electrical conductivity up to a critical frequency, f_0, above which the electrical conductivity again increases with frequency. f_0 increases with p and for $p \geq 0.02$ the electrical conductivity remains frequency independent over the entire range studied here.

For the purpose of a qualitative evaluation of these findings, the experimental set-up used for AC characterization, i.e. thin films of MWCNT – PDMS nanocomposites sandwiched between two silver paint electrodes (cf. Section 3.3.3), can be modeled as a resistor and a capacitor in parallel [172]. The admittance of such a system is defined as:

$$Y_{AC} = \frac{1}{R} + j2\pi fC \ , \tag{3.5}$$

where R and C are the electrical resistance and capacitance of the MWCNT – PDMS nanocomposite film, respectively, j is the imaginary unit, and f is the measurement frequency.

At $p < p_c$, MWCNT modified PDMS is electrically insulating (cf. Figure 3.11) and the admittance is essentially given by the second term of Equation 3.5 as the first term is negligible for large R. The admittance as well as the electrical conductivity (cf. Equation 3.2) should then be frequency dependent over the entire frequency range, and increase with increasing frequency, as is indeed observed in Figure 3.14. As specified in the

figure, in this case the σ_{AC} vs. f plot exhibit a slope of unity, which is characteristic for dielectric materials [174].

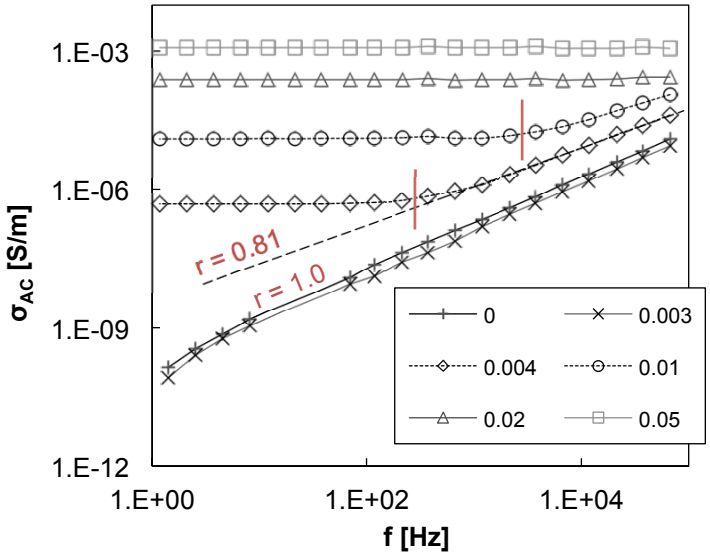

Figure 3.14. Logarithmic plot of frequency dependence of electrical conductivity as a function of particle mass fraction. The vertical lines indicate critical frequencies, and the transverse labels give ac-exponent for p = 0.003 and p = 0.004, as obtained by fitting Equation 3.6 to the experimental data at $f > f_0$.

At $p > p_c$, on the other hand, MWCNT modified PDMS is electrically conducting (cf. Figure 3.11) and the nanocomposite films are characterized by much smaller R values; consequently, the first term of Equation 3.5 gains in importance such that the admittance is now given by the sum of both terms, i.e. it should be frequency independent at low frequencies, and become frequency dependent at higher frequencies. As a matter of fact, this is what is observed in Figure 3.14. The electrical resistance of the nanocomposite films decreases with increasing particle mass fraction. The smaller R the larger the range

of frequency independent electrical conductivity, and the higher the σ_{AC} values at low frequencies, as is also observed in Figure 3.14 (cf. plots for p = 0.004 and p = 0.01).

It should be noted that the capacitance, which is a function of the relative permittivity of the material, typically increases with increasing particle mass fraction [84, 175-177]; in terms of magnitude, however, this increase is much smaller than the concurrent decrease in R. For example, it has been reported that the addition of 6 wt.% of MWCNT to PDMS increased the relative permittivity at a frequency of 1 kHz by a factor of 450, the electrical resistance, in turn, is decreased by more than six order of magnitudes [175].

From Figure 3.14 it appears that the resistive nature of the material becomes more predominant as the particle mass fraction is increased. Nevertheless, electron-conducting MWCNT – PDMS nanocomposites do not behave as ideal resistors; as will be discussed below, first, their electrical conductivity increases with temperature, which is characteristic for semiconductors, and the opposite of what would be observed for an ideal resistors, and, second, their IV characteristics are inconsistent with Ohm's law.

As reported in Table 3.2, the electrical conductivity of MWCNT modified PDMS, with particle mass fractions ranging from close to p_c to far above p_c, increases with increasing temperature. This can be understood by looking at a simplified picture of electron conduction through ideal conductors, e.g. metal conductors, vs. semiconductors. The electrical conductivity of a metal conductor typically decrease with increasing temperature, because of the added thermal energy that leads to an increase in atomic vibration and therewith to more collisions of electrons with the crystal lattice. In contrast, the electrical conductivity of a semiconductor typically increases with temperature

because the added thermal energy leads to an increased number of electrons having enough energy to surmount the potential barrier and contribute to conduction.

Table 3.2. Electrical conductivity of MWCNT modified PDMS as a function material temperature, for three different particle mass fractions, and normalized increase in electrical conductivity over a temperature difference of 75 °C.

p	σ [S/m]				$\frac{\sigma\,(T=100\,°C)}{\sigma\,(T=25\,°C)}$
	T = 25 °C	T = 50 °C	T = 75 °C	T = 100 °C	
0.004	4.4×10^{-6}	4.8×10^{-6}	5.0×10^{-6}	1.2×10^{-5}	2.47
0.01	2.9×10^{-4}	3.0×10^{-4}	3.3×10^{-4}	4.5×10^{-4}	1.52
0.02	2.1×10^{-3}	2.1×10^{-3}	2.1×10^{-3}	3.0×10^{-3}	1.41

The semiconducting behaviour of MWCNT modified PDMS is confirmed by an analysis of the high frequency region in Figure 3.14, where, for $f > f_0$, the frequency dependence of the electrical conductivity can be described as a power law [174]:

$$\sigma_{AC} \propto f^r, \tag{3.6}$$

r being the ac-exponent. Semiconducting materials typically obey Equation 3.6, with most of the reported ac-exponents in the interval $0.7 \leq r \leq 1.0$, and a majority close to r = 0.8 [178]. Equation 3.6 was used to fit the experimental data of MWCNT modified PDMS at p = 0.004, for which the region of frequency dependant electrical conductivity is reasonably large. As proposed by Kilbride et al. [174], f_0 was taken as the frequency at which σ_{AC} reached 110 % of the σ_{AC} value obtained at $f \approx 1$ Hz. The so obtained ac-exponent is r = 0.81 (cf. Figure 3.14), which is in line with what is reported for

semiconducting materials. The coefficient of determination for the fit over the given frequency range is $R^2 = 0.995$.

Figures 3.15 (a) to (c) show current vs. voltage plots for MWCNT modified PDMS with particle mass fractions ranging from p = 0.004, i.e. close to the percolation threshold, to p = 0.05, i.e. far above the percolation threshold. It appears that MWCNT – PDMS nanocomposites exhibit a non-linear IV behaviour, and that the nonlinearity of the IV curves is more pronounced at p close to p_c and becomes weaker as p increases. In line with this, the IV behaviour of a network of Baytubes C 150P without PDMS follows a linear trend, as is shown in Figure 3.15 (d); something that has also been reported for other CNT networks [179].

In the case of the MWCNT network without PDMS, the electron-conducting network is made up of many electron-conducting paths, and adjacent CNTs within these paths likely form direct contacts. The IV characteristics in this case are dominated by the behaviour of the network as a whole, which appears to be of ohmic type, as according to Ohm's law, the current passing through a conductor between two points is linearly proportional to the potential difference across the two points, and inversely proportional to the resistance between them; a current vs. voltage plot of an ohmic material sample should therefore follow a straight line. At p close to p_c, on the other hand, the electron-conducting network is made up of just a few electron-conducting paths, in which case the IV characteristics are dominated by the behaviour of the individual paths, which appears to be of non-ohmic type. A non-linear IV behaviour is characteristic of electron conduction via quantum mechanical tunnelling, as can be understood from Equation 3.4

where it is explicit that the interdependence between current and voltage is indeed non-linear. It thus appears that that electron transport through individual paths is limited by tunnelling between adjacent but non-contacting CNTs

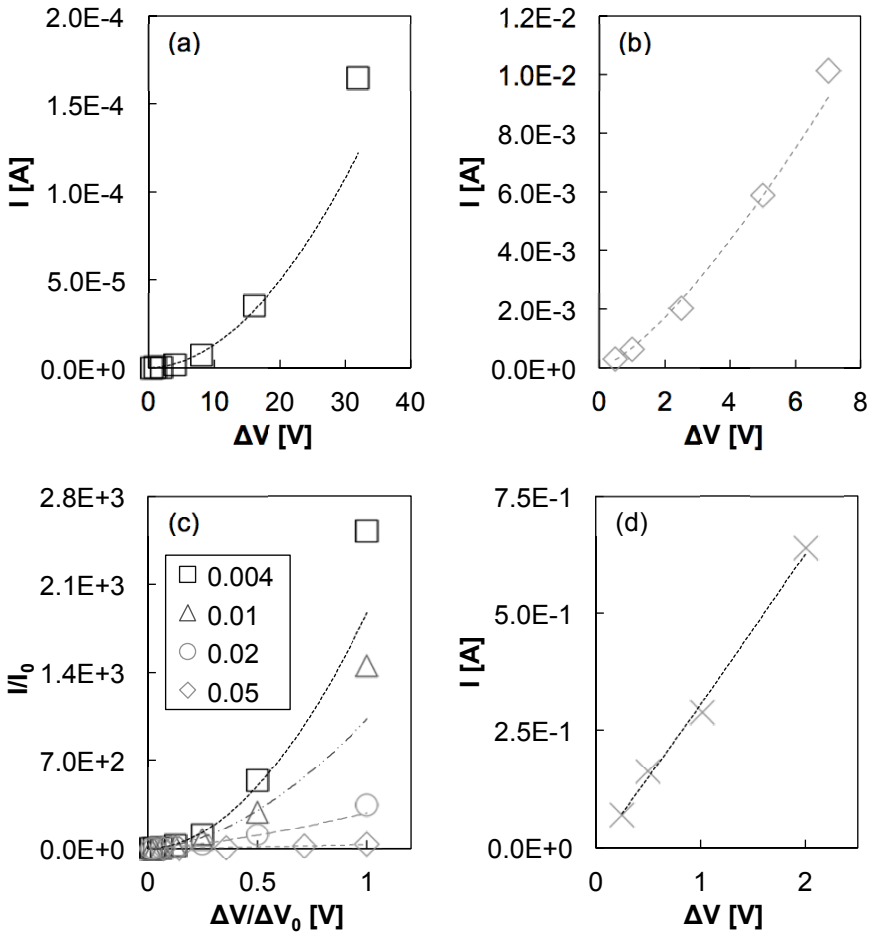

Figure 3.15. Current-voltage (IV) behaviour of MWCNT modified PDMS for particle mass fractions of (a) 0.004 and (b) 0.05, and (c) plot of normalized current vs. normalized electric potential difference for four particle mass fractions, where I_0 is the respective current measured at 0.5 V and ΔV_0 is the respective maximum voltage applied. (d) IV behaviour of a dry network of Baytubes C 150P, without PDMS. The dotted and dashed lines are trend lines for visual aid.

As shown by Dyre [178], and highlighted by Kilbride et al. [174], an approximate power law of the form of Equation 3.6, with $0.8 \leq r \leq 1.0$ is characteristic of hopping in a disordered material where hopping charge carriers are subject to spatially randomly varying energy barriers, and where the transport mechanism is probably quantum mechanical tunnelling. Accordingly, the finding that at low p the CNT network is characterized by $r = 0.81$ (cf. Figure 3.14) also indicates quantum mechanical tunnelling between adjacent but non-contacting CNTs within the electron-conducting paths.

From the above it follows that at low p the electrical characteristics of MWCNT modified PDMS are controlled by the behaviour of the individual electron-conducting paths, in which electron conduction is dominated by quantum mechanical tunnelling between adjacent but non-contacting CNTs, and that at high p the electrical characteristics of MWCNT modified PDMS are controlled by the behaviour of the network as a whole. The finding that the normalized increase in electrical conductivity with temperature is most pronounced at p close to p_c, and decreases with increasing p, affirms this picture (cf. Table 3.2). In this context It should be noted that the semiconducting behaviour in MWCNT modified PDMS is not due to the intrinsic properties of the constituent materials, but rather due to the fact that electron conduction within electron-conducting paths is dominated by the electron transfer mechanism at CNT to CNT junctions [157], i.e. quantum mechanical tunnelling, for the PDMS is electrically insulating and the electron-conducting network is likely not made up of individual MWCNTs, but small aggregates of MWCNT, in which current flow takes place predominately through the metallic MWCNTs [165].

The above picture of electron conduction in CNT modified polymers is reviewed in Chapter 4, where the electric response to uniaxial compression of MWCNT – PDMS nanocomposites is studied as a function of MWCNT mass fraction. Equation 3.4 predicts the interdependence between tunnelling probability and tunnelling gap width to be of exponential type. If mechanical deformation leads to an alteration of the average tunnelling gap width within the electron-conducting network, such an exponential relation might also be found between compressive strain and sample resistance, and should then become quite clear as p approaches p_c from above.

3.4.6 Influence of the electrode system

The evolution of the electrical conductivity of MWCNT – PDMS nanocomposites with MWCNT mass fraction has been measured with two different electrode systems, namely with a resistivity test fixture with conductive rubber pad electrodes and with an electronic circuit using conductive silver paint electrodes (cf. Section 3.3.3); the results are given in Figure 3.11.

Overall, σ values are higher if the material is contacted by conductive silver paint electrodes. At $p < p_c$, the σ values obtained by the two set-ups differ by a factor of about 20, which is likely due to a difference in the degree to which the results are affected by background currents and drifts. High resistance low current measurements are highly sensitive to background currents, which can be produced by many different phenomena (e.g., piezoelectric effects, temperature induced pole relaxation, discharging of capacitive elements, etc.), and which depend on the specifics of the measuring technique. At $p > p_c$,

background currents can be neglected. The σ values obtained by the two set-ups are close and in average differ by a factor of only 2.5. There are likely two sources for this difference. First, due to variations in sample thickness and the rubbery nature of both the conductive rubber pad electrodes and the samples being tested, it was nearly impossible to get two electrode to sample interfaces free of entrapped air. This can exemplarily been seen in Figure 3.6, were the 0.1 wt.% sample appears darker in areas where air is trapped between sample and support. Air entrapments in the electrode to sample interface reduce the effective electrode area; consequently, A of Equation 3.1 might overestimate the effective electrode area; hence σ might be underestimated. In the case of silver paint electrodes, on the other hand, air entrapment can effectively be prevented as the electrodes are painted onto the sample and form a continuous, pore-free film when dried. Second, the resistivity test fixture applies a considerable compressive force on the sample being tested, whereas in the case of the electronic circuit using conductive silver paint electrodes no compressive force is applied. As will be shown in Chapters 4 and 5, uniaxial compression of high aspect ratio particle modified polymers causes an increase in sample electrical resistance and, hence, a decrease in σ.

Despite the difference in σ values obtained by the two experimental set-ups, the electrical percolation parameters, which describe the configuration of the percolated MWCNT network, are congruent. From Table 3.1 it can be seen that p_c and t values vary by less than 3 % and 1 %, respectively (the small difference is likely due to the difference in compressive force applied during testing, cf. Chapter 5). Consequently, while electrical

conductivity values do depend on the specifics of the electrode system (e.g., contact resistance between electrodes and sample), the percolation parameters do not.

3.5 Summary and Conclusions

In the present chapter, electron conduction in MWCNT modified PDMS was studied by measuring and analysing electrical properties of MWCNT – PDMS nanocomposites as a function of particle mass fraction.

The electrical conductivity of MWCNT – PDMS nanocomposites increases with particle mass fraction, exhibiting a sudden transition from electrically insulating ($\sigma \leq 10^{-12}$ S/m at $p \leq 0.003$) to conducting ($\sigma \approx 10^{-2}$ S/m at $p = 0.05$), which is well described by percolation theory. Percolation threshold and conductivity exponent, obtained on up to 1 mm thick disc samples produced by solution casting, were $p_c \approx 0.0031$ and $t \approx 2.2$, respectively, which is in line with the majority of the data reported in literature on CNT modified polymers in general. Both the electrical conductivity and the percolation parameters have been analyzed with two different electrode systems, namely a resistivity test fixture with conductive rubber pad electrodes and an electric circuit using conductive silver paint electrodes. It is shown that while the magnitude of the electrical conductivity does depend on the specifics of the electrode system, the percolation parameters do not. This is significant as it helps understand to what expend data obtained with different measuring set-ups are comparable.

A simple measuring technique was developed to measure the electrical conductivity of a lose MWCNT network without PDMS. The latter gives an estimate of the maximum

electrical conductivity that can be achieved by adding MWCNTs to PDMS and, for the system studied here, was found to be $\sigma \approx 2$ S/m.

A study of both the frequency and temperature dependence of the electrical conductivity at particle mass fractions above the percolation threshold revealed semiconducting material characteristics. The current voltage behaviour was found to be of non-ohmic type and the ac-exponent at low particle mass fraction was found to be in the range $0.8 \leq r \leq 1.0$, thus indicating a dominant role of quantum mechanical tunnelling between adjacent but non-contacting CNTs within the electron-conducting network. This is supported by the fact that the conductivity exponent is nonuniversal, i.e. $t \neq 2$. Both the frequency and the temperature dependence of the electrical conductivity as well as the nonlinearity of the current voltage curves were found to decrease with increasing particle mass fraction. It thus follows that at particle mass fractions close to the percolation threshold the electrical behaviour of MWCNT modified PDMS is dominated by the characteristics of individual electron-conducting paths, in which electron conduction is controlled by quantum mechanical tunnelling between adjacent but non-contacting CNTs, and that at high particle mass fractions the electrical behaviour of MWCNT modified PDMS are dominated by the characteristics of the network as a whole, despite quantum mechanical tunnelling events within the individual electron-conducting paths.

CHAPTER 4

A Study of the Electric Response to Mechanical Deformation of MWCNT – PDMS Nanocomposites

---

Published in Materials Research Society Symposium Proceedings – MRS Proceedings 2012, 1410. DOI: 10.1557/opl.2012.856.

4.1 Introduction

The main determinant for the electrical properties of CNT – polymer nanocomposites is the configuration of the percolated particle network. Electrical properties of as produced CNT – polymer nanocomposites have been measured and analysed in Chapter 3. A logical next step towards a more complete understanding of electron conduction in CNT modified polymers, is to study the electric response to configurational changes within the particle network, i.e., the electric response to mechanical deformation of bulk CNT – polymer nanocomposites.

Compared to the body of literature on CNT – polymer nanocomposites in general, studies of the electric response to mechanical deformation are quite scarce. The fact that more than half of the publications have become available in the course of this dissertation research, however, points to the fact the that there is an increasing research interest. In the relevant literature the electric response to mechanical deformation is studied in

uniaxial tension [160, 180-189] and compression [87-89, 159, 185, 190-192] tests, as well as in flexural tests [193-197].

Uniaxial tension on CNT – polymer nanocomposites generally leads to an increase in electrical resistance. As discussed in Chapters 3, electron conduction through the percolated CNT network is limited by the contact resistance between neighbouring CNTs. This contact resistance is a function of interparticle separation, and is dominated by quantum mechanical tunnelling through insulating polymer layers. Accordingly, the positive interdependence of electrical resistance and uniaxial tension can be explained with a change in mean interparticle separation: as the particle network is stretched, the mean interparticle separation increases, and so does the overall electrical resistance.

The electric response to uniaxial compression, on the other hand, is less clear, as the interdependence of electrical resistance and uniaxial compression has been reported to be positive [87, 88, 159, 190-192] in some cases, but negative [89, 185] in others. There seems to be no evident dependence on the type of constituent materials; for MWCNT modified PDMS, for example, the electrical resistance has been measured to both increase [87, 88] and decrease [89] with uniaxial compression. Taking up the above argument, upon uniaxial compression, i.e., as the volume occupied by the CNT network is reduced, it would seem evident that the mean interparticle separation, and hence the overall electrical resistance, decrease. The majority of the published work, however, measured an increase in electrical resistance with increasing uniaxial compression.

In flexural test, the electric response to mechanical deformation strongly depends on the specifics of the test (e.g., measurement on the side under compression vs.

measurement on the side under tension, or freestanding beam vs. surface attached thin film), and both positive and negative interdependences of electrical resistance and mechanical deformation have been found.

The common ground in all reports is that the material reacts to changing external conditions, i.e., the electrical resistance of CNT modified polymers changes with mechanical deformation of the material, which makes CNT – polymer nanocomposites interesting with regard to implementation as functional materials in stress/strain sensing applications. A targeted use as functional materials requires an understanding of, first, electron conduction through the percolated particle network, and, second, the electric response to mechanical deformation. However, as outlined above, conclusions drawn from relevant work in literature are inconsistent and not generally applicable.

4.2 Research Objective

The goal of this chapter is to gain further insight into electron conduction in CNT modified polymers, and therewith to contribute to an understanding of the electric response to mechanical deformation of CNT – polymer nanocomposites. First, the electric response to uniaxial compression of MWCNT – PDMS nanocomposites is studied as a function of particle mass fraction. Then, the result is compared to data from the literature, and the conflicting results in literature are discussed. Finally, the use of electroconductive polymer nanocomposites as functional materials in stress/strain sensing applications is discussed.

4.3 Materials and Methods

The test method used to study the electric response to mechanical deformation was uniaxial compression. This allowed the external stimuli to be uniformly applied in parallel with the electrical current, which facilitates a correlation between the applied mechanical deformation and the resulting change in CNT network configuration, and hence the electric response. Enabling significant elastic deformation of CNT – polymer nanocomposite test specimens, required a matrix material with a low Young's modulus (e.g., PDMS). As mentioned in the introduction, the characteristics of the CNTs play a minor role, and have no phenomenological influence on the electric response to mechanical deformation.

4.3.1 Materials

PDMS (Gelest OE41) was purchased from Gelest, Inc. and MWCNTs (Baytubes C 150 P) were obtained from Bayer MaterialScience LLC. Both constituent materials are described in detail in Chapter 3.3.1.

4.3.2 Sample preparation

Preparation of MWCNT in PDMS suspensions with varying MWCNT mass fraction is described in detail in Chapter 3.3.2. Cube samples with MWCNT concentrations up to 2.0 wt.% were manufactured by solution casting of the MWCNT in PDMS suspensions into SU-8 coated aluminum moulds, followed by thermal curing in an air-circulating oven. The cube edges were 10 mm in length. A picture of both the mould and MWCNT –

PDMS nanocomposite cube samples is shown in Figure 4.1. As for the thin film samples, an electron-microscopical analysis of the cube samples indicated a percolated CNT network, with interconnected CNTs and or agglomerates of CNTs (cf. Figure 3.7).

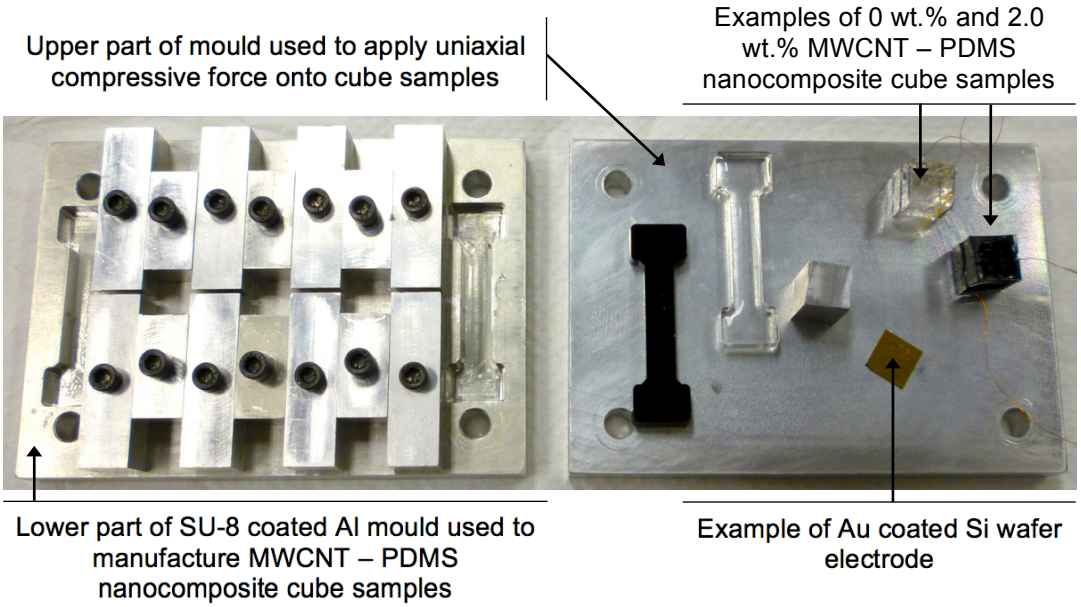

Figure 4.1. Photo showing the SU-8 coated aluminum mould used to manufacture and test MWCNT – PDMS nanocomposite cube samples, and two cube samples, with 0 wt.% and 2.0 wt.% MWCNT, respectively.

The cube samples were contacted on opposite sides with gold-coated silicon wafer electrodes that were contacted by Kapton insulated silver plated copper wires using conductive silver paint. The sample – electrode interface is a critical element in analysing the electric response to mechanical deformation of a material, as any change to area and or quality of the electrical contact, due to mechanical deformation of the material during testing, needs to be minimized. Here, the effective contact area was kept constant by

applying the compressive load and the electrical current in parallel, and the initial contact quality was optimized by mounting the electrodes on opposite sides in the mould, such that the PDMS cured directly onto the electrodes.

4.3.3 Measuring the electric response to mechanical deformation

Uniaxial compression was applied using an electromechanical testing system (MTS Insight 5, MTS Systems Corp.), and the electrical resistance was obtained simultaneously using a high resistance meter (Model 6517A, Keithley Instruments Inc.). To minimize the effect of mechanical deformation of the material on the electrical contact between material and electrodes, first the applied compressive load and electrical current were in parallel, i.e., the load was applied onto the electrodes, such that the effective contact area remained constant, and, second, a 0.11 pre-strain was applied to further improve the initial contact quality. A picture of the experimental set-up, together with a schematic representation, is shown in Figure 4.2. The applied crosshead displacement rate was 0.5 mm/min, and the DC voltage was 10 V. All measurements were taken at room temperature. The resistance was calculated from the applied voltage and the measured current, and the compressive strain was obtained by dividing the applied crosshead displacement of the electromechanical testing system by the initial edge length of the sample. As an example, Figure 4.3 shows the simultaneously recorded absolute crosshead displacement, d_c, compressive force, F_c, and electrical current, I, and the calculated electrical resistance, R.

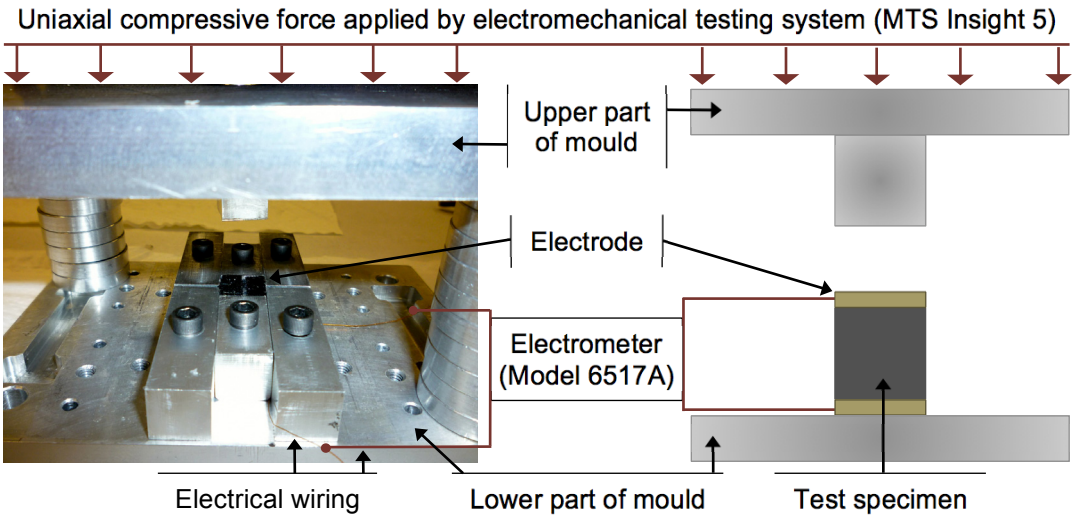

Figure 4.2. Picture and schematic representation of experimental set-up used to study the electric response to uniaxial compression of MWCNT – PDMS nanocomposite test specimens. The set-up allows for constrained and unconstrained uniaxial compression testing. The data reported in this thesis were obtained in the unconstrained mode, for which the fixation surrounding the sample (used for sample manufacturing) was removed. Upper and lower parts of the mould were mounted onto the electromechanical testing system. For electrical insulation, the aluminum mould was SU-8 coated and the silver plated copper wires were Kapton insulated.

Fife or more samples per concentration were manufactured. For the applied compressive strain range, the test – retest variability on different samples is shown in Figure 4.4. The presentation of the results in terms of a normalized electrical resistance, R/R_0, vs. compressive strain, ε_c, plot will be discussed in Chapter 4.4. The test – retest variability on one and the same sample was better. Interestingly, the test – retest variability improves as the CNT mass fraction increases. This is likely related to the number of electron-conducting paths within the CNT network, which increases with

increasing CNT content. The smaller that number the paths, the bigger the influences of small differences between CNT networks in different samples, and vice versa. The reported data in Chapters 4.4 and 5 are average values or 'best case results'.

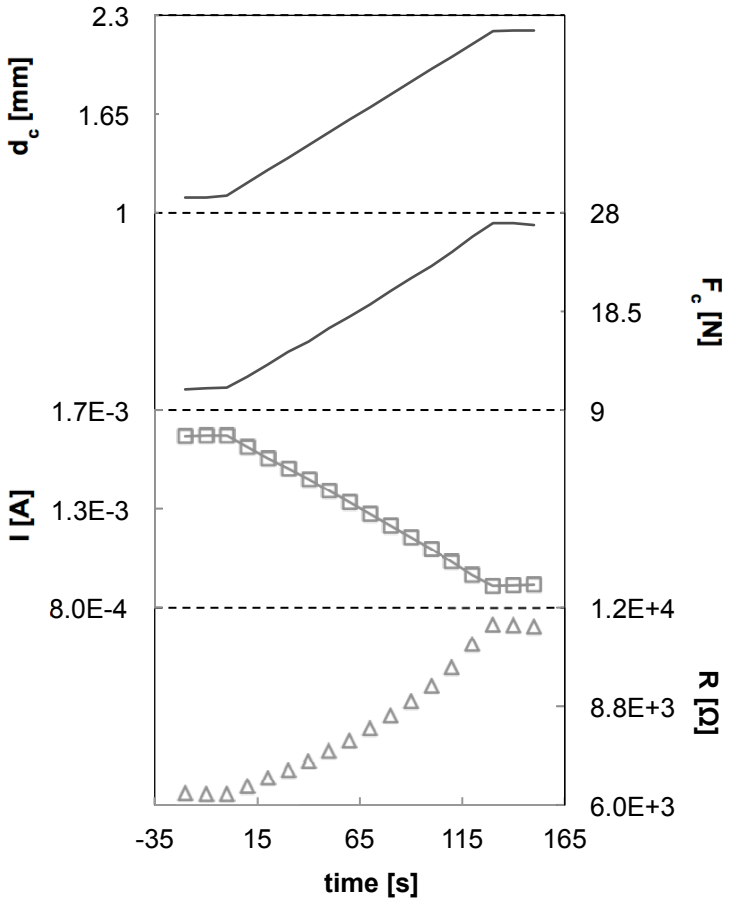

Figure 4.3. Example of data recording: applied absolute crosshead displacement, d_c, required compressive force, F_c, measured electrical current, I, and calculated electrical resistance, R. The test specimen was a 2.0 wt.% MWCNT – PDMS nanocomposite.

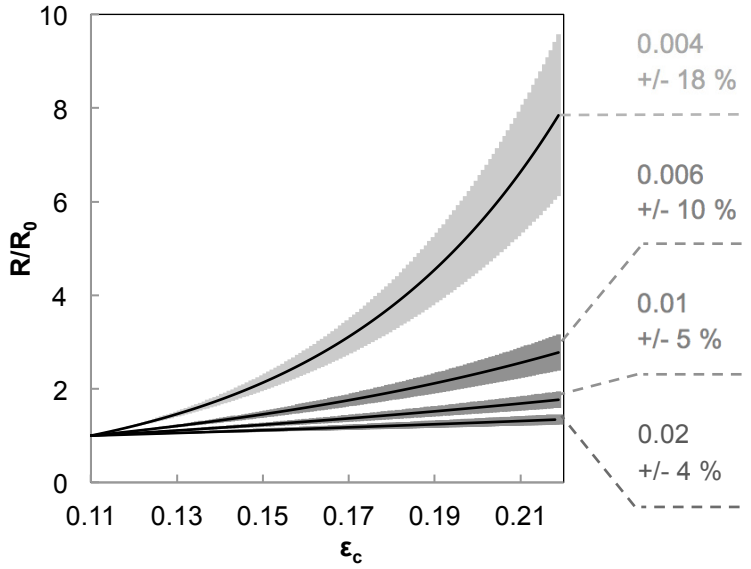

Figure 4.4. Test – retest variability on different samples as a function of MWCNT mass fraction (indicated on the right). Test – retest variability on one and the same sample was better.

4.4 Results and Discussion

The DC volume conductivity of the MWCNT – PDMS nanocomposite as a function of particle content was evaluated in Chapter 3: the electrical conductivity scales positively with MWCNT concentration, shows a sudden transition from a non-conducting to a conducting regime at a percolation threshold of around 0.003, and increases relatively moderately at high particle content.

4.4.1 Electric response to uniaxial compression of MWCNT – PDMS nanocomposites

The measured electric response to uniaxial compression of MWCNT – PDMS nanocomposites is shown in Figure 4.5, where the electrical current is plotted as a function of absolute crosshead displacement of the electromechanical testing system, for

a CNT mass fraction, p, close to the percolation threshold, i.e., p = 0.004, a high CNT mass fraction, i.e., p = 0.02, as well as two CNT mass fractions in between, i.e., p = 0.006 and p = 0.01. The corresponding calculated variation in normalized electrical resistance, R/R_0, with compressive strain, ε_c, is plotted in Figure 4.6. As the material is uniaxially compressed, the characteristics of the particle network are altered such that current flow is continuously impeded, and the electrical resistance increases with increasing mechanical deformation. The positive interdependence of R and ε_c is particle concentration dependent and more pronounced at lower particle mass fraction. In addition, this interdependence appears to be exponential in type.

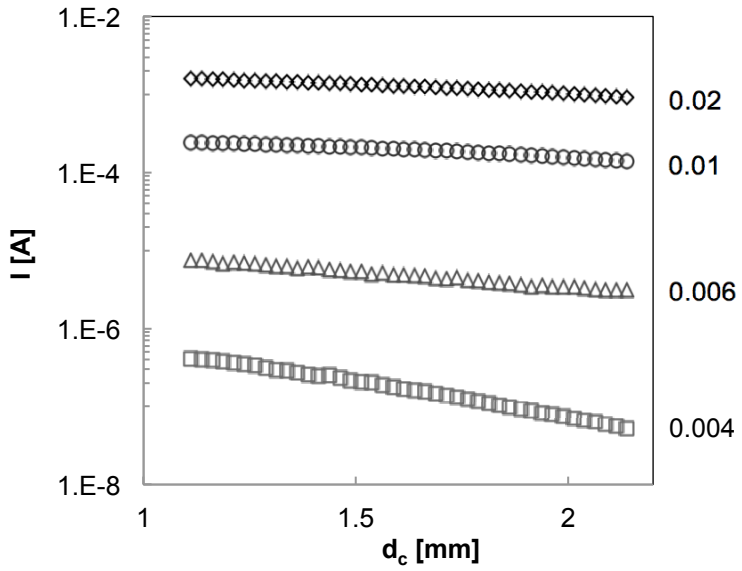

Figure 4.5. Semilogarithmic plot of change in electrical current, I, with crosshead displacement, d_c, measured at 10 V on PDMS – MWCNT cube samples with varying MWCNT mass fraction (indicated on the right)).

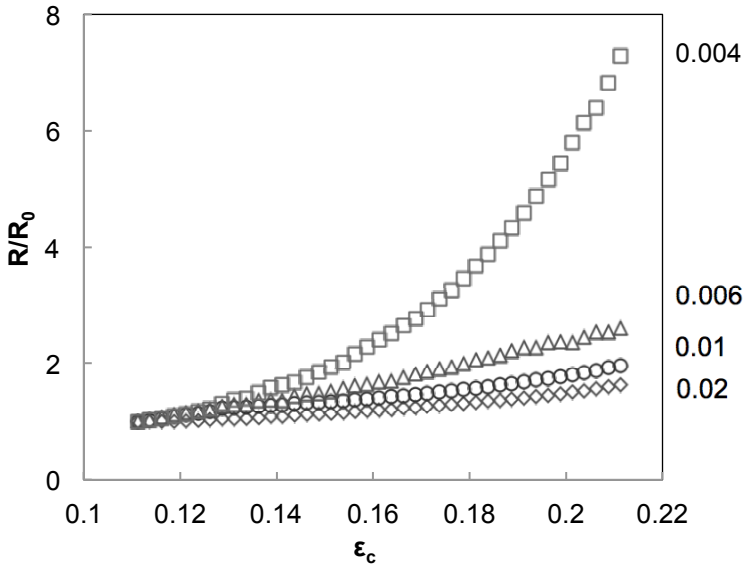

Figure 4.6. Variation in normalized electrical resistance, R/R_0, with uniaxial compressive strain, ε_c, of MWCNT – PDMS nanocomposites with varying MWCNT mass fraction (indicated on the right), R_0 being the resistance obtained at $\varepsilon_c = 0.11$.

The electrical resistance of a test specimen generally depends on its geometry and on the electrical resistivity, ρ, of the material and can be expressed as:

$$R = \rho \frac{l}{A}, \tag{4.1}$$

where l and A are the specimen thickness and cross-sectional area, respectively. In metallic foil strain gauges, for example, the resistance change with mechanical deformation is mostly due to changes in thickness and cross-sectional area of the metallic foil [198, 199]. In semiconductor strain gauges, on the other hand, the resistance change is typically dominated by a change in the electrical resistivity of the semiconducting strain gauge material, where strain induced changes in inter-atomic spacing affect the bandgap structure, and hence the probability for an electron to be raised into the

conduction band [200, 201]. During uniaxial compression of a MWCNT – PDMS test specimen, A is given by the size of the electrodes (cf. Figures 4.2 and 5.4) and remains unchanged, l, on the other hand, is decreased; hence, the geometrical factor in Equation 4.1 decreases with increasing ε_c. If ρ remained unchanged, an increase in ε_c would therefore lead to a decrease in R. In Figure 4.6, however, the opposite is observed; hence, the electrical resistivity of the material changes with compressive strain. MWCNT – PDMS nanocomposites therefore are piezoresistive materials.

Given the insulating nature of PDMS ($\sigma < 10^{-12}$ S/m, cf. Chapter 3.4.2), electron conduction is limited to the MWCNT network. The overall resistance change can thus be associated with a change in electrical resistance of the CNT network due to CNT deformation, on the one hand, and or changes in the CNT network configuration (e.g., change in average value and distribution of the interparticle contact resistances, or a change in the number of electron-conducting paths within the CNT network), on the other hand. In this regard Oliva-Aviles et al. [202] have investigated the contribution of CNT deformation to the piezoresistance of a CNT – polymer nanocomposite, and found that it is marginal, and that the overall electric response to mechanical deformation is dominated by changes in the configuration of the CNT network. The electric response to mechanical deformation of MWCNT – PDMS nanocomposites might thus be compared to the one in semiconductor strain gauges, in the sense that the resistance change is also dominated by a change in the electrical resistivity of the material, where the strain induced changes to the particle network affect the inter-particle spacing, and hence the probability for an electron to pass from one particle to an adjacent one.

In Chapter 3, electron conduction in MWCNT modified PDMS was found to be dominated by quantum mechanical tunnelling through insulating polymer layers between adjacent but non-contacting CNTs. The exponential relation between R and ε_c further evidences this. As emphasized in Figures 4.7 (a – c), where the electric response to uniaxial compression is presented in a R vs. ε_c plot, for a high MWCNT mass fraction, i.e., p = 0.02, a low MWCNT mass fraction, i.e., p = 0.004, and a MWCNT mass fraction just above the percolation threshold, the exponential behaviour is universal, but increasingly pronounced the closer p to p_c. The coefficient of determination, R^2, of an exponential fit to the data points is $R^2 \geq 0.99$ for both p = 0.02 and $0.003 < p < 0.004$; for a linear fit do the data points, however $R^2 = 0.97$ for p = 0.02 but $R^2 = 0.82$ for $0.003 < p < 0.004$. This might be interpreted as discussed in the following two paragraphs.

At p just above p_c, the number of electron-conducting paths within the CNT network is small, and the electric response to mechanical deformation is dominated by the resistance change within a path (cf. Figure 4.8 a). The resistance of a path is controlled by the contact resistance of non-contact CNT – CNT junctions, where electrons pass from one CNT to an adjacent one via quantum mechanical tunnelling. The interdependence between tunnelling probability and tunnelling gap width is exponential in type (cf. Equation 3.4). Hence, a strain induced alteration of the tunnelling gap width in CNT – CNT junctions within an electron-conducting path leads to an exponential change in the corresponding contact resistances, thus explaining the overall exponential change of R with ε_c at low p.

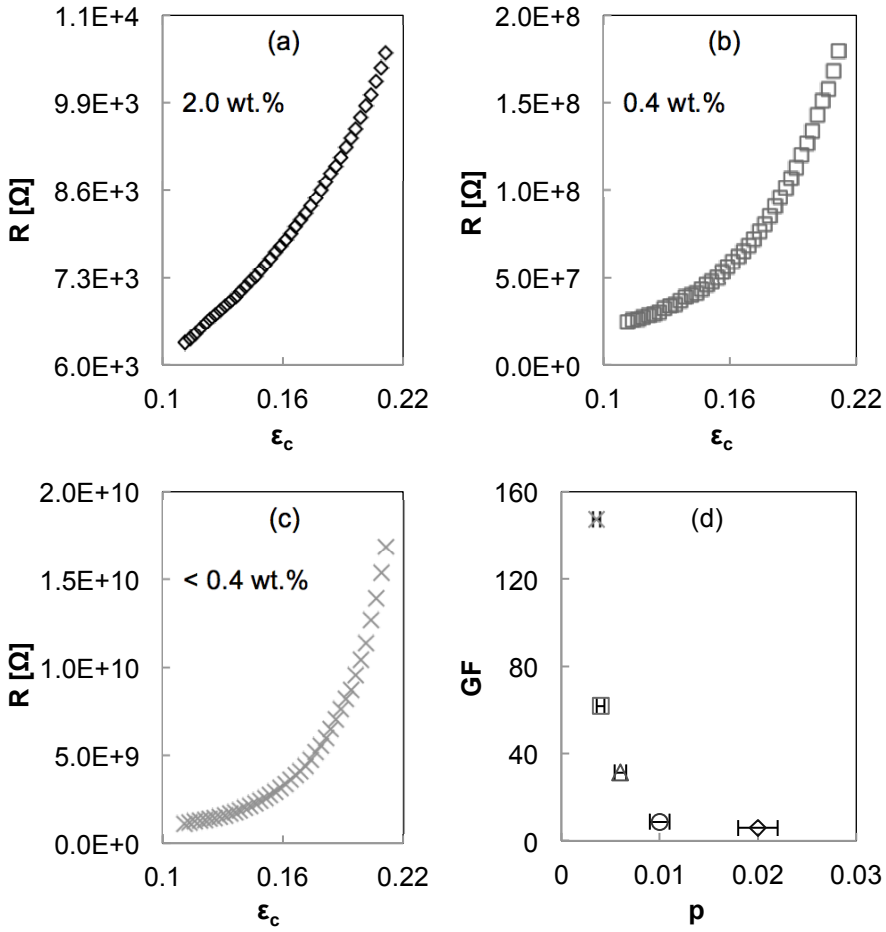

Figure 4.7. Resistance change with uniaxial compression of MWCNT – PDMS nanocomposites, at varying CNT mass fraction: (a) 0.02, (b) 0.004, and (c) just above the percolation threshold. (d) Gauge factor of MWCNT – PDMS nanocomposites as a function of CNT mass fraction.

At $p >> p_c$, the number of electron-conducting paths within the CNT network is much higher (cf. Figure 4.8 b), and the electric response to mechanical deformation is dominated by the resistance change of the CNT network as a whole. The CNT network

can be viewed as a resistor network, with electron-conducting paths of resistance R_p connected in parallel. The resistance of the network, R_n, can then be expressed as:

$$\frac{1}{R_n} = \sum_i^N \frac{1}{R_{p,i}}, \tag{4.2}$$

where N is the total number of electron-conducting paths. If R_p is assumed to be the same for all paths, Equation 4.2 can be rewritten as:

$$R_n = \frac{R_p}{N}, \tag{4.3}$$

where it is made explicit that R_n depends linearly on N. A strain induced alteration of the tunnelling gap width in CNT – CNT junctions leads to an exponential change in R_p, on the one hand, and to a breakup of electron-conducting paths, or to the creation of new ones, on the other hand. As N varies continuously with applied mechanical deformation to the CNT network, R_n varies linearly with N, thus explaining the more linear character of the electric response to ε_c at high p.

Accordingly, with respect to the positive interdependence of R and ε_c (cf. Figure 4.6), uniaxial compression of MWCNT – PDMS nanocomposites leads to an increase in CNT – CNT separation such that R_p increases, i.e., the resistance of the electron-conducting paths increase with mechanical deformation, and N decreases, i.e., electron-conducting paths are continuously broken up. It is worth noting that this is somewhat unobvious. Upon uniaxial compression, the volume occupied by the CNT network is reduced and a decrease in mean interparticle distance, and hence a decrease in R_p, and an increase in N, might seem more intuitive. This will be further discussed in Chapter 5.

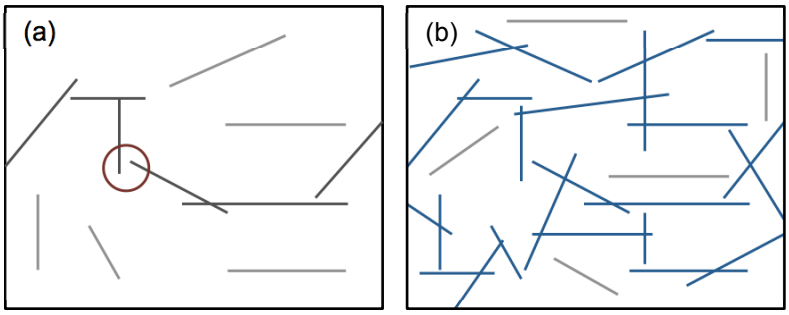

Figure 4.8. Schematic illustrating a CNT network at (a) p close to p_c, and (b) p >> p_c. Black lines in (a) and blue lines in (b) represent CNTs which are part of the electron-conducting network, grey lines in (a) and (b) represent CNTs which are not part of the electron conducting network. The red circle in (a) highlights the CNT – CNT junction with the highest local resistance within the electron-conducting path.

4.4.2 Piezoresistance in polymer nanocomposites with high aspect ratio particles

The result presented in the previous section is in line with the majority of the data from the literature on polymer nanocomposites with CNTs [87, 88, 159, 190-192] and high aspect ratio particles (e.g., graphene or high structure carbon black) in general [203-205]. The exceptions are [185] and [89]. In MWCNT – PDMS and MWCNT – polyethylene (PE) nanocomposites, and for particle concentrations varying from 3.0 to 6.0 wt.%, Rizvi et al. [89] found the resistance to decrease with increasing applied stress, i.e., increasing compressive strain. The reported percolation thresholds for the MWCNT – PDMS and the MWCNT – PE systems are 0.03 and 0.022, respectively, values that are 20 to 30 times higher than what is typically observed in CNT – polymer nanocomposites [26], and comparable to percolation thresholds typically observed in low aspect ratio particle based polymer nanocomposites (e.g., low structure carbon black – polymer nanocomposites [206, 207]). These high percolation thresholds indicate extremely poor

particle dispersion with relatively large MWCNT agglomerates. In terms of electric response to mechanical deformation, the two material systems therefore should be regarded as low aspect ratio particle based polymer nanocomposites, for which the electrical resistance typically decreases with increasing compressive strain [208-212]. Kang et al. [185] characterized SWCNT – polyimide (PI) nanocomposites, and, at a SWCNT concentration of 0.05 wt.%, found the interdependence of electrical resistance and compressive strain to be negative. Tests were performed on 50 μm thin film samples. As reported by some of the co-authors in an earlier paper [213], individual SWCNTs were 3 μm long and agglomerated into bundles, which formed micrometer scale agglomerates. Given the low ratio of agglomerate size to sample thickness, it is likely that reorientation, reshaping, and relative movement of the agglomerates within the polymer matrix is restricted. The reported electric response to uniaxial compression therefore can not be viewed as that of bulk SWCNT – PI nanocomposites, but rather of a designed SWCNT – PI system, namely of a SWCNT – PI nanocomposite thin film with oriented agglomerates of SWCNT. Given the relatively small deformation, i.e., up to ε_c = 0.0017, and the fact that no pre-strain was applied, it is also possible that the measured decrease in electrical resistance is due to a decrease in contact resistance between electrodes and samples.

Based on the results presented in Chapter 4.4.1, and on the above discussion of the conflicting results in literature, it can be concluded that high aspect ratio particle based bulk polymer nanocomposites are piezoresistive materials, exhibiting a positive interdependence between electrical resistance and compressive strain. This is in contrast

to low aspect ratio particle based bulk polymer nanocomposites, for which the interdependence between electrical resistance and strain is typically positive in tension [186, 189, 214], but negative in compression [208-212]. The piezoresistive effect in polymer nanocomposites, and in polymer nanocomposites with high aspect ratio particles in particular, will be discussed in detail in Chapter 5.

As outlined in the introduction, the electric response to mechanical deformation has also been measured in flexural tests. In contrast to uniaxial tension and compression tests, however, flexural mechanical deformation parallel to the electrical current is non-uniform, and a correlation between mechanical deformation and electric response therefore is non-trivial. In a simple 4-point beam-bending test (cf. [197]), for example, one side of the beam will be under tension whereas the opposite side will be under compression. By measuring the current on the compressive side, it cannot be concluded that the measured electric response to mechanical deformation is characteristic to the test-material under compression, as paths of low resistance to electrical current might pass through the sample half under tension. Other work reports on the electric response to mechanical deformation of specifically designed high aspect ratio particle based architectures in polymer matrices (e.g., CNT film attached to polymer substrate [215], CNT films layered with thin films of pure polymer [216], foams [217], or more advanced architectures [39, 218]). The measured electric response to mechanical deformation in these cases is a function of the specifics of the respective design, and, thus, not representative for the corresponding bulk particle – polymer nanocomposite. It should be

noted that data reported in [193-197] and [39, 215-218], and related work, has therefore not been included in the above considerations.

4.4.3 Application as a piezoresistive sensing material

The piezoresistive character of MWCNT modified PDMS, and CNT – polymer nanocomposites in general, makes them interesting candidates as functional materials in stress/strain sensing applications. On the one hand, CNT – polymer nanocomposites can be employed in applications where the polymeric characters of the material (e.g., transparency and or flexibility) are key requirements, as, for example, in flexible tactile sensors [8], or where polymers are generally preferred to metals or ceramics for others reasons, such as weight savings, cost savings, ease of fabrication or biocompatibility. On the other hand, as will be discussed below, CNT – polymer nanocomposites are interesting because of a potentially very high, and, most notably, tunable Gauge factor.

The piezoresistive strain coefficient of a material, i.e., its Gauge factor, GF, can be determined by dividing the fractional change in resistance by the corresponding applied compressive strain:

$$GF = \frac{\Delta R}{R_0 \varepsilon_c}, \tag{4.4}$$

where R_0 is the reference resistance. For the MWCNT – PDMS nanocomposite studied here, the variation of the piezoresistive strain coefficient with MWCNT mass fraction is shown in Figure 4.7 (d), where R_0 is the resistance at $\varepsilon_c = 0.11$. As can be seen, GF decreases by one order of magnitude as the MWCNT mass fraction is increased from p =

0.004 to p = 0.02. At high p, and for small Δp, GF can be considered constant. At low p, in contrast, GF varies strongly with p and can reach values of 150 and more for p just above p_c. By comparison, metallic foil strain gauges typically have GFs between 2 to 5 [198], and silicon based semiconductor strain gauges can have GFs as high as 200 [219], but usually have GFs between 50 and 100 [220]. The high piezoresistive strain coefficients in MWCNT modified PDMS are due to the piezoresistive character of the material, and the exponential interdependence of electrical resistance and compressive stain.

It should be noted that the higher the strain – sensitivity of the material, the more demanding the technical requirements to read the electric response to mechanical deformation. For the results presented here, at 10 V the ratio of I at $\varepsilon_c = 0.22$ to I at $\varepsilon_c = 0.11$ is 17 at p just above p_c, but only 1.7 at p = 0.02. In addition, at p close to p_c, I is in the nA – range, whereas at p = 0.02 I is 6 orders of magnitude higher. The electronic circuit accessing at highly strain – sensitive MWCNT – PDMS nanocomposites with p close to p_c needs to be able to track currents in the nA range and current variations in the 10^{-10} to 10^{-11} A range, whereas the requirements for the electronic circuit accessing a MWCNT – PDMS nanocomposites with high p are less demanding, as it needs to be able to track currents in the mA range and current variations in the 10^{-4} A range only.

In this context it is interesting to note that at $\varepsilon_c = 0.22$, the applied pressure, calculated by dividing the applied compressive force (cf. Figure 4.3) by the cross-sectional area of the test sample, is less than 0.3 MPa for all MWCNT concentrations, which is within the

finger-pressure range, cf. [204], and thus makes the studied MWCNT – PDMS nanocomposites interesting for tactile sensing applications.

4.5 Summary and Conclusions

With the goal of gaining further insight into electron conduction in CNT – polymer nanocomposites, and to contribute to an understanding of the electric response to mechanical deformation in bulk CNT – polymer nanocomposites, the present chapter measured and analyzed the electric response to uniaxial compression of MWCNT modified PDMS as a function of CNT content.

The electrical resistance is found to increase with compressive strain. The interdependence between the two parameters is exponential in type, and shows a particle concentration dependent behaviour, with increasing strain-sensitivity for decreasing particle mass fraction. It is shown that bulk MWCNT modified PDMS, and high aspect ratio particle based polymer nanocomposites in general, are piezoresistive materials, showing positive interdependences between electrical resistance and compressive strain as well as between electrical resistance and tensile strain.

The exponential relation between electrical resistance and compressive strain supports the previous finding that electron conduction in bulk CNT modified polymers is dominated by quantum mechanical tunnelling through insulating polymer layers between adjacent but non-contacting CNTs. It is argued that at low CNT mass fractions, the electric response to mechanical deformation is dominated by the resistance change within electron-conducting paths, which is caused by strain induced alterations of the tunnelling

gap widths, and that at high CNT mass fractions, the electric response to mechanical deformation is dominated by the resistance change of the CNT network as a whole, which is caused by a strain induced alteration of the number of electron-conducting paths within the CNT network.

It is further shown that at CNT mass fractions close to the percolation threshold, MWCNT modified PDMS can exhibit piezoresistive strain coefficients as high as 150, and that the Gauge factor varies as a function of particle mass fraction, i.e., that it is tunable. This makes MWCNT modified PDMS, and CNT – polymer nanocomposites in general, interesting candidates as functional materials in stress/strain sensing applications where the polymeric characters of the material are key requirements, or where polymers are generally preferred to metals or ceramics.

CHAPTER 5

Piezoresistance in Polymer Nanocomposites with High Aspect Ratio Particles

Published in ACS Applied Materials & Interfaces –
ACS Applied Materials & Interfaces 2014, 6 (3). DOI: 10.1021/am404808u.

5.1 Introduction

As introduced in Chapter 2 and analyzed in Chapter 3, adding electrically conducting nanoparticles to polymers allows for the design of electroconductive polymer nanocomposites, where electron flow is enabled through the formation of a particle network throughout the polymer matrix. In Chapter 4, the characteristics of the particle network (e.g., the mean interparticle separation) and, consequently, the electrical conductivity of the material were found to change with mechanical deformation, which makes such nanocomposites piezoresistive materials.

Uniaxial tension on electroconductive polymer nanocomposites generally leads to an increase in electrical resistance [160, 180-186, 188, 189, 214], whereas the electric response to uniaxial compression seems to depend on particle shape: the electrical resistance typically decreases with compressive strain in the case of low aspect ratio particles (e.g., low structure carbon black and metal powder) [208-212, 221] but increases with compressive strain in the case of high aspect ratio particles (e.g., high structure carbon black agglomerates, carbon nanotubes and graphite nanosheets) (cf.

Chapter 4 and [87, 159, 190-192, 203-205, 214, 222]). In either case the piezoresistance strongly depends on particle concentration and increases with decreasing particle content (cf. Chapter 4 and [87, 183, 184, 192, 204, 210, 211]). The determinant for the overall electrical resistance in electroconductive polymer nanocomposites is the contact resistance between neighbouring particles within the conducting network, which in turn, is dominated by quantum mechanical tunnelling through insulating polymer layers (cf. Chapters 3), and so is a function of interparticle separation (cf. Equation 3.4). Accordingly, the positive interdependence of electrical resistance and uniaxial tension, as well as the negative interdependence of electrical resistance and uniaxial compression, can be explained with the change in mean interparticle separation: as the particle network is stretched, the overall electrical resistance increases because the mean interparticle separation is increased, and as the particle network is compressed the overall electrical resistance decreases because the mean interparticle separation is decreased. In both cases, the experimentally observed piezoresistance is found to be well described by models based on quantum mechanical tunnelling or thermal activation over barriers [182, 185, 186, 208, 210, 211, 214]. Such modeling, however, involves nontrivial parameters, namely, the height of the tunnelling potential barrier and the average initial interparticle separation, and generally is concentration specific, hence inapplicable to predicting the experimentally observed concentration dependence of the piezoresistance.

In contrast to the above, the positive interdependence of electrical resistance and uniaxial compression, as it is found in polymer nanocomposites with high aspect ratio particles, is not well understood. An increase in interparticle separation with uniaxial

compression of the particle network, i.e., as the occupied volume is reduced, seems unobvious. Oliva-Aviles et al. [202] have investigated the contribution of carbon nanotube deformation to the piezoresistance of a CNT – polymer nanocomposite and found that it is marginal and that the overall electric response to mechanical deformation is dominated by changes in the configuration of the CNT network. Accordingly, by considering the electrical resistance of the conducting particles as constant, it has been proposed that the piezoresistance in polymer nanocomposites with high aspect ratio particles can be explained by a combination of two distinct mechanisms, namely, a change in interparticle separation, and a change in the number of conducting paths within the particle network [192, 204, 208]. Quantum mechanical tunnelling based models, that have been extended to account for such changes in the number of conducting paths, were found to fit the electric response to uniaxial compression in well-defined systems [192, 204]; they remain, however, concentration specific and are not generally applicable.

In electroconductive polymer nanocomposites, the percolation threshold, i.e., the minimum particle concentration needed to form an electron-conducting network throughout the polymer matrix, is inversely proportional to the aspect ratio of the particles [26, 169]. With regard to applications as functional materials where the polymeric characteristics of the material, e.g., transparency and or flexibility, are key requirements (e.g., flexible tactile sensors [8]), high aspect ratio particle based polymer nanocomposites are therefore of particular interest, as the added properties, i.e., electrical conductivity and piezoresistance, can be obtained at much lower particle content. Thence, there is a clear need for a better understanding of the piezoresistance in such materials.

Moreover, as mentioned before, the piezoresistance of electroconductive polymer nanocomposites is tunable because it is concentration dependent. Having the capacity to predict this concentration dependence of the piezoresistance would be highly instrumental in the selection of functional materials for piezoresistive sensing applications.

5.2 Research Objective

This chapter addresses the problem of positive vs. negative piezoresistance in uniaxially strained polymer nanocomposites with high aspect ratio particles, and aims to provide new insight into piezoresistance in polymer nanocomposites in general. A percolation theory based model relating the variation in electrical resistance to compressive strain is developed and applied to the piezoresistance characterization of a CNT based polymer nanocomposite, as well as to related data from the literature on CNT, graphene, and high structure carbon black based polymer nanocomposites. It is then shown why current theories fail to generally describe the experimental findings and the electric response to compressive and tensile deformation of both high aspect ratio particle and low aspect ratio particle based polymer nanocomposites is discussed.

5.3 Theoretical Basis and Model

The overall electrical conductance, G, of an electroconductive polymer nanocomposite scales positively with the fractional particle content, p, and for $p > p_c$ typically follows the power-law behaviour:

$$G \propto (p - p_c)^t, \tag{5.1}$$

where p_c is the percolation threshold, i.e., the particle concentration below which G vanishes, and t is the so-called conductivity exponent. For the case of direct contact between adjacent particles, classical percolation theory predicts the conductivity exponent to be universal, i.e., not dependent upon the nature of the particles and the configuration of the network, and solely dependent on the network dimensionality (e.g., t = 2 for all three-dimensional direct-contact networks) (cf. Chapter 3). By fitting Equation 5.1 to experimental results, many bulk electroconductive polymer nanocomposites, however, are found to be characterized by nonuniversal conductivity exponents (cf. Figure 6.2 and [26, 170]). Studying this discrepancy between experimental data and available theories, Balberg proposed a tunnelling-percolation model [173], in which electron conduction through the percolating network is dominated by tunnelling between adjacent but non-contacting particles and identified quantum mechanical tunnelling as the potential origin of this nonuniversality. Experimental evidence for a determinant role of quantum mechanical tunnelling is found in both polymer nanocomposites with low aspect ratio particles [223] and polymer nanocomposites with high aspect ratio particles (cf. Chapters 3 and 4, and [146]), and on the basis of Balberg's work, it is now understood that the magnitude of the deviation from the universal value of t is governed by the distribution of local conductances [224-227].

The tunnelling probability and, so, the local conductance depend exponentially on interparticle separation. It therefore seems likely that, due to reorientation, reshaping, and relative movement of the particles, uniaxial compression of a polymer nanocomposite

with high aspect ratio particles will affect the local conductances, such that part of it increases, part of it remains unchanged, and part of it decreases, leading to a net broadening of the distribution of local conductances. Recently, Scardaci et al. [14] found the conductivity exponent of a high aspect ratio particle based polymer nanocomposite to scale linearly with network non-uniformity, suggesting higher t values for broader distributions of local conductances. Accordingly, it is assumed that uniaxially compressed bulk polymer nanocomposites with high aspect ratio particles are characterized by an increased conductivity exponent; hence that t scales positively with applied compressive strain, ε_c. It is therefore propose that t can be replaced by a compressive strain dependent conductivity exponent, t_c:

$$t_c(\varepsilon_c) = t_0(1 + c_p|\varepsilon_c|), \tag{5.2}$$

where $0 \leq |\varepsilon_c| \leq 1$, t_0 is the reference conductivity exponent characterizing the particle network at compressive strain ε_0 (typically $\varepsilon_0 = 0$), and c_p is a factor taking into account the concentration dependence of the influence of compressive strain on the distribution of local conductances. By inverting Equation 5.1 and replacing t by t_c given in Equation 5.2, one so obtains an expression for the compressive strain dependent overall electrical resistance of the material, R_c:

$$R_c(\varepsilon_c) \propto (p - p_c)^{-t_0(1+c_p|\varepsilon_c|)}. \tag{5.3}$$

As discussed before, the piezoresistance in polymer nanocomposites is concentration dependent and increases with decreasing particle content. It is therefore assumed that the influence of ε_c on the distribution of local conductances decreases as the number of local

conductors, i.e., two particles within the electron-conducting network close enough to allow for quantum mechanical tunnelling, increases; thence as the particle concentration increases it is highest at p close to p_c and decreases as $(p - p_c)$ increases. A simple expression for this is given by:

$$c_p = \frac{p_c}{p}. \tag{5.4}$$

Thus, by substituting the above expression in Equation 5.3, and normalizing $R_c(\varepsilon_c)$ to the reference electrical resistance at ε_0, $R_c(\varepsilon_0)$, the variation in normalized electrical resistance with uniaxial compression of a polymer nanocomposite with high aspect ratio particles, i.e., its piezoresistance, can conveniently be described as:

$$\frac{R_c(\varepsilon_c)}{R_c(\varepsilon_0)} = (p - p_c)^{t_0 \frac{p_c}{p}(|\varepsilon_0| - |\varepsilon_c|)}. \tag{5.5}$$

Prominent features of this model are that it captures the concentration dependence of the piezoresistance and that no assumptions need to be made with respect to the nature of the particles and or the configuration of the network, as both of them are described by parameters p_c and t_0, which are experimentally definable.

5.4 Results and Discussion

First, provided p_c and t_0 are known, Equation 5.5 enables one to evaluate the piezoresistance at any particle concentration of $p > p_c$. Second, given that parameters p_c and t_0 are specific to a particle network, Equation 5.5 should apply to any uniaxially compressed polymer nanocomposite with high aspect ratio particles. The underlying assumptions are that the particle network at ε_0 is indeed well characterized by the

parameters p_c and t_0 and that the evolution of the characteristics of the particle network, and, consequently, of the overall electrical resistance of the material, is captured by the strain dependence of the conductivity exponent. Next, the first point is studied by applying Equation 5.5 to the piezoresistance characterization of a high aspect ratio particle based polymer nanocomposite, where parameters p_c and t_0 are experimentally define, and the fit of the model at different particle concentrations is studied. The second point is then verified by applying the model to appropriate data from the literature on various polymer nanocomposites.

5.4.1 Predicting the concentration dependence of the piezoresistance

The high aspect ratio particle based electroconductive polymer nanocomposite studied herein is a multiwalled carbon nanotube modified polydimethylsiloxane. The details regarding constituent materials are given in Chapter 3.3.1. Figure 5.1 shows the electrical conductivity, σ, of the MWCNT – PDMS nanocomposite at eight different CNT mass fractions (empty symbols). The DC volume conductivity as a function of MWCNT content was evaluated on both thin film samples according to ASTM D257 (cf. Chapter 3.3.3) and cube samples at $\varepsilon_0 = 0.11$, using a high resistance meter with a DC voltage of 10 V. Cube sample manufacturing and electrical connection is described in Chapter 4.3.1, and the electrical characterization technique is detailed in Chapter 4.3.2. The results from the two test methods were in good agreement. As expected, the electrical conductivity scales positively with CNT concentration, showing a sudden transition from a non-conducting to a conducting regime, with a relatively moderate

increase at high CNT content. Parameters p_c and t_0 of Equation 5.5, characterizing the MWCNT network throughout the PDMS matrix at ε_0, are obtained by means of a logarithmic plot of σ vs. $(p - p_c)$ (cf. inset in Figure 5.1) where p_c is incrementally varied until the best linear fit of Equation 5.1 to the experimental data is obtained. Note that the power-law behaviour in Equation 5.1 also applies to the electrical conductivity, and that G is replaced by σ (cf. Equation 3.3).

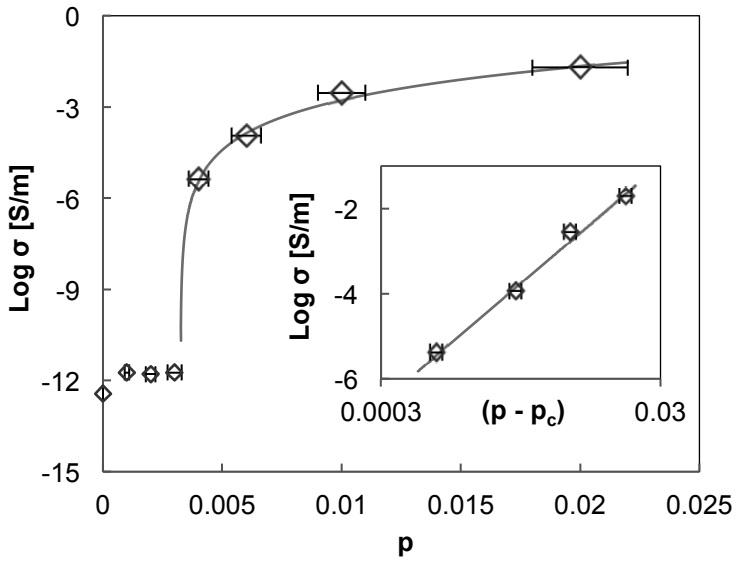

Figure 5.1. Semilogarithmic plot of measured (empty symbols) and calculated (solid line) change in electrical conductivity with MWCNT mass fraction, p. Reported σ values for $p \leq 0.003$ were obtained according to ASTM D257, and σ values for $p \geq 0.004$ were obtained on cube samples at the reference point, i.e., at $\varepsilon_0 = 0.11$, taking into account the corresponding sample dimensions. Inset: logarithmic plot of σ vs. $(p - p_c)$ showing the best fit of Equation 5.1 to the experimental data.

For the system at hand, the parameters were found to be $p_c = 0.00325$ and $t_0 = 2.8$, respectively, with a coefficient of determination of 0.99232. The proportionality constant, σ_x, used to fit Equation 5.1 to the semilogarithmic plot of σ vs. p (solid line), which was also obtained through the fitting procedure, was $\sigma_x \approx 2.2 \times 10^3$ S/m.

The measured electric response to uniaxial compression of the MWCNT – PDMS nanocomposite is shown in Figure 5.2 a (empty symbols), for a CNT mass fraction close to the percolation threshold, i.e., p = 0.004, and a high CNT mass fraction, i.e., p = 0.01, as well as one in between, i.e., p = 0.006. In line with data reported for other high aspect ratio particle based bulk polymer nanocomposites, first, the electrical resistance increases with compressive strain and, second, the interdependence of electrical resistance and compressive strain is exponential in type and shows a particle concentration dependent behaviour, with increasing strain-sensitivity for decreasing particle content. Figure 5.2 a also shows the calculated electric response to uniaxial compression as obtained by Equation 5.5 for the same CNT mass fractions (solid lines), using the previously determined values for parameters p_c and t_0. It appears that both the piezoresistance of the MWCNT – PDMS nanocomposite as well as its concentration dependence are well described by the proposed model, indicating that the electric response to uniaxial compression is indeed dominated by a net broadening of the distribution of local conductances and that the influence of compressive strain on this distribution is inversely proportional to particle concentration. Although other expressions for c_p cannot be ruled out, the goodness of the fit further indicates that this interdependence is well captured by the simple expression given in Equation 5.4.

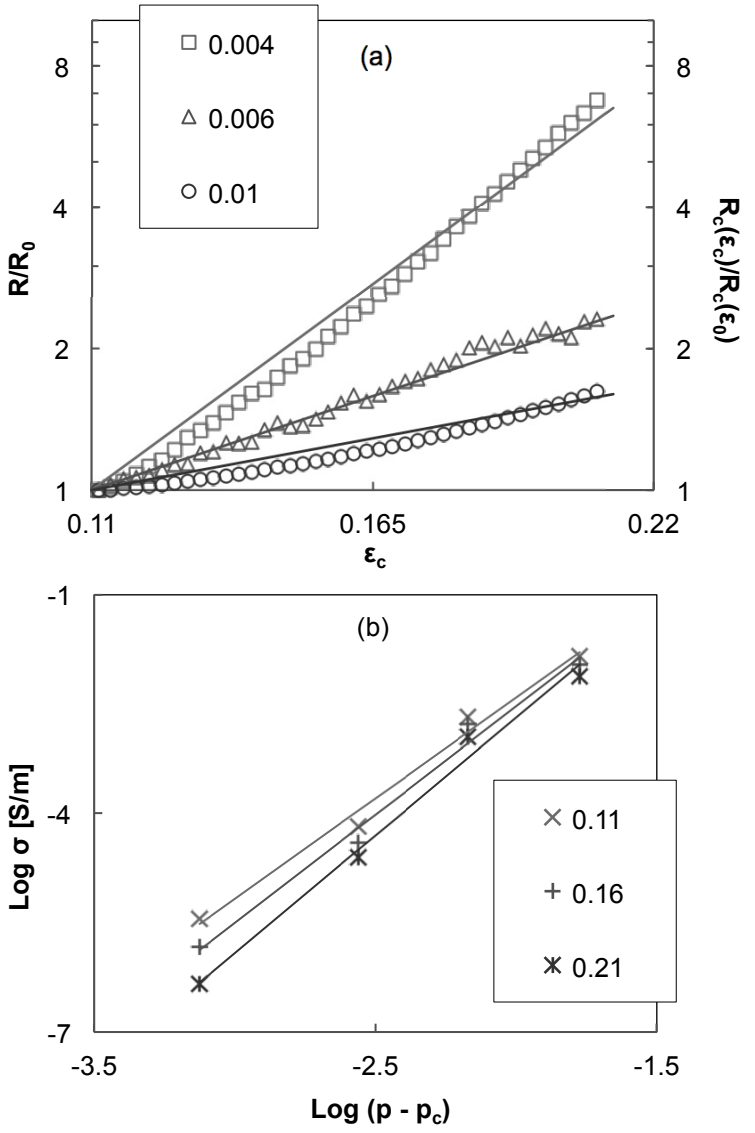

Figure 5.2. (a) Semilogarithmic plot of variation in normalized electrical resistance, R/R_0, with uniaxial compression, ε_c, of the MWCNT – PDMS nanocomposite at three CNT mass fractions (empty symbols), R_0 being the resistance measured at $\varepsilon_0 = 0.11$, and calculated electric response, $R_c(\varepsilon_c)/R_c(\varepsilon_0)$, to uniaxial compression, as obtained by Equation 5.5 for the same CNT mass fractions (solid lines). (b) Logarithmic plot of σ vs. $(p - p_c)$ showing the linear fits (solid lines) to the experimental data (line symbols) at three compressive strains ε_c.

Analyzing the σ vs. $(p - p_c)$ trends at different compressive strains (cf. Figure 5.2 b), the conductivity exponent (slope of the linear fits to the experimental data) is found to increase with increasing compressive strain, which confirms the corresponding assumption made leading up to Equation 5.2 (i.e., that t scales positively with ε_c).

Given the dependence of $t_c(\varepsilon_c)$ on p_c and t_0 (cf. Equation 5.2 and 5.4), it is worth noting that both p_c and t_0 are considered strain independent. Parameters p_c and t_0 characterize the particle network at the reference point p_0 and, for a given p, $t_c(\varepsilon_c)$ then captures the change in the distribution of local conductances with compressive strain $|\varepsilon_c| \geq |\varepsilon_0|$. Parameters p_c and t_0 are a function of constituent materials, processing method and reference point (e.g., pre-compression); a change of any of those parameters would likely lead to different p_c and t_0 values.

5.4.2 Applying the model to data from the literature

For the purpose of applying the model to different polymer nanocomposites a number of papers that study the electric response to uniaxial compression of bulk polymer nanocomposites with high aspect ratio particles have been identified, namely [87, 159, 190-192, 205, 214]. The extracted data for seven CNT, graphene and high structure carbon black based polymer nanocomposites are shown in a R/R_0 vs. ε_c plot in Figure 5.3 (full and empty symbols). In case the electric response was given as a function of pressure, P, or compressive force, F_c, the corresponding compressive strain was derived by taking into account the Young's modulus, Y, of the material:

$$\varepsilon_c \approx \frac{P}{Y} = \frac{F_c}{A_c Y}\,, \tag{5.6}$$

where A_c is the area onto which F_c was applied. The degree to which a polymer nanocomposite resists uniaxial compression or tension typically increases with increasing deformation; for elastomers and small deformations, however, this effect is small (cf. Figure 5 in [204]); the above approximation therefore seems acceptable. Y values are specified in Table 5.1 and 5.2. For the same polymer nanocomposites, Figure 5.3 also shows the calculated electric response to uniaxial compression as obtained by Equation 5.5 (solid and dashed lines), using the respective parameters listed in Table 5.1.

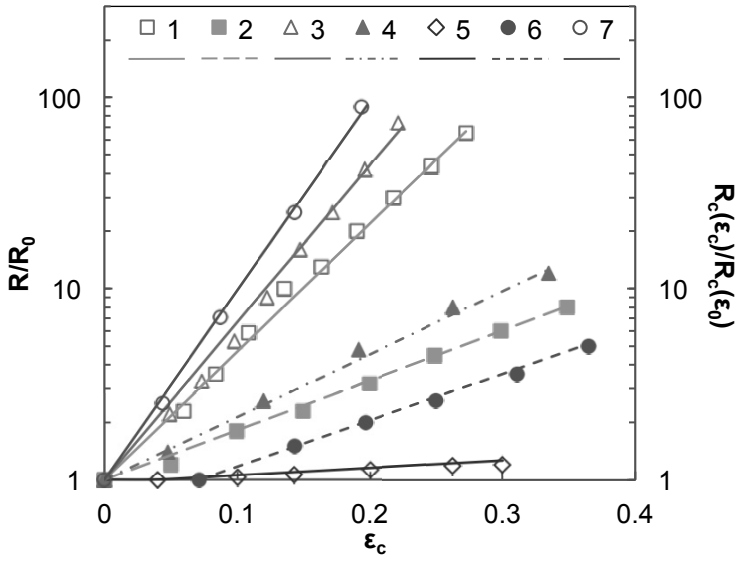

Figure 5.3. Semilogarithmic plot of variation in normalized electrical resistance, R/R_0, with uniaxial compression, ε_c, for seven high aspect ratio particle based polymer nanocomposites (full and empty symbols), and the corresponding calculated electric response, $R_c(\varepsilon_c)/R_c(/_0)$, to uniaxial compression as obtained by Equation 5.5 (solid and dashed lines). Data sources and parameters p, p_c, t_0 and Y are specified in Table 5.1. For improved facility of inspection, ε_c values of data set 5 were multiplied by 10.

First of all, in spite of the large range of variations in relative resistance, the piezoresistance of all seven polymer nanocomposites is well characterized by the model. The model was applied to data from [192], by using the p, p_c, and t_0 values given in the paper and incrementally changing Y until the best fit was obtained. The so found values for the Young's modulus of the material seem reasonable, and higher Y values were found for higher CNT concentrations, as is expected for MWCNT – methylvinyl silicone rubber (VMQ) nanocomposites. In both systems, i.e., for MWCNT – VMQ nanocomposites with CNTs having an average aspect ratio of around 50 (data sets 1 and 2) as well as for MWCNT – VMQ nanocomposites with CNTs having an average aspect ratio of around 500 (data sets 3 and 4), Equation 5.5 also captures well the concentration dependence of the piezoresistance. To fit Equation 5.5 to data from [159], values for p and p_c were taken from the paper; an assumption for Y was made based on data from the material supplier, and t_0 was the fitting parameter. Again, the so obtained value falls within the expected range.

Given the difference in MWCNT aspect ratio for the polymer nanocomposites presented in [192] (e.g., data sets 1 and 3) and the fact that the polymer nanocomposite characterized in [159] (data set 5) is composed of modified MWCNTs and a different matrix material, it seems self-evident that the corresponding CNT networks at $\varepsilon_0 = 0$ differ from each other. The equally good fits of Equation 5.5 to data sets 1, 3, and 5, for different respective sets of p_c and t_0 values (cf. Table 5.1), therefore strongly support the assumptions that the particle network at ε_0 is well characterized by the corresponding p_c

and t_0 values and that the variation in electrical resistance with uniaxial compression is indeed captured by the strain dependence of the conductivity exponent.

Table 5.1. Parameters p, p_c, t_0 and Y used to fit Equation 5.5 to data from the literature (cf. Figure 5.3).

Label	Ref.	Material system	Comment	p	p_c	t_0	Y [MPa]
1	[192]	MWCNT | VMQ	CNT aspect ratio: 50	0.011	0.0082	3.52	6.6 [b]
2				0.021			7.1 [b]
3	[192]	MWCNT | VMQ	CNT aspect ratio: 500	0.013	0.0102	4.16	7.2 [b]
4				0.025			7.4 [b]
5	[159]	MWCNT | PDMS	Modified CNTs	0.01	0.0075	2.3 [b]	4 [a]
6	[205]	Graphene | PDMS	-	0.0119	0.0063	2.12	1.4 [b]
7	[214]	HS-NCB [c] | PI	-	0.1	0.09 [a]	5.5 [b]	0.4 [a]

[a] estimated value; [b] fitting parameter; [c] high structure nanosized carbon black (HS-NCB).

In [192], a higher percolation threshold was found for the nanocomposite with the higher aspect ratio CNTs. This is unusual as, typically, the percolation threshold is inversely proportional to the particle aspect ratio [26, 169]. The authors explain this discrepancy with the agglomeration of CNTs, which decreases the effective aspect ratio and appears to be more pronounced for the higher aspect ratio ones. It is worth noting that, despite this discrepancy, Equation 5.5 describes data sets 1 to 4 equally well. The reason for this is that the description of the respective CNT networks is based on experimentally defined parameters and does not rely on assumptions regarding particle geometry and or network configuration, and that Equation 5.5 is equally applicable to networks of well-dispersed particles and networks comprising particle agglomerates.

Same as for data sets 1 to 4, Equation 5.5 was applied to the graphene – PDMS nanocomposite (data set 6) by using the p, p_c, and t_0 values given in the corresponding paper and incrementally changing Y until the best fit was obtained. For the high structure carbon black – polyisoprene (PI) nanocomposite (data set 7), an estimation of p_c is given by the same authors in [181]; Y was estimated on the basis of data reported in the literature [228], and t_0 was the fitting parameter. In both cases, the so obtained values lie within the expected range, and the piezoresistance is well characterized by the above model. This suggests that the notion of a net broadening of the distribution of local conductances with compressive strain applies to all polymer nanocomposites with high aspect ratio particles, and it is therefore concluded that Equation 5.5 can be applied to high aspect ratio particle based bulk polymer nanocomposites in general. It is worth noting that the piezoresistance of the polymer nanocomposites studied in [87, 190, 191] are equally well described by Equation 5.5.

5.4.3 Understanding piezoresistance in bulk polymer nanocomposites

To conclude, an attempt is made to demonstrate that the framework of the proposed model is not limited to high aspect ratio particle based polymer nanocomposites but that it can describe piezoresistance in electroconductive polymer nanocomposites in general. To this end, it is assumed that the dispersion of the particles within the polymer matrix is such that the local conductances, g, follow some distribution around a mean value. The overall electrical conductance, G, of a bulk polymer nanocomposite is then a function of both the mean local conductance, $\mu(g)$, and the variance of this distribution of local

conductances, Var(g). On the one hand, for a given Var(g), G increases with increasing μ(g), i.e., decreasing mean interparticle separation, and decreases with decreasing μ(g), i.e., increasing mean interparticle separation. On the other hand, for a given μ(g), G increases with decreasing Var(g) and decreases with increasing Var(g). The reason for this is that the range of g is finite, with a maximum in the case of physical contact between particles and a minimum in the case of high interparticle separation, where the corresponding particle-particle junction can no longer be considered as a conductor.

Upon mechanical deformation, μ(g) is increased or decreased, depending on whether the particle network is compressed or stretched. Var(g), in contrast, is always increased. To illustrate this, a case of uniaxial compression, as is schematically shown in Figure 5.4, is discussed. On the one hand, as the bulk polymer nanocomposite is compressed, the overall volume occupied by the particle network is reduced and so is the mean interparticle separation, with the consequence that μ(g) is increased. On the other hand, upon compression, the distance between two adjacent particles either decreases (cf. mode 1 in Figure 5.4) or increases (cf. mode 2 in Figure 5.4) or remains unchanged (mode 0, not shown in Figure 5.4), depending on the details of this individual particle-particle junction (e.g., orientation with respect to the direction of the applied compressive load or position within the particle network). The probability of occurrence for the three modes is typically not equal. However, because the probability of occurrence for the three modes is typically independent of the interparticle separation at ε_0, the probability for an increase in g is therefore equal for all g, as is the probability for a decrease in g or a zero-change. Consequently, as the number of particle-particle junctions for which $g = g_i$ is

highest for $g_i = \mu(g)$ and lower for $g_i < \mu(g)$ and $g_i > \mu(g)$, the compression of the particle network results in a net broadening of the distribution of local conductances and, hence, an increase in Var(g). From this follows that in the case of uniaxial compression of bulk polymer nanocomposites, the overall electrical resistance, R = 1/G, can increase or decrease, because the increase of μ(g) and the increase of Var(g) have opposites effects on R (i.e., because R scales with Var(g) but with the inverse of μ(g)), whereas in the case of uniaxial tension, R increases because μ(g) decreases and Var(g) increases. This is in good agreement with experimental evidence, as the interdependence of electrical resistance and mechanical deformation can be positive or negative in the case of uniaxial compression [87, 159, 190-192, 203-205, 208-212, 214, 221, 222], but is generally positive in the case of uniaxial tension [160, 180-186, 188, 189, 214].

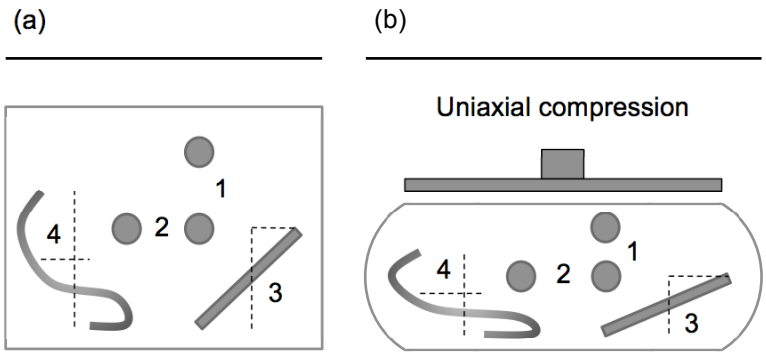

Figure 5.4. Schematic, two-dimensional representation of interparticle distances (a) prior to and (b) after uniaxial compression of an unconstrained bulk polymer nanocomposite. The changes are due to, first, relative movement of the particles (modes 1 and 2) and, second, reorientation and reshaping of the particles (modes 3 and 4).

The fact that the electrical resistance typically decreases with uniaxial compression of low aspect ratio particle based polymer nanocomposites [208-212, 221] but increases with uniaxial compression of high aspect ratio particle based polymer nanocomposites (cf. Chapter 4 and [87, 159, 190-192, 203-205, 214, 222]) suggests that in the first case the electric response is dominated by the change in $\mu(g)$, $\Delta\mu(g)$, whereas in the second case, it is the change in Var(g), ΔVar(g), that dominates the electric response. This can be understood by looking at the nanoscale mechanisms that lead to a change in the distribution of local conductances. In low aspect ratio particle based polymer nanocomposites, the change in the distribution of local conductances due to mechanical deformation of the particle network is caused by relative movement of particles (cf. modes 1 and 2 in Figure 5.4). In this case, for a given deformation, ΔVar(g) is inversely proportional to $\Delta\mu(g)$ (e.g., ΔVar(g) is at a maximum in the case of equal and nonzero probabilities for the distances between adjacent particles to increase or decrease, in which case $\Delta\mu(g) = 0$). As $\Delta\mu(g)$ typically is nonzero, ΔVar(g) is reduced accordingly and it appears to be likely that the electric response is then dominated by $\Delta\mu(g)$. In high aspect ratio particle based polymer nanocomposites, in contrast, the distribution of local conductances within the particle network is affected not only through relative movement of the particles but also through reorientation and reshaping of the particles (cf. modes 3 and 4 in Figure 5.4). It seems self-evident that particle reorientation and reshaping is a more random process, with closer probabilities for the distances between adjacent particles to increase or decrease, which consequently, for the same deformation, leads to smaller $\Delta\mu(g)$ and larger ΔVar(g), such that ΔVar(g) dominates the electric response.

From the above, it follows that electroconductive polymer nanocomposites are piezoresistive materials because the distribution of local conductances within the particle network changes with mechanical deformation of the latter, and that this change in distribution of local conductances is described by $\Delta\mu(g)$ and $\Delta Var(g)$. Models based on quantum mechanical tunnelling or thermal activation over barriers have in common that the change in R with deformation is given as a function of the change in mean interparticle separation. Thence, such modeling considers the influence of $\Delta\mu(g)$ on the electric response but ignores the effect of $\Delta Var(g)$. In the case of uniaxial tension, qualitatively good fits are obtained because the effects of $\Delta\mu(g)$ and $\Delta Var(g)$ on R are similar in type, and neglecting the effect of $\Delta Var(g)$ does not change the general trend. Similarly, in the case of uniaxial compression of low aspect ratio particle based polymer nanocomposites, qualitatively good fits are obtained because the electric response is dominated by $\Delta\mu(g)$. In the case of high aspect ratio particle based polymer nanocomposites, however, where the electric response is dominated by $\Delta Var(g)$, such modeling fails to describe the experimental findings.

The model presented in this chapter considers the influences of both $\Delta\mu(g)$ and $\Delta Var(g)$. The influence of $\Delta Var(g)$ is accounted for by considering a positive interdependence of t and ε_c, and the influence of $\Delta\mu(g)$ is factored in by considering the strain dependence of the conductivity exponent in the first place. Note that Equation 5.5 can be rewritten as:

$$\frac{R_C(\varepsilon_C)}{R_C(\varepsilon_0)} = (p - p_c)^{t_0\frac{p_c}{p}(|\varepsilon_0|-|\varepsilon_c|)} = e^{t_0\frac{p_c}{p}\ln(p-p_c)(|\varepsilon_0|-|\varepsilon_c|)}, \quad (5.7)$$

where in the second equality it is made explicit that the interdependence of R_c and ε_c is exponential in type, as it is expected for percolated networks where electron conduction is dominated by tunnelling between adjacent but non-contacting particles and where the mean interparticle separation and, hence, $\mu(g)$, is a function of applied strain. The model might therefore be generalized to describe the electric response to mechanical deformation of bulk polymer nanocomposite in general. Such a generalized relation between the overall electric resistance, $R(\varepsilon)$, and the applied strain, ε, might be given by:

$$\frac{R(\varepsilon)}{R(\varepsilon_0)} = (p - p_c)^{(1-\theta(\alpha)\xi(\varepsilon))t_0 c_p(|\varepsilon_0|-|\varepsilon|)}, \tag{5.8}$$

where $R(\varepsilon_0)$ is the reference resistance at strain ε_0, α is the de facto aspect ratio of the particles or agglomerates, $\theta(\alpha) = 2$ for $\alpha \approx 1$ and $\theta(\alpha) = 0$ for $\alpha >> 1$, and $\xi(\varepsilon) = 1$ for $\varepsilon < 0$ and $\xi(\varepsilon) = 0$ for $\varepsilon > 0$.

Table 5.2. Parameters $\theta(\alpha)$, $\xi(\varepsilon)$, p, p_c, t_0 and Y used to fit Equation 5.8 to data from the literature (cf. Figure 5.5).

Label	Ref.	Material system	$\theta(\alpha)$	$\xi(\varepsilon)$	p	p_c	t_0	Y [MPa]
1	[210]	NCB [c] | polyethylene	2	1	0.25	0.15 [a]	3.2 [a]	95 [b]
2					0.30			105 [b]
3	[186]	NCB [c] | epoxy	2	0	0.005	0.0025 [a]	2.3 [b]	-
4		MWCNT | epoxy	0	0	0.003	0.002 [a]	3.2 [b]	-
5	[210]	Sn/Pb [d] | polyethylene	2	1	0.3	0.25 [a]	4.4 [b]	125 [a]
6	[221]	SnO_2: Sb [e] | f-epoxy [f]	2	1	0.244	0.21	2.6 [b]	55 [a]

[a] estimated value; [b] fitting parameter; [c] nanosized carbon black (CB); [d] nanosized tin/lead alloy powder; [e] nanosized antimony-doped tin oxide powder; [f] flexible epoxy resin.

In Figure 5.5, Equation 5.8 is applied to appropriate data from the literature on uniaxially compressed bulk polymer nanocomposites with low aspect ratio particles on the one hand, and on uniaxially stretched bulk polymer nanocomposites with both low and high aspect ratio particles on the other hand. Equation 5.4 was used to calculate c_p and all other parameters are listed in Table 5.2.

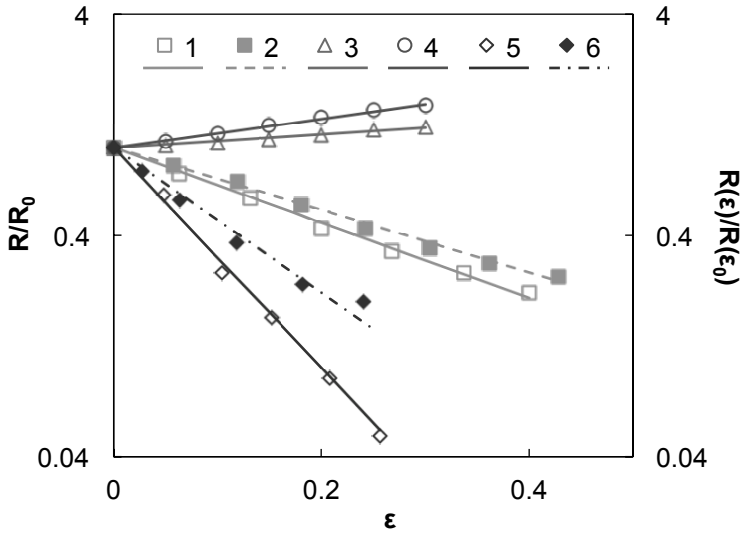

Figure 5.5. Semilogarithmic plot of measured variation in normalized electrical resistance, R/R_0, (full and empty symbols), and corresponding calculation, $R(\varepsilon)/R(\varepsilon_0)$, as obtained by Equation 5.8 (dashed and solid lines), for uniaxial compression of four low aspect ratio particle based polymer nanocomposites (squares and diamonds) and uniaxial tension on both a low aspect ratio particle (triangles) and a high aspect ratio particle (circles) based polymer nanocomposite. Data sources and parameters $\theta(\alpha)$, $\xi(\varepsilon)$, p, p_c, t_0 and Y are specified in Table 5.2. For improved facility of inspection, ε values of data sets 3 and 4 were multiplied by 10.

It appears that the electric response to mechanical deformation in all six examples is well described by Equation 5.8. This illustrates that piezoresistance in polymer nanocomposites in general can indeed be understood in terms of a change in the distribution of local conductances, which is characterized by $\Delta\mu(g)$ and $\Delta Var(g)$, and well described by a deformation dependent conductivity exponent, which scales positively with applied strain. This applies to different polymer nanocomposites as well as to different particle contents for a given material system (cf. fits to data sets 1 and 2).

5.5 Summary and Conclusions

High aspect ratio particle based polymer nanocomposites are at the center of research on flexible piezoresistive materials. The electric response to uniaxial compression of such materials is tunable because it is concentration dependent and it can be highly sensitive because it is exponential in type. Whereas in low aspect ratio particle based polymer nanocomposites the experimentally found decrease in electrical resistance can generally be well explained with the corresponding decrease in mean interparticle separation, the experimentally observed increase in electrical resistance in high aspect ratio particle based polymer nanocomposites was not well understood.

The present chapter addressed this problem theoretically and experimentally. By considering the conductivity exponent to be strain dependent and, therefore, to scale with the change in distribution of local conductances, a percolation theory based model is developed, which relates the variation in electrical resistance of bulk polymer nanocomposites with high aspect ratio particles to compressive strain. The model captures the characteristics of the particle network through the experimentally definable

percolation threshold, p_c, and reference conductivity exponent, t_0, and does not rely on assumptions regarding the nature of the particles and or the configuration of the network.

It is shown that the model fits extremely well to experimental data for carbon nanotube, graphene and high structure carbon black based polymer nanocomposites and it is therefore concluded that it is applicable to high aspect ratio particle based polymer nanocomposites in general. Accordingly, it is reasoned that the electric response to uniaxial compression of such materials is dominated by a net broadening of the distribution of local conductances, which in turn, is caused by reorientation, reshaping, and relative movement of the particles. It is further shown that piezoresistance in polymer nanocomposites in general can be understood in terms of a change in the distribution of local conductances. Both the mean local conductance and the variance of the distribution of local conductances are well described by the strain dependent conductivity exponent, which scales with the magnitude of applied mechanical deformation.

By applying the model to the piezoresistance characterization of MWCNT – PDMS nanocomposites with varying MWCNT content, it is also shown that the concentration dependence of the piezoresistance in such materials is well captured by the proposed model. Provided parameters p_c and t_0 are known, the model therefore allows for predicting the piezoresistance at any particle concentration above the percolation threshold. With regard to piezoresistive sensing applications with set key requirements for the functional material (e.g., flexibility, transparency, dimensions, operating voltage/current, applied pressure and or required sensitivity), it is likely that the presented model will be instrumental in material selection and performance evaluation.

CHAPTER 6

Investigations into Particle Network Formation and Optimized Percolation

Parts published in Nanotechnology and in Materials Research Society Symposium Proceedings – Nanotechnology 2012, 23 (28). DOI: 10.1088/0957-4484/23/28/285701, MRS Proceedings 2012, 1410. DOI: 10.1557/opl.2012.856.

6.1 Introduction

Electron conduction in CNT – polymer nanocomposites is controlled by percolation and involves quantum mechanical tunnelling at CNT junctions (cf. Chapters 3 and 4), and is primarily dependant on the configuration of the particle network, which can be described by two parameters; the percolation threshold, p_c, and the conductivity exponent, t (cf. Chapters 5).

For isotropic distributions of particles, continuum representations based on the excluded volume concept [229] found that p_c decreases with increasing particle aspect ratio, α, [169], and that in the limit of large α, $p_c \approx \alpha^{-1}$ [26, 230]. Accordingly, for typical CNT aspect ratios of $100 \leq \alpha \leq 1000$, a CNT – polymer nanocomposite would be characterized by $0.001 \leq p_c \leq 0.01$. Percolation thresholds reported in literature, however, span a much larger range and vary from 0.000021 [134] to 0.15 [231], which suggests that the assumptions with respect to the nature of the particles (rigid cylindrical rods) and or the configuration of the particle network (isotropic distribution of the particles within

the matrix), typically made for modelling and theoretical considerations such as the above continuum representations, are too stringent. CNTs are not rigid cylindrical rods but are flexible through bending and buckling [29] (cf. SEM and TEM images in Chapter 3), and the configuration of the network not only depends on the aspect ratio of the CNTs but also on the quality of the CNT dispersion during nanocomposite processing. The inverse proportionality $p_c \approx \alpha^{-1}$ is indeed found experimentally, cf. [147, 232-234], but the opposite, i.e., increasing p_c with increasing α, has also been observed, cf. [111, 119, 192, 234], in part even for a same class of nanocomposites, which affirms that material processing is key as regards particle network formation.

A very high percolation threshold can be attributed to poor CNT dispersion, i.e. an electron-conducting network formed by agglomerates of CNTs with comparatively low effective aspect ratios. A very low percolation threshold, on the other hand, can be attributed to a non-isotropic particle distribution enabling network formation at particle mass fractions, p, below the statistical percolation threshold. Hereinafter the latter situation is referred to as *optimized percolation*. For the use of CNT – polymer nanocomposites in applications where electrical conductivity and or piezoresistance are desired material properties, but where the polymeric characters of the material (e.g., transparency and or flexibility) are also key requirements, as, for example, in flexible tactile sensors [8], optimized percolation is the tool that allows for maximizing the electrical performance at a minimal impairment of the polymeric characters of the material. It allows not only for very low percolation thresholds but also for high maximum electrical conductivities, σ_{max}, as shown in Figure 6.1, which, based on relevant

data from the literature, illustrates that for a given CNT concentration and matrix material σ_{max} increases with decreasing p_c.

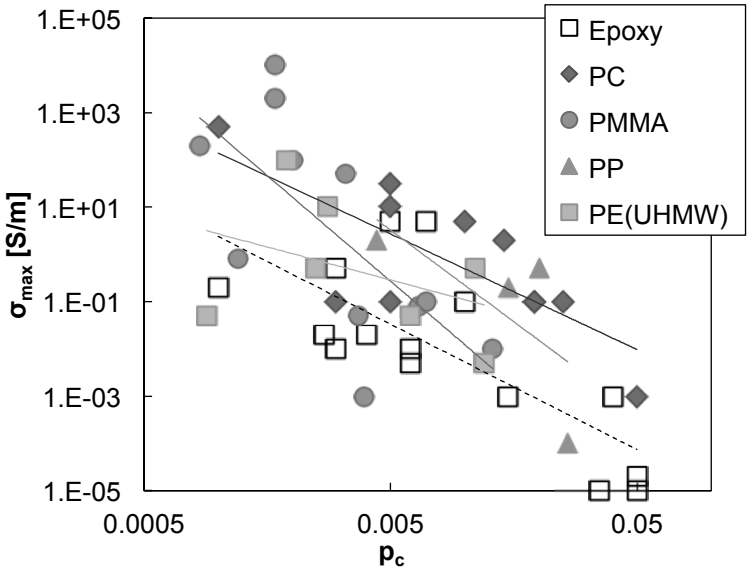

Figure 6.1. Logarithmic plot of σ_{max} as a function of p_c, for both thermosetting (empty symbol and dashed line) and thermoplastic (full symbols and solid lines) polymers. Dashed and solid lines indicate the negative interdependence between the two parameters. References can be found in Table 1 of [26], from where the data has been taken for σ_{max} measured at $p \geq 0.01$ and $0.0005 \leq p_c \leq 0.05$.

For a particle network with direct contacts between adjacent particles, classical percolation theory predicts the conductivity exponent to be universal and to solely dependent on network dimensionality, such that $t = 1.3$ for any two-dimensional direct-contact network, and $t = 2$ for any three-dimensional direct-contact network [166, 167]. However, just as for p_c, reported experimental conductivity exponents differ from the theoretical predictions: most polymer nanocomposites are characterized by nonuniversal

conductivity exponents [26, 170], with values as high as t = 7.6 [235]. As discussed in Chapters 3 to 5, this is because electron conduction through the percolated network is dominated by quantum mechanical tunnelling between adjacent particles, which does not require direct contact between particles, as is assumed by the classical percolation theory.

As further discussed in Chapter 5, the magnitude of the deviation from the universal value of t is governed by the distribution of local conductances within the electron-conducting network. The more uniform the network, the narrower the distribution of local conductances, and the smaller the conductivity exponent. In contrast, the less uniform the network, the broader the distribution of local conductances, and the higher the conductivity exponent [14]. If electron conduction through the percolated network is dominated by quantum mechanical tunnelling, adjacent particles can but do not have to be in direct contact, and the local conductance depends exponentially on interparticle separation. In this case the distribution of local conductances would naturally be much broader than in the case of a direct contact network; thence, conductivity exponents as predicted by the classical percolation theory can be considered as lower limits for t. Just as p_c, t depends on material processing; the distribution of local conductances is naturally a function of particle dispersion, which is not determined statistically but rather by the rheological properties of the matrix material when it is in a fluid state [236].

The formation of an electron-conducting network at $p \leq p_c$ can be induced by processing the material under an external field, which can be a stress field produced by shear flow [134, 145, 151, 237, 238], an electric field [125, 239-248], or a magnetic field [249-251]. In all cases the particle network is restructured through reorientation,

reshaping, and relative movement of the particles, and the extent to which network restructuring is possible depends on the rheological properties of the fluid matrix. By definition, network optimization leads to a decrease in p_c, and it typically causes an increase in σ_{max} (cf. Figure 6.1), it is however unclear to date if and in what way it affects t. From relevant data reported in the literature, there seems to be no obvious interdependence between p_c and t, as shown in Figure 6.2, where the two parameters are plotted for more than 30 different CNT – polymer nanocomposites.

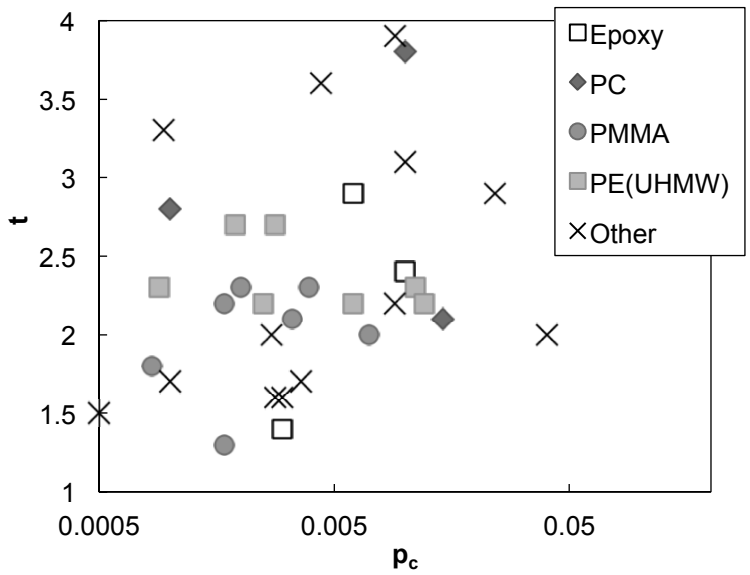

Figure 6.2. Semi-logarithmic plot of t vs. p_c, for both thermosetting (empty symbol and part of x symbols) and thermoplastic (full symbols and part of x symbols) polymers. References can be found in Table 1 of [26] from where the data has been taken for σ at p ≥ 0.01 known and $0.0005 \leq p_c \leq 0.05$.

With regard to applications as functional materials, controlling t is important as it directly influences the electrical performance of the material. An example is the use as low-

resistance, high-transparency films, such as electrodes in solar cells, where the optoelectronic properties of the material are controlled by the network non-uniformity, and for which low t values are essential [14].

In this regard it is also important to understand what microstructural changes cause the increase in electrical conductivity, σ, which is something that with hitherto published work remains unclear. Essentially, the increase in electrical conductivity due to network optimization can be due to (i) a decrease in the mean interparticle distance, i.e. decrease in average contact resistance within electron-conducting paths, and or (ii) the growth of the particle network, i.e. formation of additional electron-conducting paths. With respect to piezoresistive sensing, for instance, it does make a difference whether network optimization is dominated by (i) or (ii), as particle networks with few electron-conducting paths would offer high piezoresistive strain coefficients but would also pose high demands on the read-out system, whereas particle networks with a larger number of electron-conducting paths would be less sensitive, but also less demanding in terms of technical requirements (cf. Chapter 4).

6.2 Research Objectives

This chapter looks at network formation and optimized percolation in MWCNT modified PDMS. First, given the strong dependence of both percolation threshold and conductivity exponent on material processing, and notably on the viscosity of the matrix when it is in a fluid state, the rheological properties of MWCNT modified PDMS prior to polymerization are analyzed. Second, network optimization by means of an external field

is studied, and it is examined in what way this affects the conductivity exponent and what configurational changes form the basis for the increase in electrical conductivity. Third, it is also studied how the electrical conductivity of MWCNT modified PDMS evolves during polymerization of the elastomeric matrix, and how this depends on particle mass fraction.

6.3 Materials and Methods

The materials used in this study were MWCNTs and two types of PDMS. The rheological characteristics of MWCNT modified PDMS prior to polymerization were analyzed by rotational and oscillatory parallel plate rheometry, and the parallel plate setup was also used for the study of network optimization by means of an electric field as well as for monitoring electrical and viscoelastic properties during polymerization.

6.3.1 Materials

PDMS (Gelest OE41 and Gelest Gel D200) was purchased from Gelest, Inc. and MWCNTs (Baytubes C 150 P) were obtained from Bayer MaterialScience LLC. Gelest OE41 is an addition cure, filler-free, two-part, pure silicon elastomer, that was selected for its higher tensile strength (> 2 MPa), its relatively low viscosity of the catalyzed mix (1.75 – 2.5 Pa.s), and its moderate cure temperatures (e.g., cure at 55 °C for 4 h). Its pot-life at room temperature is 18 h. Baytubes are agglomerates of MWCNTs, with a loose agglomerate size in the range of 0.1 to 1 mm. Detailed information about both materials can be found in Chapter 3.3.1. Gelest Gel D200 is an addition cure, filler-free, two-part

medium penetration gel, that was selected for its typical dimethylsilicone properties, namely its ideal-viscous flow behaviour, its low viscosity of the catalyzed mix (1 Pa.s), and its moderate cure temperatures (e.g., cure at 115 – 120 °C for 30 – 60 min). Its pot-life at room temperature is 3 – 4 h. Because it is an addition cure system, no byproducts are formed, which allows for a good dimensional stability if the material is polymerized during testing. The base polymer (vinyl-terminated polydimethylsiloxane and vinyl-modified Q silica resin) and the curing agent (methylhydrosiloxane–dimethylsiloxane copolymer) react via platinum catalyzed hydrosilylation. Both the reacting groups and the bond forming chemistry are schematically illustrated in Figure 3.1, with values for a, b, and c being different for Gelest Gel D200 and Gelest OE41, respectively. Gelest OE41 was used as matrix material for the dispersion analysis (cf. Chapter 6.3.5, Figures 6.13 – 6.15, and Table 6.4) as well as the study of the evolution of the resistance ratio during network restructuring (cf. Figure 6.18). For all other work the matrix material was Gelest Gel D200.

6.3.2 Sample preparation

Toluene, purchased from Sigma-Aldrich Canada Corp., was used as an organic solvent to facilitate MWCNT deagglomeration and mixing of the constituent materials to produce MWCNT in PDMS suspensions. For each concentration the desired amount of MWCNTs was first dispersed in toluene for 90 min, using an ultrasonic bath (Model 2510, Branson Ultrasonics Corp.), and then added to the PDMS base polymer and the PDMS curing agent, such that the MWCNT/toluene to PDMS weight ratio was 1:3.

Subsequently the mixture was shear-mixed for 5 min, using a disperser (T 10 basic Ultra-Turrax, IKA Works, Inc.) rotating at 940 rad/s, degassed in low vacuum, and toluene was evaporated in an air-circulating oven at 40 °C. Degassing and evaporation times were 30 min. The variability in MWCNT mass fraction was estimated at < 10 %.

6.3.3 Rheological characterization

The rheological characteristics of the material were analyzed with a rotational rheometer (AR2000 Rheometer, TA Instruments) with parallel plate geometry, using aluminum plates with a diameter of 25 mm. The viscous behaviour of MWCNT modified PDMS as a function of particle mass fraction was studied by means of rotational tests at room temperature, with a gap, λ, of 1020 ± 40 μm and the shear rate, γ', varying from 0.1 to 100 s^{-1}. The viscoelastic behaviour of the material was evaluated by means of oscillatory tests at room temperature, with a gap of 980 ± 80 μm and the angular frequency, ω, varying from 0.06283 to 628.3 rad/s. Plate and gap size were as recommended by The Rheology Handbook [252]. All measurements were taken in the linear viscoelastic region in which the storage modulus, G', and the loss modulus, G'', are independent of the stain amplitude. The limits of the linear viscoelastic regions were determined by means of amplitude sweeps with controlled shear strain, at an angular frequency of 6.283 rad/s, and the stability of the selected equilibrium strains, γ, at which the oscillatory tests were performed, was confirmed by means of oscillatory time sweeps for 15 minutes, at the same angular frequency. Equilibrium strains are specified in Table 6.1. Roughly 0.5 g of MWCNT modified PDMS were needed per test, which were

poured onto the bottom aluminum plate by means of a cylindrical glass rod and contacted by the top aluminium plate such that the gap was entirely filled with material.

6.3.4 Measuring the electric current during exposure to an electric field

Network optimization by means of an electric field and simultaneous monitoring of the electrical resistance, R, was performed using the parallel plate set-up of the rheometer. 40 mm aluminum plates were used as electrodes and were contacted by Kapton insulated silver plated copper wires using conductive silver paint. The electrodes were electrically insulated from the rheometer head and base. A picture together with a schematic diagram of the set-up is given in Figure 6.3.

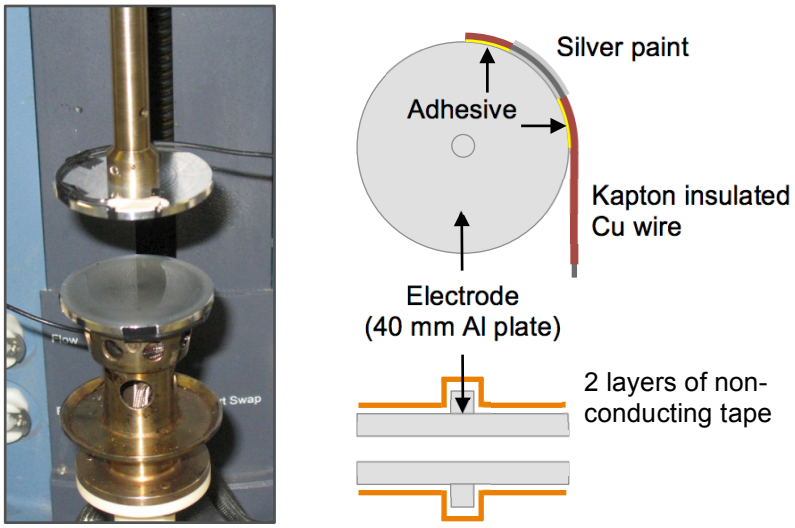

Figure 6.3. Picture and schematic diagram of the set-up used to monitor the electrical resistance during exposure to an electric field, as well as during polymerization of the elastomeric matrix. A high-temperature adhesive (LePage Speed Set Epoxy, Henkel Canada Corp.) was used to fix the wiring onto the electrodes. Two layers of non-conducting high-temperature tape (Flashbreaker 2 tape from Airtech International, Inc.) per electrode were used for electrical insulation.

A high resistance meter (Model 6517A, Keithley Instruments, Inc.) was used to apply a potential difference, ΔV. The magnitude of the electric field, E, generated this way can be approximated by:

$$E = \frac{\Delta V}{\lambda}. \quad (6.1)$$

The high resistance meter was also use to monitor the resulting current, I, simultaneously. R was calculated from the applied voltage and the measured current, and the electrical resistivity, ρ, was obtained according to Equation 4.1, taking into account the electrode area and the sample thickness. The potential difference was applied using the alternating polarity method with an alternating voltage, V_{AV}, and a non-zero offset voltage, V_{OV}; i.e. the applied voltage alternated between a high voltage, $V_h = V_{OV} + V_{AV}$, and a low voltage $V_l = V_{OV} - V_{AV}$. If not specified otherwise, hold times, τ, were 10 s. V_{OV} and V_{AV}, together with λ, are specified in the captions and footnotes of the respective figures and tables. Depending on λ, 1.2 to 2.1 g of MWCNT modified PDMS were needed per test, which were poured onto the bottom electrode and contacted by the top electrode such that the gap was entirely filled with material.

6.3.5 Dispersion analysis

The dispersion analysis was conducted on thin film samples, which were cured in the rheometer. 2 mm thick samples of MWCNT modified PDMS were produced, which required roughly 2.5 g of material per sample. For non-optimized networks, the material was poured onto the bottom plate, contacted by the top plate such that the gap was

entirely filled with material, and cured at 55 °C for 4 h. Optimized networks were obtained by pouring the material onto the bottom electrode, contacting it by the top electrode such that the gap was entirely filled with material, exposing it to an electric field of 25 kVm^{-1} for 10 min, and curing it at 55 °C for 4 h, while maintaining the electric field. Subsequently, the samples were prepared as detailed in Figure 6.4 such that a transverse section could be analyzed by SEM.

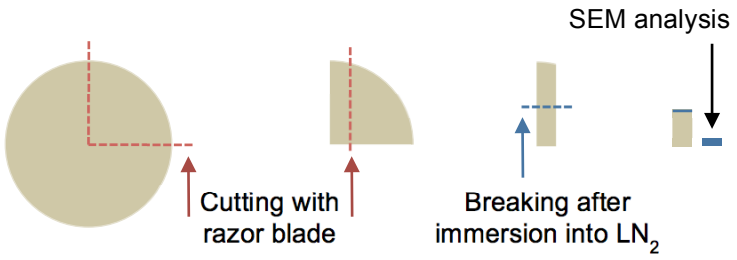

Figure 6.4. Preparation of MWCNT modified PDMS samples for SEM analysis.

SEM images were recorded on a Hitachi SU-8000 cold-field emission scanning electron microscope, using an accelerating voltage of 0.5 kV and a working distance as specified in the caption of Figure 6.13. Secondary electrons (SE) were collected with two through-the-lens detectors and a conventional SE detector located in the specimen chamber. The main images were not enhanced and are shown as recorded (raw data).

6.3.6 Monitoring the electrical resistance during polymerization

The set-up used for monitoring the electrical resistance during polymerization is shown in Figure 6.3 and described in Chapter 6.3.4. The experimental details are

provided in the captions of the respective figures. Although the readings of storage modulus and complex viscosity were affected by the wiring mounted onto the rheometer plates, the recordings clearly indicate beginning and end of polymerization. Depending on λ, 1.2 to 2.4 g of MWCNT modified PDMS were needed per test, which were poured onto the bottom electrode by means of a cylindrical glass rod and contacted by the top electrode such that the gap was entirely filled with material.

6.4 Results and Discussion

The effect of particle addition on the rheological properties of the matrix as well as the influence of various processing conditions on particle network formation have been relatively well studied for both thermoplastic and thermosetting polymers, cf. [83, 84, 86, 92, 95-98, 102, 108, 111, 112, 114, 115, 118, 120-123, 125-128, 237, 238, 243, 245, 248, 250, 253-276] and [26, 128, 134, 145, 151-155, 239-242, 246, 249, 277-282], respectively. Given that such characterization requires the matrix to be in a fluid state, thermoplastic polymers are generally characterized at high temperatures, whereas thermosetting polymers are characterized at low temperatures. In comparison, for elastomeric polymers, such as the PDMS used in this work, studies looking at the influence of particle addition on the rheological properties and or processing dependent network formation are quite scarce, cf. [282-287]. Just as for thermosetting polymers, PDMS and most other elastomeric polymers form irreversible chemical bonds during polymerization and therefore are generally also characterized at low temperatures. In

contrast to thermosetting polymers though, elastomeric polymers form wider meshed crosslinking and typically have longer polymer chains.

Polymer chain mobility, which depends on temperature, and polymer chain length both have an influence on the interaction between particles and matrix, and therefore also on the network formation process and the configuration of the percolated network. This is why experimental results from one class of nanocomposites can normally not be transferred to another class of nanocomposites, and systems have to be looked at individually. A good example for this is rheological percolation, i.e. the transition from a liquid-like to a solid-like behaviour of a nanocomposite as the particle mass fraction is increased beyond the rheological percolation threshold, p_r. Even within the same class of nanocomposites, some systems exhibit $p_r < p_c$ [86, 95, 102, 114, 122, 127, 256, 259], whereas other systems are characterized by $p_r > p_c$ [83, 84, 98, 108, 120, 123, 126, 263]. This will be discussed in more detail at the end of Section 6.4.1.

6.4.1 Rheological characterization of MWCNT modified PDMS

6.4.1.1 Flow behaviour

As mentioned in Chapter 6.3.1, Gelest Gel D200 is an ideal-viscous (or Newtonian) material, i.e. it exhibits a shear rate independent shear viscosity, η. For dispersions of MWCNTs in PDMS, shear flow can cause agglomerates to disintegrate and or particles to be oriented into flow direction [252]. In this case the viscosity depends on the degree of shear load and decreases with increasing shear rate; such materials exhibit shear-thinning (or pseudoplasic) behaviour. This is what is observed for the MWCNT – PDMS

system studied in this work, as is shown in Figure 6.5, where η vs. γ' is given for pure PDMS and MWCNT modified PDMS with three different particle mass fractions. The shear-thinning index, ϒ, which has been calculated by:

$$\Upsilon = \frac{\eta(\gamma_1')}{\eta(\gamma_2')}, \tag{6.2}$$

with $\gamma_1' = 1\ s^{-1}$ and $\gamma_2' = 10\ s^{-1}$, increases with increasing p and is ϒ = 1 for pure PDMS, ϒ = 1.8 at p = 0.004, ϒ = 2 at p = 0.01, and ϒ = 2.5 at p = 0.05. Thus, the higher p, the more pronounced the shear-thinning behaviour of MWCNT modified PDMS. It can also be seen in Figure 6.5 that MWCNTs addition has a strong influence on the shear viscosity of the material: at low shear rates, 5 wt.% of MWCNTs increase the room temperature shear viscosity by a factor of 50.

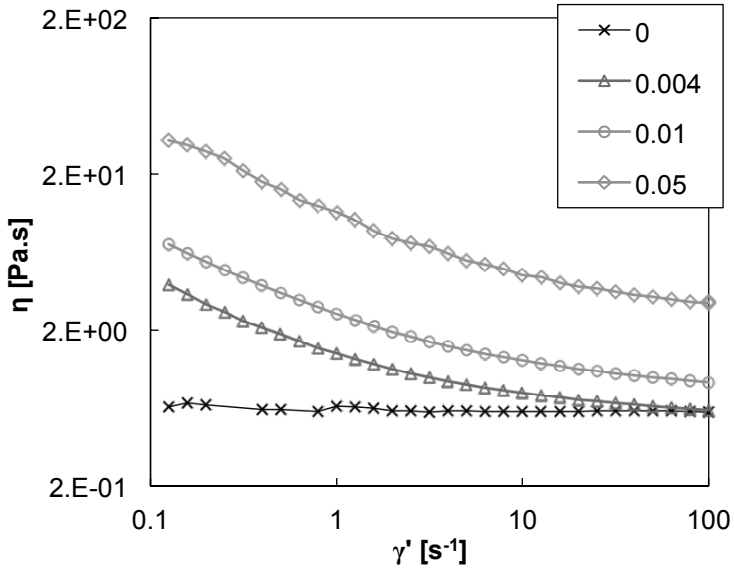

Figure 6.5. Logarithmic plot of shear viscosity vs. shear rate for pure PDMS and MWCNT modified PDMS, showing ideal-viscous behaviour of pure PDMS and shear-thinning behaviour of MWCNT modified PDMS. MWCNT mass fractions are specified in the legend.

The strong influence of MWCNTs on the flow behaviour of PDMS is also apparent in Figure 6.6, where the 1st normal stress coefficient, ψ_1, is plotted as a function of shear rate, for pure PDMS and the same MWCNT in PDMS dispersions. The 1st normal stress coefficient gives the difference between the normal stress in the flow direction and the normal stress in the gradient direction, divided by the square of the shear rate [252]. The raw data measured by the rheometer used to determine this difference in normal stresses is the force in the direction perpendicular to the parallel plates. Accordingly, positive values of ψ_1 indicate that the parallel plates are being pushed apart, whereas negative values of ψ_1 indicate that the parallel plates are being pulled together [288].

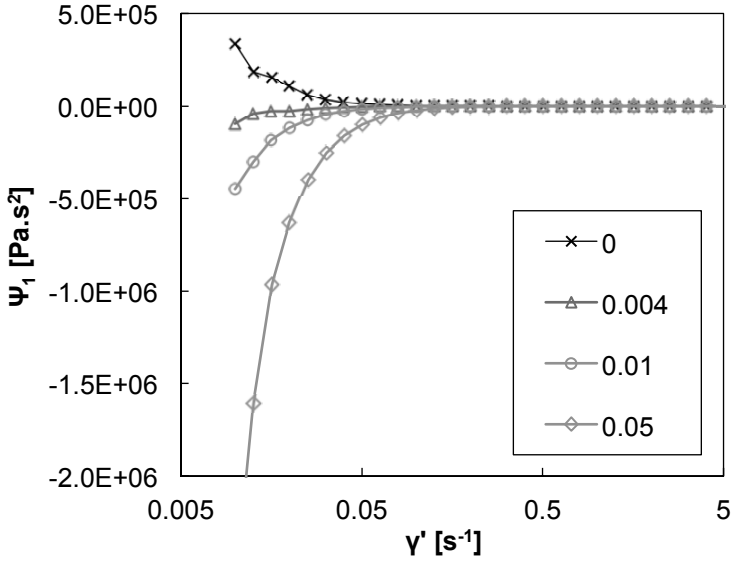

Figure 6.6. Logarithmic plot of 1st normal stress coefficient vs. shear rate for pure PDMS and MWCNT modified PDMS for four different MWCNT mass fractions. The latter are specified in the legend.

Normal stresses are associated with shear-induced anisotropy in the fluid. In the case of pure PDMS, the molecules are being forced away from their equilibrium average shape, which results in a positive normal stress (29 Pa at $\gamma' = 1\ s^{-1}$) pushing the plates away from each other, as is expected for entangled polymers [96]. The same normal stresses cause a cross-linked rubber rod to get longer when it is twisted. In the case of MWCNT modified PDMS, in addition to the above, particle agglomerates can be broken up and or particles oriented into flow direction. It appears that in this case the resulting normal stresses pull the plates together, as for all MWCNT mass fractions the normal stresses are negative. The negative stress increases with increasing particle mass fraction: at p = 0.01 its magnitude is comparable to pure PDMS, i.e. - 36 Pa at $\gamma' = 1\ s^{-1}$, at p = 0.05, however, the normal stress is 7 times higher, i.e. -256 Pa at $\gamma' = 1\ s^{-1}$. This has implications for material processing. Extruded PDMS parts, for example, typically display post-extrusion die swelling, which is caused by recoiling of PDMS chains that, during extrusion, have been deformed and oriented into shear direction. Such extrudates have cross sections larger than the die area and suffer from shape-distortion instability. It has been reported that modifying the polymer with CNTs allows for suppressing the die swell as well as controlling the dimensional characteristics of the extruded parts [96].

6.4.1.2 A way to influence processablity of nanocomposites

Figures 6.5 and 6.6 show that, on the one hand, MWCNT addition to PDMS strongly affects polymer chain mobility, rendering an ideal-viscous material viscoelastic, with a negative 1st normal stress coefficient, and that, on the other hand, flow during processing

affects MWCNT network formation, as particle agglomerates can be disintegrated and or particles oriented into flow direction. Both the quality of particle dispersion and the effect of particle addition on polymer chain mobility are influenced by the surface chemistry of the particles. Surface functionalization can therefore be used to tailor the effects of particle addition on the processablity of nanocomposites. This is shown in Figure 6.7 where η vs. γ' is given for pure epoxy and SWCNT modified epoxy, for a particle mass fraction of 0.005 and four different types and degrees of surface functionalization.

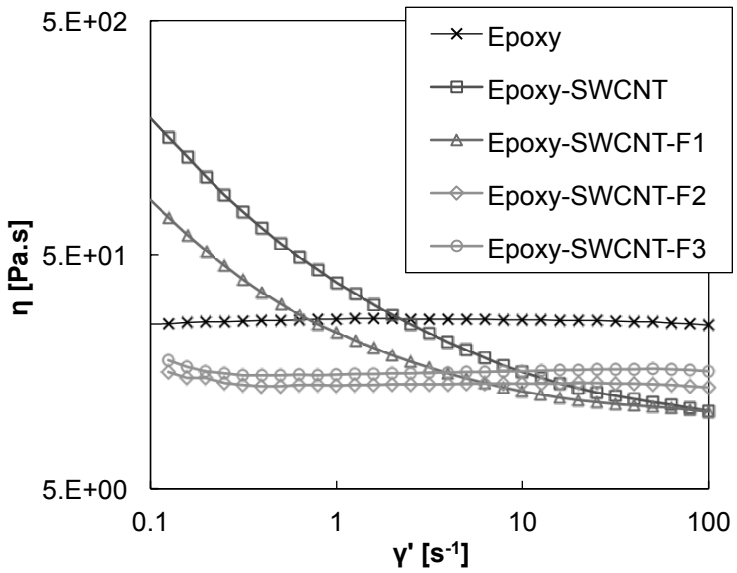

Figure 6.7. Logarithmic plot of shear viscosity vs. shear rate for a pure epoxy resin and epoxy resin modified with non-functionalized and functionalized SWCNTs. SWCNT mass fraction is 0.005. Types of functionalization (F1 – F3) are specified in [63].

As can be seen, SWCNT modified epoxy exhibits the expected shear-thinning behaviour with non-functionalized SWCNTs, but shear rate independent shear viscosity with selected degree and type of functionalization. The SWNCT epoxy system is one of the

other systems that has been looked at in the course of this dissertation research, it will, however, not be discussed in further detail here; for more information the reader is referred to [63].

6.4.1.3 Viscoelastic behaviour

Given the viscoelastic nature of MWCNT – PDMS nanocomposites, the material has also been characterized by means of dynamic mechanical analysis. The viscoelastic behaviour of the material consists of a viscous and an elastic portion. In Figure 6.8, the complex shear modulus, G^*, which characterizes the complete viscoelastic behaviour of the material, and which can be imagined as the rigidity of the material, is plotted as a function of angular frequency, for pure PDMS and MWCNT modified PDMS with five different particle mass fractions.

For pure PDMS G^* increases linearly with ω, as is typical for unlinked polymers. For PDMS containing MWCNTs, the G^* vs. ω curves indicate a plateau in the low angular frequency range, which indicates from-stability at rest. With increasing MWCNT mass fraction the rigidity of the material increases and the plateau becomes more pronounced; the viscoelastic character of the material thus changes from liquid-like to solid-like. On a microstructural level this is due to MWCNTs hindering polymer chain mobility and this effect being more pronounced at higher particle mass fractions [95, 127].

It should be noted that, although it has been argued that the low angular frequency plateau is due the MWCNTs forming an interconnected network [83, 108], this is not the case for the MWCNT – PDMS system studied here. A MWCNT – PDMS nanocomposite

with an interconnected particle network would naturally be characterized by $p > p_c$ and a σ value near σ_{max}. In the G^* vs. ω plot, a plateau appears already at $p = 0.0005$, the corresponding σ value obtained after polymerization, however, is only $\sigma = 2.5 \times 10^{-12}$ S/m, i.e. comparable to σ of pure PDMS, which shows that at $p = 0.0005$ no interconnected MWCNT network is formed. In line with this it is also interesting to note that the liquid-like to solid-like transition observed in Figure 6.8 is comparable to the insulator to semiconductor transition reported in Chapter 3 (cf. Figure 3.14), with the difference that in Figure 3.14 the low frequency plateau appears at much higher p values.

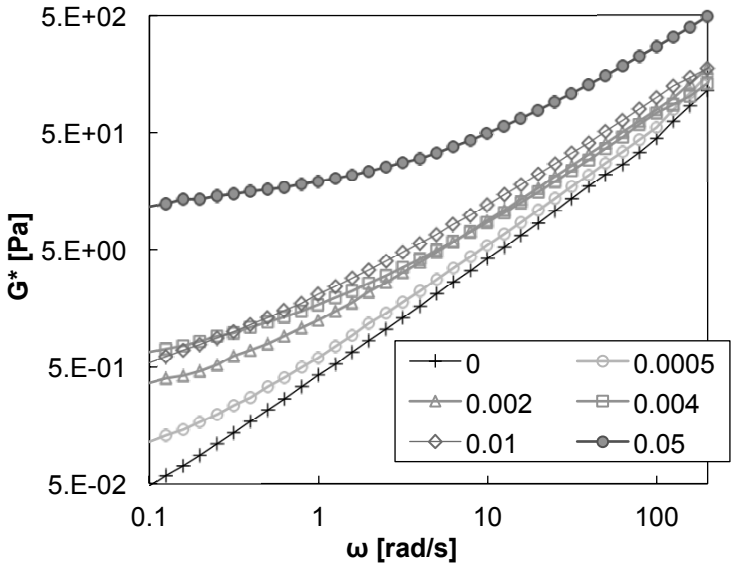

Figure 6.8. Logarithmic plot of complex shear modulus vs. angular frequency for pure PDMS and MWCNT modified PDMS. MWCNT mass fractions are specified in the legend and equilibrium strains at which the test were performed are given in Table 6.1.

The increase in rigidity as observed in Figure 6.8 is accompanied by an increase in complex viscosity, η^*, which can be imagined as the viscoelastic flow resistance of the

material. As can be seen in Table 6.1, η^* increases with p and, at low angular frequency, is around 60 times higher at p = 0.05 compared to pure PDMS. The interaction between particles and matrix increases with the quality of particle dispersion [289]. The fact that the G^* vs. ω behaviour as well as η^* at ω = 0.6283 rad/s are different at p = 0.0005, compared to pure PDMS, thus indicates good MWCNT dispersion.

Table 6.1. For pure PDMS and MWCNT modified PDMS: equilibrium strains at which oscillatory test were performed, as well as complex viscosity, storage modulus, and inverse loss tangent measured at ω = 0.6283 rand/s.

p	0	0.0005	0.002	0.004	0.01	0.05
γ [%]	50	10	8	10	5	1
η^* [Pa.s]	0.4235	0.642	1.445	2.105	2.381	27.05
G' [Pa]	0.01732	0.02981	0.2243	0.7294	0.7105	15.29
1/tanδ	0.0652	0.0741	0.2548	0.6609	0.5394	2.0567

The ratio of viscous to elastic portion of the viscoelastic behaviour is best represent by the loss factor, tanδ, which is calculated as:

$$tan\delta = \frac{G''}{G'}. \quad (6.3)$$

G' is a measure of the deformation energy stored by the sample during the shear process and G'' is a measure of the deformation energy used up by the sample during the shear process because the relative motion between molecules and or particles causes frictional forces. The smaller tanδ, the firmer the material [96]; as can be seen in Table 6.1, where values of the inverse loss tangent are given for pure PDMS and MWCNT modified

PDMS with five different particle mass fractions, just as the rigidity of the material, its firmness increases with increasing MWCNT mass fraction.

6.4.1.4 Rheological percolation

Similar to electrical percolation, the dependence of rheological properties on particle mass fraction is typically described by percolation where the rheological percolation threshold is correlated with the onset of a power-law behaviour [84, 86, 95, 102, 108, 114, 122, 126, 127, 259]. Various rheological parameters, e.g., G', G'', η^*, and 1/tanδ, have been used in this regard. Kota et al. [108] have studied the informative value of these parameters in conjunction with electrical percolation; they found that the elastic load transfer was more sensitive to percolation than the dissipation mechanisms that affect the viscous response, and concluded that among the directly measured rheological properties G' was the most suitable parameters to study rheological percolation. In line with Equation 5.1, rheological percolation can thus be described as:

$$G' \propto (p - p_r)^u, \tag{6.4}$$

where u is the elasticity exponent. Figure 6.9 shows the electrical conductivity (empty squares) as well as the storage modulus (empty triangles) of MWCNT modified PDMS as a function of MWCNT mass fraction. In line with the above discussion, both parameters scale positively with MWCNT concentration, showing a power law behaviour above the respective percolation thresholds. Parameters p_c and t, characterizing electrical percolation, were obtained by means of a logarithmic plot of σ vs. $(p - p_c)$ where p_c was incrementally varied until the best linear fit of Equation 3.3 to the experimental data was

obtained. Parameters p_r and u, characterizing rheological percolation, were obtained by means of a logarithmic plot of G' vs. $(p - p_r)$ where p_r was incrementally varied until the best linear fit of Equation 6.4 to the experimental data was obtained. All four parameters are given in Table 6.2, together with the corresponding proportionality constants σ_x and G'_x used to fit Equations 3.3 and 6.4 to the semilogarithmic plots of σ vs. p (dashed line) and G' vs. p (solid line), respectively, as well as the coefficients of determination R^2.

First, the rheological percolation threshold of the MWCNT – PDMS system studied here under shear flow is at 0.00015. For $p < 0.00015$, the addition of MWCNTs to PDMS has no signification effect on the rheological characteristics of the material, whereas for $p \geq 0.00015$, polymer chain mobility is reduced such that the elastic portion of the viscoelastic behaviour of the material is increased. This increase then depends on MWCNT mass fraction and is well described by Equation 6.4. Second, it becomes apparent that $p_r < p_c$, by a factor of about 10.

Table 6.2. Electrical and rheological percolation parameters p_c, t, p_r, and u, proportionality constants σ_x and G'_x, and coefficients of determination R^2, used to fit Equations 3.3 and 6.4 to the experimental data in Figure 6.9.

Percolation	p_c | p_r	t | u	σ_x | G'_x	R^2
Electrical (Equation 3.3)	0.00145	2.07	55.1	1
Rheological (Equation 6.4)	0.00015	0.98	445.2	0.9806

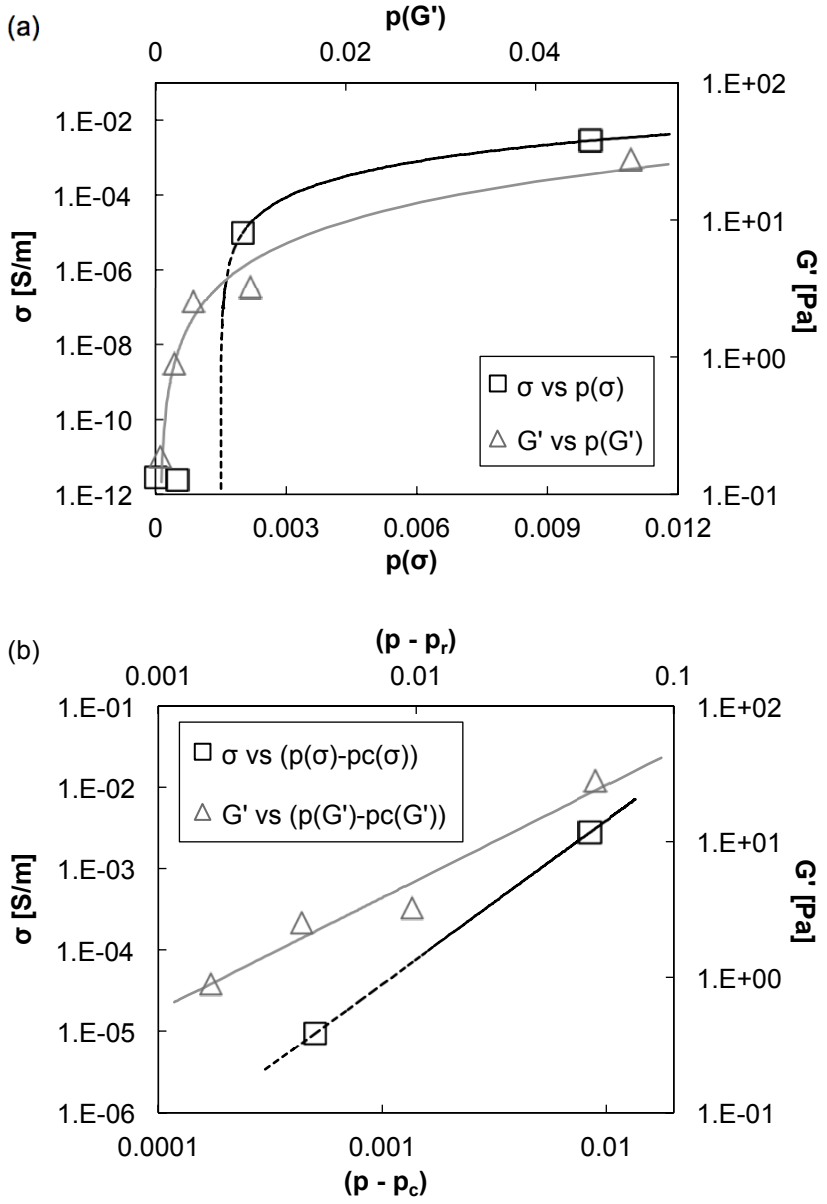

Figure 6.9. (a) Semilogarithmic plot of measured (empty squares) and calculated (dashed line) change in conductivity as well as measured (empty triangles) and calculated (solid line) change in storage modulus with MWCNT mass fraction. σ was obtained at room temperature after polymerization, G' was taken at ω = 9.958 rad/s, and equilibrium strains at which the oscillatory test were performed are specified in Table 6.1. (b) Logarithmic plot of σ vs. $(p - p_c)$ and G' vs. $(p - p_r)$ showing the best fit of Equations 3.3 and 6.4 to the experimental data. Parameters p_c, t, p_r, and u are given in Table 6.2.

The finding that $p_r < p_c$ can be best explained in terms of interparticle separation required for rheological and electrical percolation, respectively. On the one hand, polymer chain mobility is effectively restrained if the interparticle separation is smaller than the size of the polymer chain. The molecular weight of the vinyl-terminated polydimethylsiloxane used in this work is 25000 – 30000. By means of neutron scattering measurements the average radius of gyration of linear PDMS with a molecular weight of 20880 has been determined to be 4.94 nm [290], which correlates well with theoretical considerations taking 0.163 nm for the Si – O bond length, 145° for the Si – O – Si bond angle and 109° for the O – Si – O bond angle. Taking into account the difference in terms of molecular weight, the radius of gyration of the vinyl-terminated polydimethylsiloxane component of the PDMS can thus be estimated to be around 6 nm and the total length of a polymer chain is then roughly 110 nm. The radius of gyration provides an estimate of the size of a PDMS chain when it is in its relaxed state forming a random coil; hence it gives a lower limit for the size of a PDMS chain. Upon flow the polymer chains are deformed and oriented into shear direction and therefore grow in size from this lower limit to a maximum size given by the total chain length. On the other hand, for electrical percolation, interparticle separation within the electron-conducting network has to be small enough to allow for quantum mechanical tunnelling, i.e. a few nanometers only. Consequently, the interparticle separation required for electrical percolation is smaller than the one required for rheological percolation, and therefore $p_r < p_c$.

In conjunction with the above it should also be considered that the fact that at $p \geq p_c$ electron flow is enabled through the formation of a particle network throughout the

polymer matrix does not imply that all particles added to the system contribute to the electron conduction. In fact, as will be discussed with the help of the visualization given in Figure 6.10, the network is formed by only a fraction of these particles.

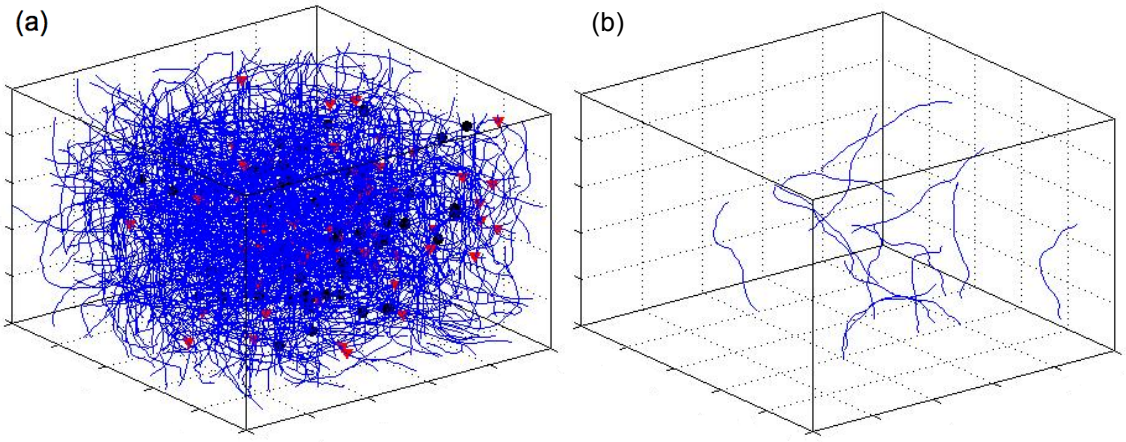

Figure 6.10. (a) Figure obtained with MatLAB visualization script, depicting 1000 CNTs with an aspect ratio of 1000 (blue lines) distributed randomly, and with random orientation, in an element of polymer matrix (white cube), such that CNT volume fraction is 0.0001. Electrical contacts between CNTs are shown as black circles (CNTs in physical contact) and red triangles (distance between CNTs ≤ 5 nm). (b) All CNTs from (a) that have two contact points (CNT to CNT contact or CNT to side of element contact), and can thus potentially contribute to electron conduction. The CNT fraction that fulfills this requirement is 0.014.

Figure 6.10 (a) shows the result of a MatLAB visualization script, depicting 1000 CNTs with an aspect ratio of 1000 (blue lines) distributed randomly and with random orientation in an element of polymer matrix (white cube), such that the CNT volume fraction is 0.0001. The CNTs are not rigid cylindrical rods but are allowed to bend and buckle. Electrical contacts between adjacent CNTs are shown as black circles (CNTs in

physical contact) and red triangles (distance between CNTs ≤ 5 nm). For the nanocomposite to conduct electrons, an electrically interconnected CNT network has to span the material. Figure 6.10 (b) shows all CNTs from Figure 6.10 (a) that have at least two contact points (CNT to CNT contact or CNT to side of element contact), and can thus potentially contribute to electron conduction. As can be seen, the number of CNTs is reduced drastically, as only 1.4 % of the CNTs fulfill this requirement. In fact no electron-conducting path spans the entire sample and the nanocomposite as shown in Figure 6.10 (a) would not conduct electrons, as can actually be expected given the low particle volume fraction. For it to become electroconductive, more CNTs would need to be added to the element of polymer matrix.

Now, the particle fraction contributing to electron conduction naturally depends on the limit set for interparticle separation; i.e., if in addition to the electrical contacts shown in Figure 6.10 (a), adjacent CNTs with an interparticle separation between 5 nm and 15 nm would also be considered as electrical contacts, the number of CNTs in Figure 6.10 (b) would be much higher. Correspondingly, at a given particle mass fraction above both the rheological and the electrical percolation threshold, the particle fraction contributing to rheological percolation is higher than the particle fraction contributing to electrical percolation; thence, $p_r < p_c$.

6.4.1.5 A first look at network optimization

As introduced in Chapter 6.1, the application of an external field allows for the formation of electron-conducting CNT – polymer nanocomposites at $p < p_c$, where p_c is

the percolation threshold of the CNT – polymer nanocomposite produced without the external field. In Table 6.3, the p_c and t values obtained in this Chapter (cf. Table 6.2) are compared to the ones reported in Chapters 3 and 5.

Table 6.3. Percolation thresholds and conductivity exponents obtained by fitting Equation 3.3 to experimental data obtained on (a) thin films produced by solution casting (cf. Chapter 3), (c) thin films produced by solution casting followed by shear flow (this chapter), and (b) cube samples produced by solution casting (cf. Chapter 5).

	Sample type and processing technique	p_c	t
(a)	Thin films (± 1mm thick) produced by solution casting onto flat surface	0.00313	2.2
(b)	Thin films (± 1mm thick) produced by solution casting and shear flow	0.00145	2.07
(c)	Strained 1 cm^3 cube samples produced by solution casting into mould	0.00325	2.8

A comparison between (a) and (b) reveals that shear flow during material processing leads to lower p_c and t values. In parallel, the electrical conductivity of the material is increased significantly: at $p = 0.01$, $\sigma = 2.9\times10^{-4}$ S/m for (a) whereas $\sigma = 2.8\times10^{-3}$ S/m for (b). It appears that network restructuring during flow (disintegration of agglomerates as well as reshaping, reorientation, and relative movement of the particles) leads to an optimized MWCNT network, with an increased fraction of MWCNTs contributing to electron conduction (decrease in p_c and increase in σ) and a more uniform three-dimensional network, with a narrower distribution in local conductances (convergence of t towards $t = 2$). It should be noted that (a) and (b) differ in the type of PDMS used as matrix material (Gelest OE41 and Gelest Gel D200, respectively); it is however unlikely that this has an influence on the difference in percolation parameters because both types

of PDMS are formed by the same reacting groups and have the same bond forming chemistry. The above finding is supported by data reported in Figure 2 of [151], which studies the influence of material processing on p_c and reports a decrease in both p_c and t when an external force field is used during material processing. The matrix material in [151] was the same for all processing routes. The influence of the use of an external field on t was not discussed.

It can further be seen in Table 6.3 that t depends on sample volume and shape. For (a) and (c) matrix material and processing technique were the same, the samples differ in shape and volume though. While p_c remains more or less unchanged, t increases with increasing volume. This is in line with information provided above: first, p_c is only dependent on network configuration and should not depend on the size of the network, and second, it seems plausible that the larger the distance spanned by the electron-conducting network, the wider the distribution of local conductances, and thus the larger t. Studying the effect of network optimization on t therefore requires constant sample geometry, which is not the case for the data reported in Figure 6.2.

6.4.2 Network optimization by means of an electric field

6.4.2.1 Exposure to an electric field

In the following, the process of network optimization by means of an external field will be looked at in more detail. The external field was an electric one. MWCNTs dispersed in fluid PDMS react to an electric field by both electrophoresis and dielectrophoresis [241, 246]: on the one hand, charged MWCNTs can migrate in the

suspension under the effect of the electric field, and, on the other hand, induced dipoles react with each other, which results in translational and rotational forces exerted by the electric field on the MWCNTs. Figure 6.11 shows the evolution of electrical resistivity, ρ, with time of exposure to an electric field, for varying particle mass fractions and electric field strengths.

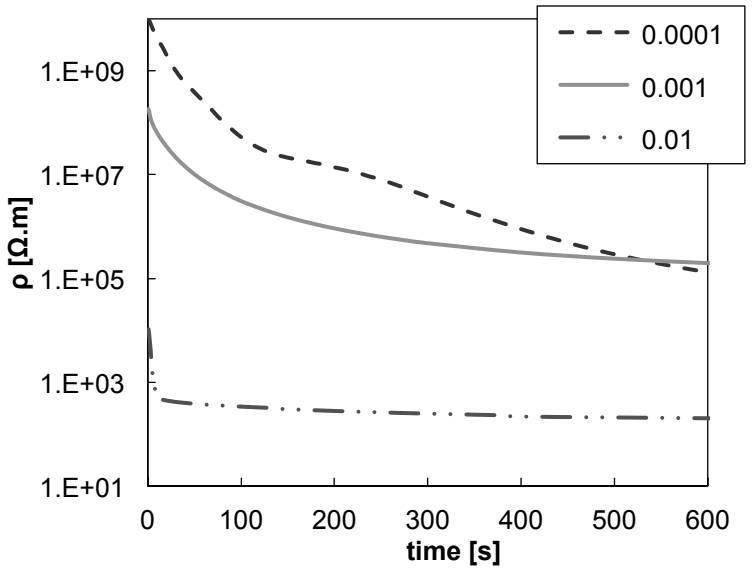

Figure 6.11. Semilogarithmic plot of evolution on electrical resistivity with time of exposure to an electric field, for MWCNT modified PDMS with three different MWCNT mass fractions, which are specified in the legend. (V_{OV} [V], V_{AV} [V], λ [μm]) were (200, 50, 1050) at p = 0.0001, (40, 0, 1250) at p = 0.001, and (10, 0, 1650) at p = 0.01.

For all p, ρ decreases with increasing time of exposure to the electric field. The attainable decrease in ρ depends on both p and E: after 550 s of exposure, for instance, $\rho = 2\times10^5$ Ω.m for both p = 0.0001 and p = 0.001 when exposing MWCNT modified PDMS at p = 0.0001 to E = 190.4 $kV.m^{-1}$ and MWCNT modified PDMS at p = 0.001 to E = 32.0 $kV.m^{-1}$. It can also be seen that as p increases the MWCNT network reacts faster to the

electric field; the slopes at the beginning of the ρ vs. time curves increase with p, despite the fact that E was lower for higher p.

In Figure 6.12 the evolution of electrical resistivity with time of exposure to an electric field is given for a constant p but varying electric field strengths.

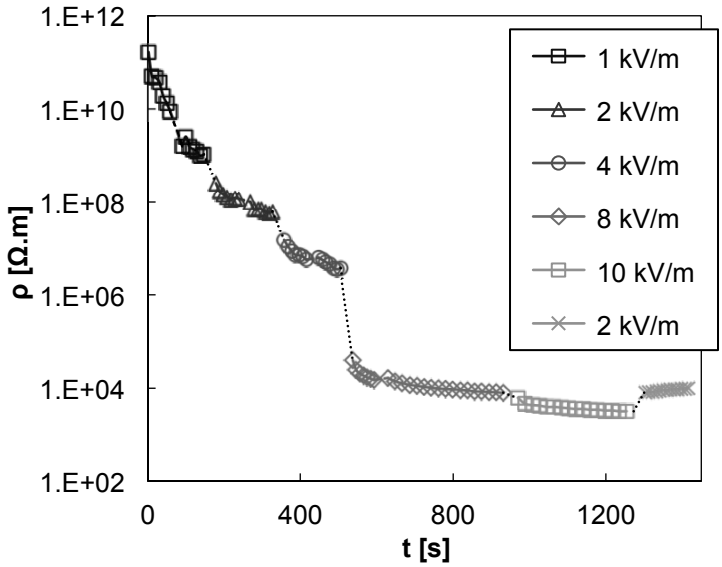

Figure 6.12. Semilogarithmic plot of evolution on electrical resistivity with time of exposure to an electric field with varying field strength. Electric field strengths are specified in the legend, p = 0.002, λ = 990 μm, and τ = 60 – 300 s.

As can be seen, network optimization allows for a signification increase in electrical performance. Without exposure to the electric field, a MWCNT – PDMS nanocomposite with 0.2 wt.% MWCNT is electrically insulating, with $\sigma = 2.4\times10^{-12}$ S/m., whereas after exposure to the electric field it is electroconductive, with $\sigma = 4\times10^{-4}$ S/m, which corresponds to a nine order of magnitude increase in electrical conductivity. As will be shown in Chapter 6.4.3, σ after exposure but prior to polymerization does not directly

translate to σ after polymerization; the increase in electrical conductivity with exposure to an electric field is significant all the same. By looking at the last set of data in Figure 6.12 it can further be seen that the highly reorganized MWCNT network is not in equilibrium, a reduction of the electric field strength results in a steady recovery in ρ.

6.4.2.2 Dispersion analysis

SEM images of 1.0 wt. MWCNT modified PDMS samples produced (a) without and (b) with the use of an external field are shown in Figure 6.13. MWCNTs are clearly distinguishable as bright spots from the dark grey PDMS matrix. The bright lines are part of the cleavage pattern that stems from freeze breaking during sample preparation (cf. Chapter 6.3.5).

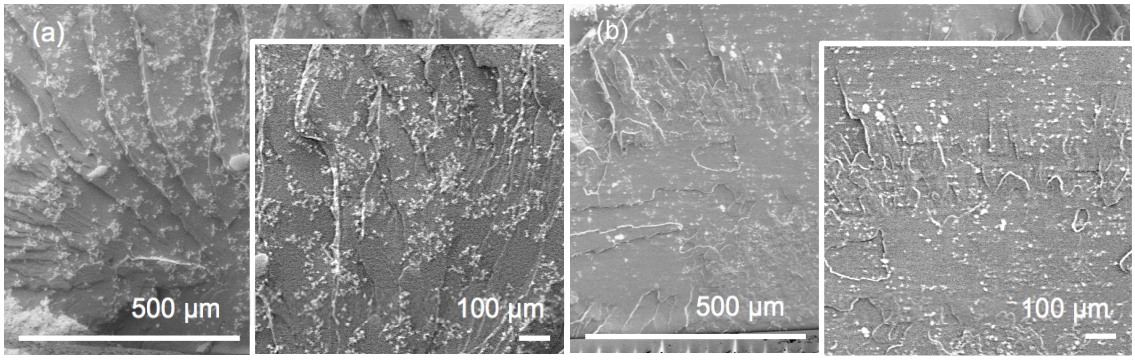

Figure 6.13. SEM images of (a) non-exposed and (b) exposed MWCNT modified PDMS, recorded on a Hitachi SU-8000 cold-field emission scanning electron microscope as described in Section 6.3.5. p = 0.01, and working distances were 7.0 mm in (a) and 7.2 mm in (b). Inset show sharpened images.

As is brought out in the insets of Figure 6.13, qualitatively, image (b) clearly appears to be more organized and its network to be more uniform. In order to assess the MWCNT

dispersion also quantitatively, the images were analysed using an algorithm developed for this purpose [291]. Image processing is outlined in Figure 6.14. Different square regions (115 × 115 pixels in size) of the SEM images were selected manually to leave the cleavage pattern from freeze breaking out from the analysis. The squares were transformed to binary images, that were then divided into matrix and particle elements, based on which the distance between each matrix element to the nearest particle element was calculated. With that, for each image a dispersion index, DI, was defined by comparing the mean value of the nearest neighbour distances for the given image with that of an ideal uniformly dispersed case; DI = 100% for the case of uniform dispersion while it decreases as the non-uniformity of the network increases. More information can be found in the reference. Subsets of 3 × 3 pixels were defined as individual MWCNTs (cf. Figure 6.15). Results from the quantitative dispersion analysis are given in Table 6.4, where the dispersion indices are given together with the corresponding white pixel fractions, WPF.

Table 6.4. Result from application of quantitative dispersion analysis [291] to the SEM images given in Figure 6.13, giving the dispersion index, DI, as well as the white pixel fraction, WPF, for non-optimized (a) and optimized (b) MWCNT in PDMS networks.

Region		1	2	3	4	5	6	Average
(a)	DI [%]	73.12	69.75	69.34	75.20	71.82	72.76	72
	WPF	0.14	0.09	0.14	0.09	0.11	0.11	0.11
(b)	DI [%]	87.50	84.99	91.74				88
	WPF	0.05	0.07	0.03				0.05

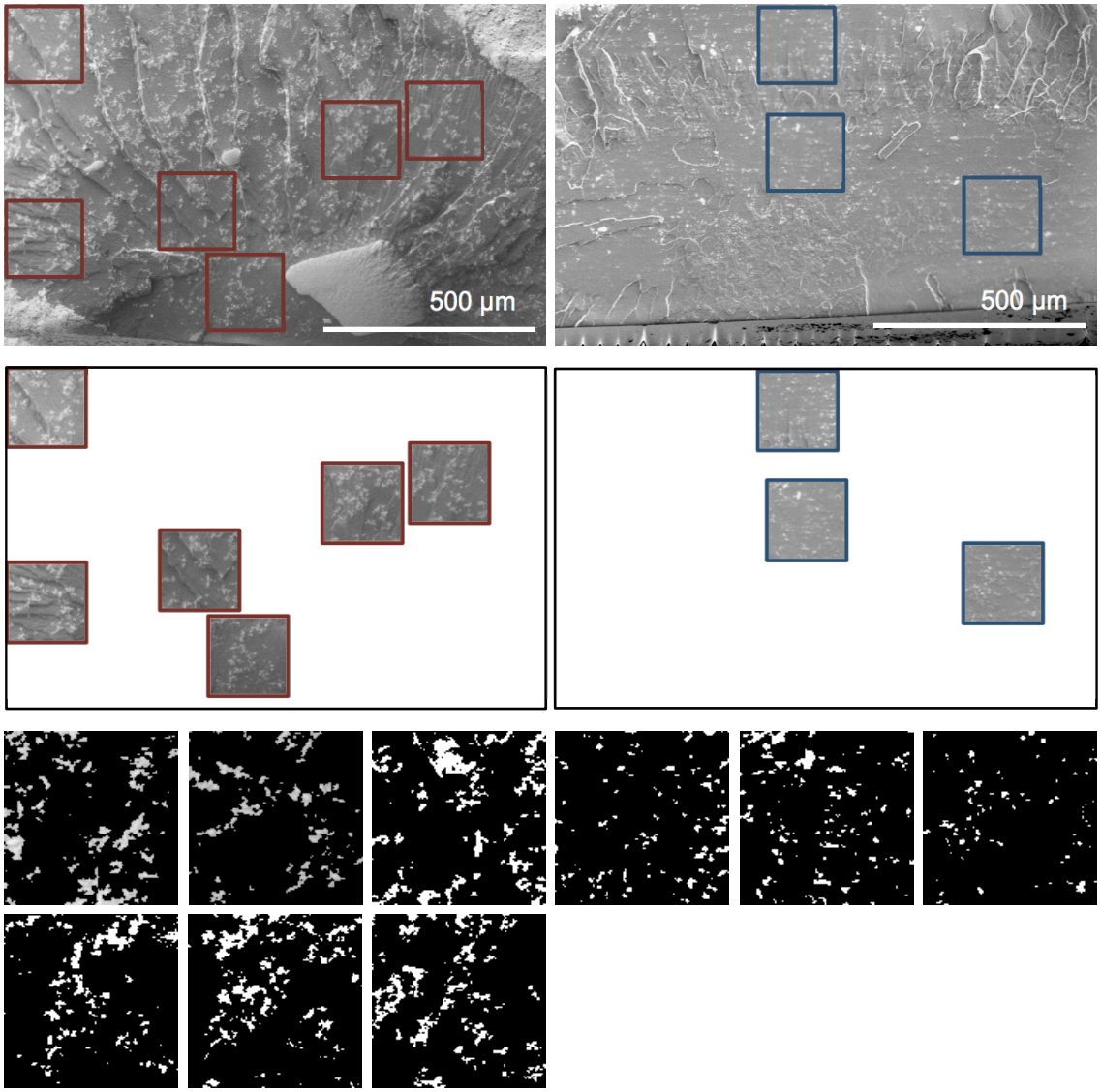

Figure 6.14. Image processing for application of quantitative dispersion analysis [291] to SEM images shown in Figure 6.13. Different regions of the SEM images were selected manually (top, red and blue squares) to leave the cleavage pattern from freeze breaking out from the analysis (middle). Each square was 115 × 115 pixels and has then been transformed to a binary image (bottom, black and white images).

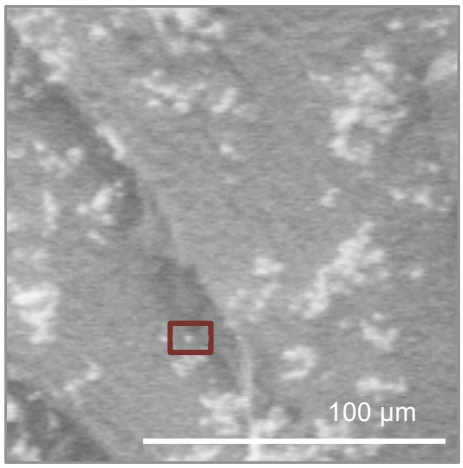

Figure 6.15. Definition of the size of an individual particle that can be recognized in the images as a subset of 3 × 3 pixels. An example is highlighted in the red rectangle.

The DI values show that the MWCNT network in (b) is indeed more uniform. The WPF values confirm the visual impression that the number of bright spots is lower in (b) compared to (a). The reason for this is that the SEM analysis is restricted to a small area of the sample and therefor prone to local variations in particle mass fraction. The overall particle mass fraction was the same in (a) and (b) as both samples have been produced from the same MWCNT in PDMS suspension. Note that a difference in WPF does not affect the result, as the analysis does not depend on p.

6.4.2.3 The influence of optimized percolation on t

The more uniform the network, the narrower the distribution of local conductances, and the smaller the conductivity exponent [14]. Accordingly, if sample volume and shape remain unchanged, optimized MWCNT in PDMS networks should exhibit not only lower p_c values but also lower t values. This has been observed in Chapter 6.4.1.4 and is looked

at in Figure 6.16, where the electrical conductivity as a function of MWCNT mass fraction is given for MWCNT – PDMS nanocomposites produced with (empty triangles) and without (empty squares) the use of an electric field. Parameters p_c and t, characterizing electrical percolation, were obtained by means of a logarithmic plot of σ vs. $(p - p_c)$ (cf. Figure 6.16 b) where p_c was incrementally varied until the best linear fit of Equation 3.3 to the experimental data was obtained; p_c and t values are given in Table 6.5, together with the corresponding proportionality constants σ_x used to fit Equations 3.3 to the semilogarithmic plots of σ vs. p (solid and dashed line), as well as the coefficients of determination R^2.

Table 6.5. Electrical percolation parameters p_c and t, proportionality constant σ_x, and coefficient of determination R^2, for fit Equations 3.3 to experimental data in Figure 6.16.

	p_c	t	σ_x	R^2
Non-optimized	0.00305	2.2	7	0.99527
Optimized	0.00192	2.05	54	0.99856

Figure 6.16 and Table 6.5 reveal that the use of an electric field during MWCNT – PDMS nanocomposite preparation, just as the use of a force field (cf. Chapter 6.4.1.4), first, shifts the σ vs. p curve to higher σ and lower p_c values and, second, leads to a decrease in t. An optimized MWCNT network, with an increased fraction of MWCNTs contributing to electron conduction (decrease in p_c and increase in σ) and a more uniform three-dimensional network, with a narrower distribution in local conductances (convergence of t towards t = 2) is formed through network restructuring due to electrophoretic and dielectrophoretic effects.

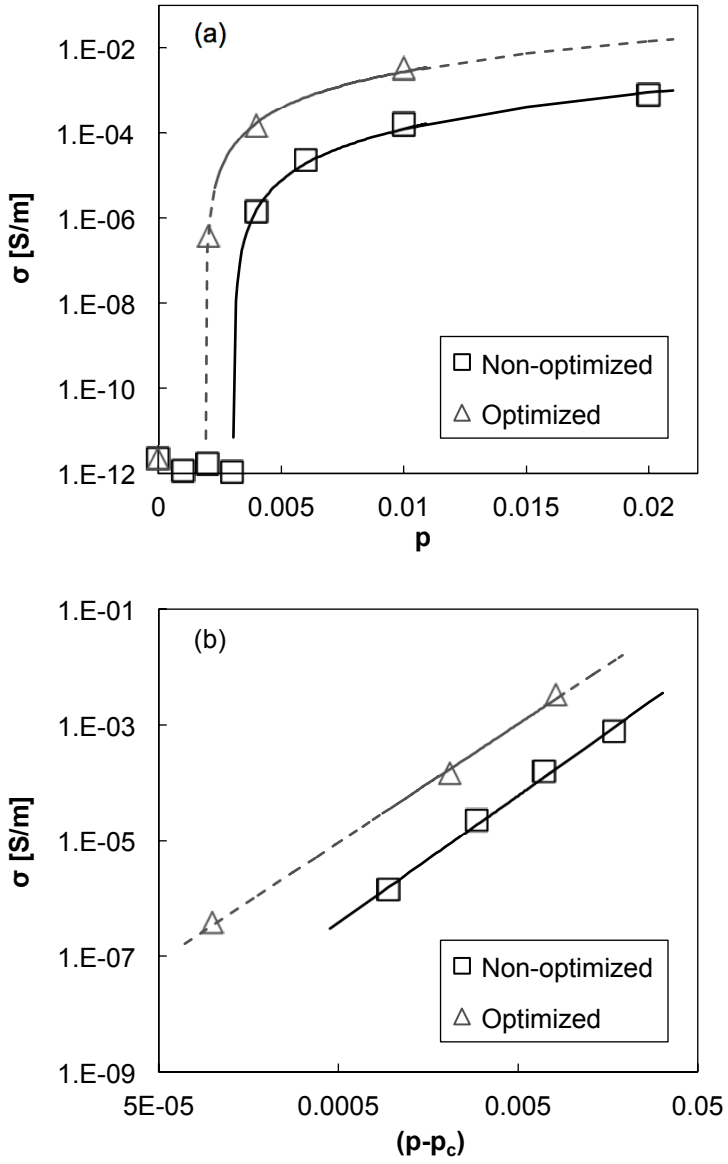

Figure 6.16. (a) Semilogarithmic plot of measured (empty squares and triangles) and calculated (full and dashed lines) change in electrical conductivity with MWCNT mass fraction for both non-optimized and optimized MWCNT in PDMS networks. σ was obtained at room temperature, after polymerization. (b) Logarithmic plot of σ vs. $(p - p_c)$ showing the best fit of Equations 3.3 to the experimental data. Parameters p_c and t are given in Table 6.5.

As outlined in Chapter 6.1 it was originally thought that t was limited to universal values depending only on the dimensionality of the particle network. Although it has been accepted for some time now that t can have higher values, it should be noted that until quite recently, it was believed that no geometrical information about the particle network could be obtained from t [26]. Based on Balberg's theoretical work [224-227], and their own experimental findings, Scardaci et al. [14] proposed that the distribution of local conductances can vary with network morphology such that non-uniform networks would display higher t values. The present study is the first comprehensive experimental proof for this view. By studying electrical percolation with and without network optimization, in combination with a quantitative dispersion analysis of both optimized and non-optimized networks it was possible to correlate the evolutions in network morphology and conductivity exponent.

Scardaci et al. showed that the optoelectronic properties of high aspect ratio particles based nanocomposites scale with network non-uniformity, which in turn increases with t; low-resistance, high-transparency films therefore require low t values. With the here presented results this observation can be explained as follows: as t is decreased, the particle fraction contributing to electron conduction is increased; for a given sheet resistance, R_S, an optimized particle network (characterized by a low t value) will therefore exhibit higher optical transparency because fewer particles need to be added to the system in order to achieve R_S. More generally, for a given electrical performance of a bulk CNT – polymer nanocomposite, low t values are essential for a minimal impairment of the polymeric characters of the nanocomposite.

6.4.2.4 The origins of the increase in electrical conductivity

It remains however the questions what microstructural changes cause the electrical conductivity to increase during network optimization, for a narrower distribution in local conductances does not per se imply higher electrical conductivity. An increase in σ can be due to (i) a decrease in the mean interparticle distance within the electron-conducting network (decrease in average contact resistance within electron-conducting paths) and or (ii) a growth of the particle network (formation of additional electron-conducting paths). As has been discussed in Chapter 3.4.5, MWCNT – PDMS nanocomposites exhibit non-linear current voltage characteristics due to the fact that electron conduction is dominated by quantum mechanical tunnelling. It can be derived from Equation 3.4 that the current density decreases exponentially with increasing distance between adjacent particles. Consequently, the non-linearity of the IV characteristics increases as the average interparticle distance within electron-conducting paths increases. A measure of this non-linearity is the resistance ratio, R_R:

$$R_R = \frac{R_l}{R_h}, \tag{6.5}$$

where R_l is calculated from an applied voltage V_l and the corresponding measured current I_l, and R_h is calculated from an applied voltage $V_h > V_l$ and the corresponding measured current I_h. A non-linear IV behaviour is characterized by $R_R > 1$, and the higher R_R the more pronounced the non-linearity. Figures 6.17 and 6.18 give the evolution of R_R during network optimization in MWCNT modified PDMS for three different MWCNT mass fractions, a particle mass fraction below the optimized percolation threshold, $p_c^{optimized}$, a

particle mass fraction between $p_c^{optimized}$ and the non-optimized percolation threshold, p_c, and a particle mass fraction above p_c (cf. Table 6.5).

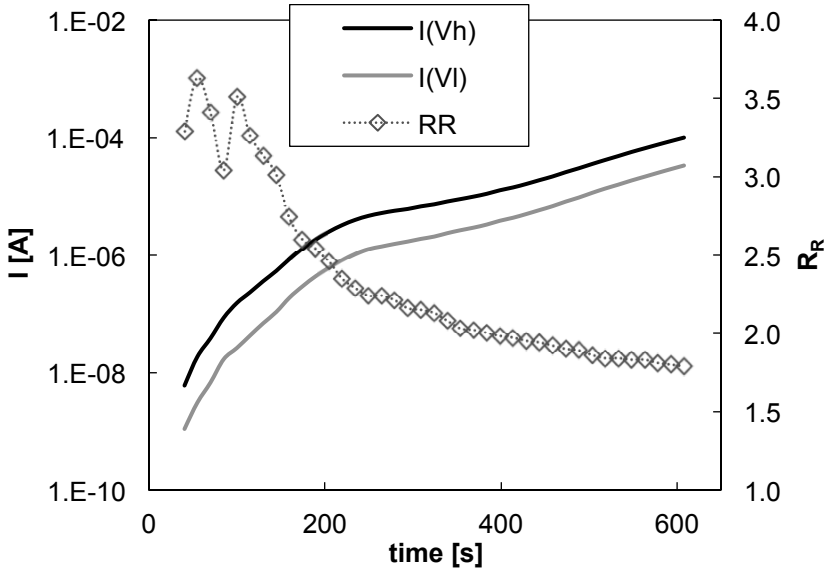

Figure 6.17. Semi-logarithmic plot of evolution of current and resistance ratio with time of exposure to an electric field, for a MWCNT modified PDMS with p = 0.0001. V_{OV} = 200 V, V_{AV} = 50 V, and λ = 1050 μm.

R_R was obtained by means of the alternating polarity method (cf. Chapter 6.3.4) and the results are plotted together with the measured currents I_l and I_h. As expected $R_R > 1$ for all p. Interestingly, the result at $p < p_c^{optimized}$ differs from the one at $p > p_c^{optimized}$, but is the same for $p_c^{optimized} < p < p_c$ and $p > p_c$. At $p < p_c^{optimized}$ R_R decreases with increasing time of exposure to the electric field, while the electrical currents, and, hence, the electrical conductivity of the material, increase. Accordingly, electrophoretic and dielectrophoretic effects lead to the formation of electron-conducting paths and to a mutual approach between the particles within the electron-conducting paths, which

decreases the mean interparticle distance within the electron-conducting paths. In contrast, at $p > p_c^{optimized}$ the increase in electrical conductivity is not accompanied by a decrease in R_R, which remains more or less constant; thus it appears that the increase in electrical conductivity is predominantly due to the formation of additional electron-conducting paths, as the fraction of MWCNTs contributing to electron conduction is increased and the percolated network is grown.

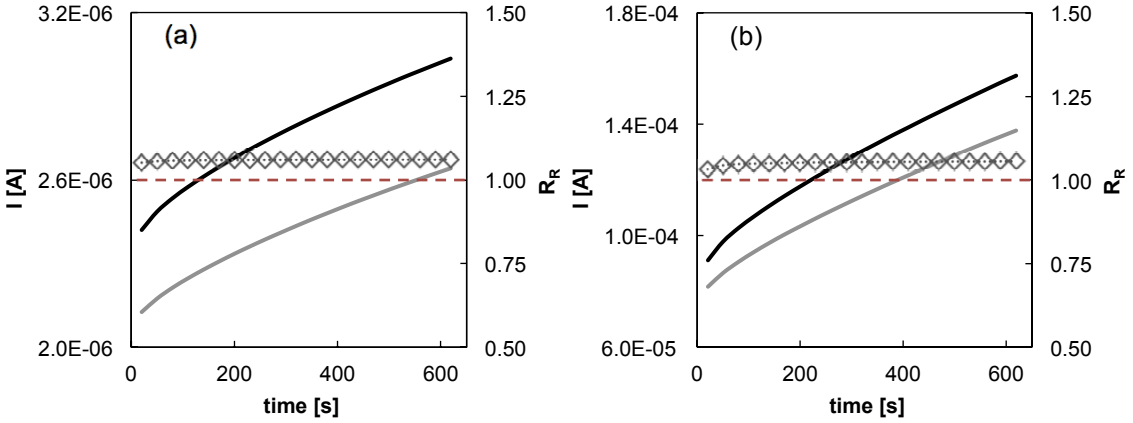

Figure 6.18. Semi-logarithmic plots of evolution of current and resistance ratio with time of exposure to an electric field, for MWCNT modified PDMS with (a) p = 0.002 and (b) p = 0.004. V_{OV} = 50 V, V_{AV} = 2 V, and λ = 1950 μm. The legend is given in Figure 6.17. The dashed red lines indicate R_R = 1.

The following picture emerges: electrophoresis and dielectrophoresis effects lead to (1) a mutual approach between particles within electron-conducting paths and (2) the formation of the additional electron-conducting paths. At sufficiently low p the electrical characteristics are mainly affected by (1), whereas at higher p, changes in the electrical behaviour are due to (2). Given that this results seems somewhat intuitive, it should be

noted that although it has been clear for some time now that the exposure to an electric field leads to an increase in electrical conductivity and that this is due to the particle network reacting to the external field, quite different viewpoints have been presented with regard to the microstructural changes within the particle network [125, 239-248]. This might be explained with the fact that the critical concentration at which the dominate microstructural features changes from (1) to (2) is not given by p_c, but by $p_c^{optimized}$ instead, which naturally depends on the optimization process itself.

6.4.3 Evolution of electrical resistance during polymerization

As mentioned before, a MWCNT network optimized by means of an electric field is not in equilibrium (cf. last set of data in Figure 6.12); if the electric field is reduced or removed, the network relaxes and part of the network restructuring is reversed, which is likely due to Brownian motion and repulsive coulombic force [292]. Producing a MWCNT – PDMS nanocomposite with a fully optimized particle network therefore requires the external field to be active during polymerization. For $p < p_c^{optimized}$, $p_c^{optimized} < p < p_c$, and $p >> p_c$ (cf. Table 6.5), Figures 6.19 and 6.20 give the evolution of electrical resistance during polymerization, which is monitored by recording the viscoelastic properties of the material simultaneously. As the temperature is increased, vinyl-terminated polydimethylsiloxane and methylhydrosiloxane–dimethylsiloxane copolymer react via platinum catalyzed hydrosilylation and form a three-dimensional network. This results in a sharp increase in the viscoelastic flow resistance of the material (η^*) as well as the elastic portion of the viscoelastic behaviour (G').

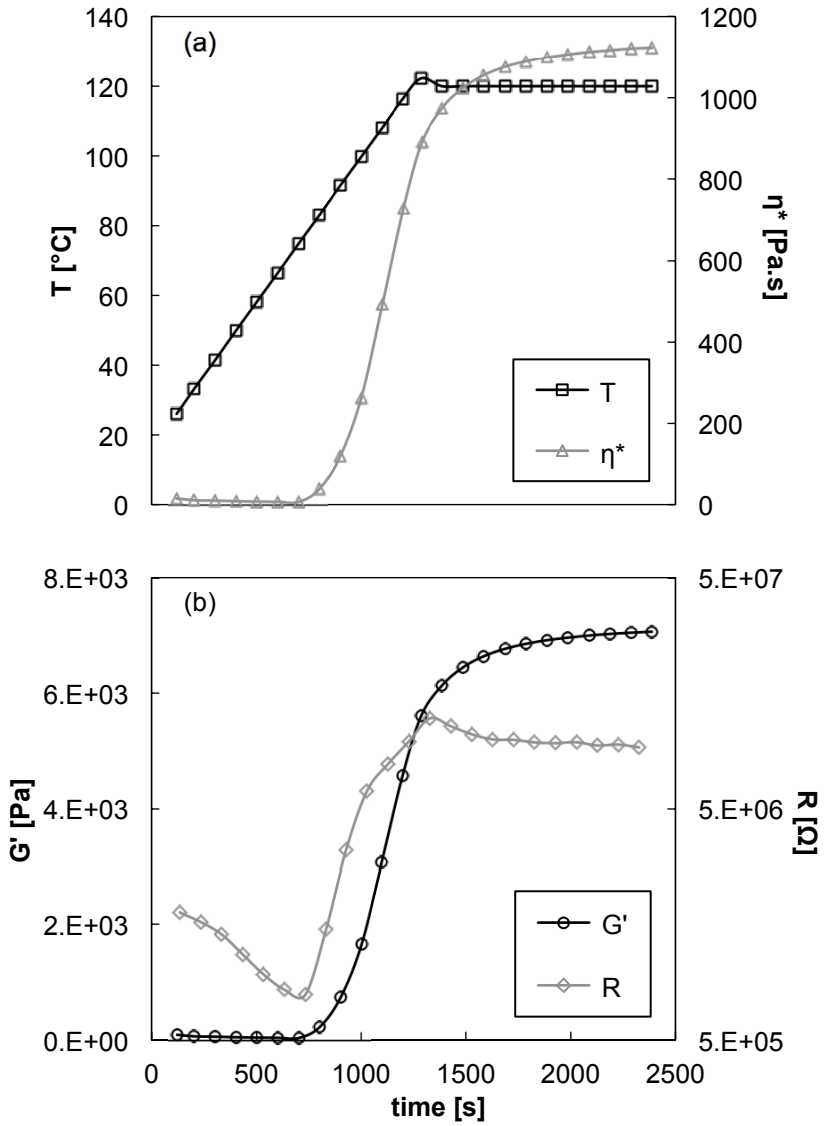

Figure 6.19. Simultaneous monitoring of rheological and electric properties during polymerization of MWCNT modified PDMS; showing (a) T and η^* vs. time and (b) G' and R vs. time. p = 0.0001, ω = 6.283 rad/s, γ = 10 %, temperature ramp = 5 °C/min, λ = 1050 µm, V_{OV} = 4 V, and V_{AV} = 2 V.

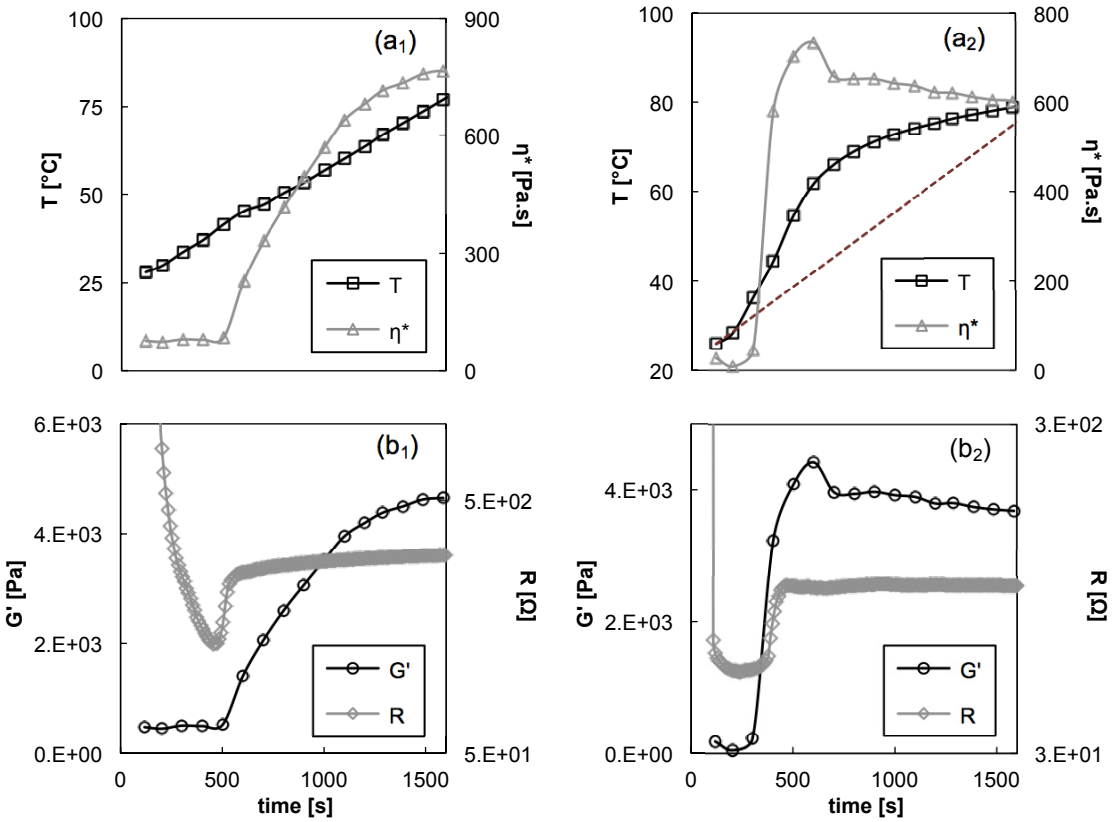

Figure 6.20. Simultaneous monitoring of rheological and electric properties during polymerization of MWCNT modified PDMS, showing (a) T and η^* vs. time, and (b) G' and R vs. time. Temperature ramp = 2 °C/min, ω = 6.283 rad/s, γ = 0.1 %, V_{OV} = 35 V, and V_{AV} = 0 V. Left: p = 0.002 and λ = 1690 µm. Right: p = 0.01 and λ = 1920 µm. The dashed line in (a_2) indicates T vs. time according to the selected ramp rate.

Prior to heating, all three MWCNT – PDMS nanocomposites were exposed to an electric field in order to induce an optimized MWCNT network (cf. Figure 6.11). A decrease in electrical resistance can be observed prior to the onset of cure, which can be explained by a combination of both a further CNT rearrangement within the uncured polymer and an increased electrical performance due to an increase in temperature. During cure, the material was exposed to a mean electrical field smaller than the one used

during network optimization; further CNT rearrangement within the uncured polymer solely due to exposure to an external electric field is therefore unlikely. The added thermal energy, however, might increase CNT mobility and, hence, enable further CNT rearrangement within the uncured polymer. In addition, CNT modified polymers are known to show semiconducting behaviour and to exhibit a positive interdependence of electrical conductivity and temperature (cf. Chapter 3.4.5).

At all MWCNT mass fractions polymerization is accompanied by an increase in electrical resistance of the material. Given that the electrical resistance of CNT modified polymers typically decreases with temperature, the observed changes cannot be caused by the rise in temperature. They can, however, be well explained with a change in the dielectric constant of the matrix, as the dielectric constant of PDMS increases with the degree of polymerization [111]. For a given interparticle separation, the tunnelling probability and, so, the local conductance decrease with increasing dielectric constant of the insulating material separating the particles. According to the picture presented in Chapter 6.4.2.4, at low p, where changes in R are primarily caused by microstructural changes within the few electron-conducting paths, this effect should then be more pronounced. The larger the percolated network (the higher the electron-conducting paths), the smaller the influence of changes within individual electron-conducting paths on the overall electrical resistance.

This is what is observed in Figures 6.19 and 6.20: at $p < p_c^{optimized}$ R increases by a factor of 13.4, whereas at $p > p_c^{optimized}$ the increase in R is about 10 times smaller, i.e. R increases by a factor of 1.89 at p = 0.002, and by a factor of 1.72 p = 0.01. It should be

noted that alterations to the structure of the particle network, e.g. due to chemical shrinkage, might also play a role in the observed change in R [293]; given the good dimensional stability during polymerization of the MWCNT – PDMS system studied here, this effect seems negligible though. Finally it is interesting to find that in contrast to Figure 6.19, the temperature profiles in Figure 6.20 are not linear but show an increase in heating rate, which correlates with the onset of the increase in R. This is likely due to the electroconductive MWCNT network providing additional heat through resistive heating.

6.5 Summary and Conclusions

As has been elaborated in Chapters 3 to 5, the electrical and multifunctional performance of CNT – polymer nanocomposites is controlled by percolation, involves quantum mechanical tunnelling at CNT junctions, and is primarily dependant on the configuration of the CNT network. As the particle network is formed during processing, when the material is in a fluid state of low viscosity, the configuration of the network depends on the processing conditions, which in turn can be adapted to optimize the structure of a percolated network (e.g., exposure to an external field). Despite a rather large body of literature on network formation and optimized percolation in CNT – polymer nanocomposites, two fundamental aspects remain unclear to date: first, although it is known that network optimization shifts the electrical percolation curve to lower percolation threshold and higher electrical conductivity values, it is unclear if and in what way it affects the conductivity exponent, and, second, a clear picture of the microstructural changes that form the basis of the increase in electrical conductivity is

missing. The present chapter addressed both of these aspects via a comprehensive study of network formation and optimized percolation in MWCNT modified PDMS.

It is shown that MWCNT addition to PDMS affects polymer chain mobility, such that the ideal-viscous PDMS becomes viscoelastic and exhibits nonlinear flow behaviour, i.e. shear thinning and large negative 1st normal stress coefficients. This is accompanied by changes in material viscosity, rigidity, and firmness, which all increase with particle mass fraction. It is further shown that the rheological characteristics of PDMS are altered at particle mass fractions as low as p = 0.0005, which indicates good particle dispersion. In line with this, the rheological percolation threshold, which was determined using the recordings of the storage modulus, is found to be at p_r = 0.00015, whereas the corresponding electrical percolation threshold is found at p_c = 0.00145. It is shown that the fact that $p_r < p_c$ is related to the difference in interparticle separation required for rheological and electrical percolation, respectively, which is smaller for electrical percolation. By comparing the percolation parameters of non-optimized MWCNT in PDMS networks with a MWCNT in PDMS network optimized by means of a force field, it is further shown that t varies with the spread of the network, unlike p_c, which does not depend on network geometry, and that, for comparable network geometries, both percolation parameters decrease with network optimization.

This is confirmed by combining a study of network optimization by means of an electric field with a quantitative dispersion analysis. It is shown that network restructuring by means of electrophoretic and dielectrophoretic effects lead to an increase in dispersion index and electrical conductivity, but a decrease in both percolation

threshold and conductivity exponent. In the optimized MWCNT in PDMS network, the fraction of MWCNTs contributing to electron conduction is increased (decrease in p_c and increase in σ) and the three-dimensional network is more uniform and exhibits a narrower distribution in local conductances (increase in DI and decrease in t). Besides, it is also demonstrated that optimized percolation enables a nine orders of magnitudes increase in electrical conductivity.

By studying the evolution of the electrical resistance ratio during network optimization it is further established that the increase in electrical conductivity is due to a combination of (i) a decrease in the mean interparticle distance within the electron-conducting network (decrease in average contact resistance within electron-conducting paths) and (ii) a growth of the particle network (formation of additional electron-conducting paths), and that at particle mass fractions below a critical one (i) dominates, whereas at particle mass fractions above that critical one (ii) dominates. The critical mass fraction is given by the optimized percolation threshold, which naturally depends on the optimization process itself. A study of the evolution of electrical resistance ratio during polymerization of the elastomeric matrix confirmed this picture, as it is shown that the increase in electrical resistance during polymerization, which is caused by a change in the dielectric constant of PDMS, is about ten times higher at particle mass fraction below the optimized percolation threshold, compared to the increase in electrical resistance at particle mass fractions above the optimized percolation threshold.

CHAPTER 7

Conclusions

7.1 Original Contributions

The thesis in hand has dealt with electron conduction in carbon nanotube modified polymers, with a focus on the configurational characteristics of the particle network that underlie the electrical behaviour of the material. The contributions of this thesis to the state-of-the-art-knowledge can be summarised as follows:

1. The particle mass fraction dependent electrical and rheological properties of a MWCNT – PDMS system were investigated in detail (cf. Chapters 3 and 6).

   Compared to thermoplastic and thermosetting polymer based electroconductive nanocomposites, information on elastomeric polymer based systems such as MWCNT modified PDMS is relatively scarce. It was shown that with increasing particle mass fraction MWCNT modified PDMS exhibits an insulator to conductor transition, which is due to the formation of an electron-conducting MWCNT network throughout the electrically non-conducting PDMS matrix. Simultaneously, the ideal-viscous PDMS becomes viscoelastic and exhibits nonlinear flow behaviour because the MWCNTs affect polymer chain mobility. The evolutions of both the electrical

conductivity and the elastic portion of the viscoelastic behaviour with particle mass fraction are characteristic of percolation. The electrical percolation threshold was found to be one order of magnitude higher than the rheological equivalent, which was identified to be a result of the difference in average interparticle separation required for electrical and rheological percolation, respectively.

2. The electrical conductivity of a loose three-dimensional network of Baytubes C 150 P without polymer matrix was measured (cf. Chapter 3).

   A simple technique was developed to measure the electrical conductivity of a loose three-dimensional network of CNTs without polymer matrix. For the MWCNTs used in the research at hand, i.e. Baytubes C 150 P, the electrical conductivity was found to be around 2 S/m. Values reported in literature for the electrical conductivity of dry MWCNT networks are typically two to three orders of magnitude higher; however, they are not representative of loose three-dimensional networks as they have been measured on thin films produced by filtration, which naturally exhibit a relatively high anisotropy in in-plane to perpendicular electrical conductivity due to CNT alignment during filtration. The electrical conductivity of a loose three-dimensional CNT network gives an estimate of the maximum electrical conductivity that can be achieved by adding CNTs to a polymer. With Baytubes C 150 P being widely used in research on MWCNT modified polymers it was highlighted that the majority of the maximum electrical conductivity values reported in literature for bulk CNT – polymer nanocomposites are ≤ 2 S/m.

3. A clear picture describing electron conduction in carbon nanotube modified polymers as well as its dependence on configurational characteristics of the particle network was presented (cf. Chapters 3 and 4).

   The dependence of the electrical conductivity on frequency and temperature, the current-voltage characteristics, and the electric response to mechanical deformation were analyzed as a function of particle mass fraction. At particle mass fractions above but close to the percolation threshold the electrical characteristics of MWCNT modified PDMS are dominated by the behaviour of individual electron-conducting paths, in which electron conduction is controlled by quantum mechanical tunnelling between adjacent but non-contacting CNTs. At higher particle mass fractions, on the other hand, despite quantum mechanical tunnelling events within the individual electron-conducting paths, the electrical characteristics of MWCNT modified PDMS are dominated by the behaviour of the network as a whole, which can be viewed as a resistor network.

4. The problem of positive vs. negative piezoresistance in high aspect ratio particle based polymer nanocomposites was addressed both experimentally and theoretically and piezoresistance in electroconductive nanocomposites in general was explained (cf. Chapters 4 and 5).

   A percolation theory based model relating the variation in electrical resistance to compressive strain was introduced and it was shown that it gives accurate theoretical fits to experimental data presented in this thesis, as well as to much of the available data in the literature. In contrast to existing theories, the model captures the

characteristics of the particle network through experimentally definable parameters and does not rely on assumptions regarding the nature of the particles and or the configuration of the network. It was explained why current theories fail to generally describe the experimental findings and it was demonstrated that the presented theoretical framework is not limited to polymer nanocomposites with high aspect ratio particles but that it can explain piezoresistance in bulk electroconductive nanocomposites in general. It was found that the piezoresistive effect in such materials is rooted in a mechanical deformation induced change in the distribution of local conductances within the electron-conducting particle network. In addition, it was shown that the findings can be applied to the experimentally observed concentration dependence of the piezoresistance in electroconductive nanocomposites and, thus, to predicting the electric response to mechanical deformation at any particle concentration.

5. It is shown that the conductivity exponent depends on the distribution of local conductances within the electron-conducting particle network, and that the latter varies with network morphology (cf. Chapters 5 and 6).

   First, it was found that the conductivity exponent varies with the spread of the network, unlike the percolation threshold, which does not depend on network geometry. Second, it was confirmed that network optimization by means of an external field shifts the electrical percolation curve to lower percolation threshold and higher electrical conductivity values, as is reported in literature. In contrast to previous work though, it was further shown that the above is accompanied by an

increase in network uniformity and a decrease of the conductivity exponent. Consequently network optimization leads to an increased fraction of MWCNTs contributing to electron conduction through a three-dimensional network that exhibits a narrower distribution in local conductances. From this it was concluded that the prevalent assumption that percolation theory presupposes direct contact between adjacent particles within electron-conducting paths is incorrect, and that, instead, percolation theory presupposes a particle network with local conductances that are equal throughout the entire network. Moreover, by studying the evolution of the resistance ratio during network optimization and polymerization it was found that the increase in electrical conductivity is due to a combination of (i) a decrease in the mean interparticle distance within the electron-conducting network and (ii) a growth of the particle network, and that at particle mass fractions below the optimized percolation threshold (i) dominates, whereas at particle mass fractions above the optimized percolation threshold (ii) dominates. The optimized percolation threshold, in turn, depends on the optimization process itself.

The experimental and theoretical findings presented in this thesis are expected to be instrumental in furthering the applicability of CNT polymers nanocomposites as functional materials, in particular with regard to their use as flexible sensors and or transparent conductors. The piezoresistive strain coefficient being highest at particle mass fractions above but close to the optimized percolation threshold, and the impairment of the polymeric characters of the nanocomposite being minimal at a conductivity exponent

close to the universal value, particle mass fraction together with processing can be adapted to optimize performance.

7.2 Suggestions for Future Work

The experimental and theoretical findings presented in the thesis at hand open new fields for further study; three areas that are deemed important are described in the following:

1. Percolation and system depend proportionality constants.

   Following Equation 3.3, the evolution of electrical conductivity with particle mass fraction can be expressed as

   $$\sigma = \sigma_x (p - p_c)^t, \tag{7.1}$$

   which applies to particle mass fractions above but close to the percolation threshold, i.e. when $p > p_c$ and $(p - p_c)$ is small. There is some ambiguity as to the range of particle mass fraction in which Equation 7.1 is applicable, which is reflected in the fact that although the proportionality constant σ_x is system-dependant, in remains unclear according to current scientific knowledge what, if any, information about the system can be obtained from σ_x. For the MWCNT – PDMS system studied in this thesis σ_x is close to the electrical conductivity of a loose three-dimensional network of MWCNTs without PDMS, which indicates that σ_x might be considered as a theoretical estimation of σ_{max}. This, however, remains to be confirmed and further in-depth research is needed.

2. Percolation and nonuniversal scaling exponents.

   As most other CNT – polymer nanocomposites, the MWCNT – PDMS nanocomposite studied in this thesis is characterized by a nonuniversal conductivity exponent. Nonuniversal scaling exponents are also found in other fields where percolation theory is applied, e.g. transport phenomena in porous media. The here presented concept of a conductivity exponent that depends on the distribution of local conductances within the electron-conducting particle network might be applied to such other fields in order to learn more about the system studied (e.g., in composites materials produced by infiltration, additional information could be gained about the distribution of local pressures, saturation, and void formation).

3. Piezoresistance and applications in tactile sensing.

   As noted in Chapter 4, the pressure needed to compress the cube samples by around 10 % is well within the finger-pressure range. The corresponding normalized change in electrical resistance varies between 1.7 at $p = 0.02$ and 17 at p close to p_c. As highlighted in Section 7.1, particle mass fraction together with processing can be adapted in order to optimize the piezoresistive strain coefficient and minimize the impairment of other characters of the nanocomposite, namely mechanical flexibility and or optical transparency. The MWCNT – PDMS nanocomposite studied in this thesis appears to be an interesting candidate for tactile sensing applications. More development in this direction would certainly be worthwhile, all the more, considering that PDMS is biocompatible, which enables its use in biomedical and wearable sensing devices.

APPENDIX A

Workplace Safety in Polymer Nanocomposite Research

Published in Materials Research Society Symposium Proceedings – MRS Proceedings 2012, 1413. DOI: 10.1557/opl.2012.197.

A.1 Introduction

In recent years research efforts to develop and advance nanoparticles and NP based composite materials have increased considerably. Well-known examples of such materials are carbon nanotubes and CNT based polymers composites. The production of CNT – polymer nanocomposites typically involves handling of dry CNTs; however, while occupational and environmental health and safety practices have been defined for the handling of most polymers and chemicals involved in such research, this is not the case for the handling of dry CNTs. For a long time it was assumed that CNTs are not particularly hazardous and little effort was devoted to evaluating the toxicity of these NPs. An in-vivo study from 2008, however, demonstrates that CNTs introduced into the abdominal cavity of mice show asbestos-like pathogenicity, and, hence, may pose a carcinogenic risk [294]. Conclusions from studies exploring the potential adverse effects of CNTs on occupational and environmental health vary considerably, review articles on CNT toxicity, however, generally conclude that CNTs can present a health hazard [295-

297]. The review articles further show that adequate knowledge of CNT toxicity does not yet exist, and recommend further research into both CNT toxicity and safe handling.

The risk associated with the handling of NPs is a function of both toxicity and exposure: the higher the toxic potential of a material the more exposure to it needs to be minimized/eliminated, and, accordingly, the less is known about material toxicity, the more should be known about occupational exposure. IRSST [298] and NIOSH [299] have published comprehensive reports on occupational exposure to NPs, in which the state of the art and the effectiveness of exposure control measures are presented [300, 301]. Both reports conclude that the current knowledge is insufficient and that additional data on the effectiveness of exposure control measures is a main research need. To date, few scientific publications report specifically on the effectiveness of exposure control measures. Among these, Cena et al. [302] have evaluated the effectiveness of two commonly used engineering controls, namely a custom fume hood and a biological safety cabinet, for exposure control to particles generated during sanding of CNT epoxy nanocomposites. They found that a biological safety cabinet was more effective in minimizing exposure to airborne particles than a custom fume hood. Moreover, respirable mass concentrations in the worker's breathing zone were higher when sanding was performed inside the fume hood compared to when sanding was performed without an engineering control. The authors point out that the poor performance of the fume hood used in their study may be explained by its lack of a front sash and rear baffles, as well as its low face velocity. With regard to exposure control during manipulation of NPs, Tsai et al. [303, 304] have investigated the effectiveness of fume hoods, likely the most popular

engineering control in laboratory research, for different fume hood designs and a range of operating conditions. Their results show that the release of airborne NPs from within a fume hood into the laboratory environment and the researcher's breathing zone is highly dependent on fume hood design and operating conditions. For some designs and operating conditions they also measured a significant release of airborne NPs from the fume hood. Interruption of the fume hood airflow patterns during the handling tasks and the resulting turbulent airflow patterns were identified as the main reason for poor fume hood performance.

The presented work addresses the need for additional data on the effectiveness of exposure control measures. A new exposure control measure to minimize/eliminate potential health, safety, and environmental risks associated with the handling of dry CNTs in laboratory research is presented and its effectiveness is analyzed.

A.2. Research Objectives

The main goal of this study is to evaluate the effectiveness of a new exposure control measure. The corresponding engineering control, namely a glove box with attached vacuum chamber for material transport and air cleaning, and working practice are described in detail, and an analysis in terms of occupational exposure to airborne NPs is presented. In addition it is studied to what extend handling of Baytubes C 150 P, the NPs used in this dissertation research, releases airborne MWCNTs and or MWCNT agglomerates.

A.3 Engineering Control and Working Practice

Figure A.1 shows a photograph of the glove box with attached vacuum chamber for material transport and air cleaning (Precise Controlled Atmosphere Glove Box, Labconco Corp., MO, USA). The vacuum chamber is connected to a vacuum pump, which, in turn, is connected to the laboratory air exhaust. When evacuated from the vacuum chamber, the air is filtered twice prior to entering the vacuum pump, using disposable particulate air filters (VACU-GUARD, GE Healthcare Bio-Sciences Corp., NJ, USA). Air is also filtered at the vacuum chamber air-inlet.

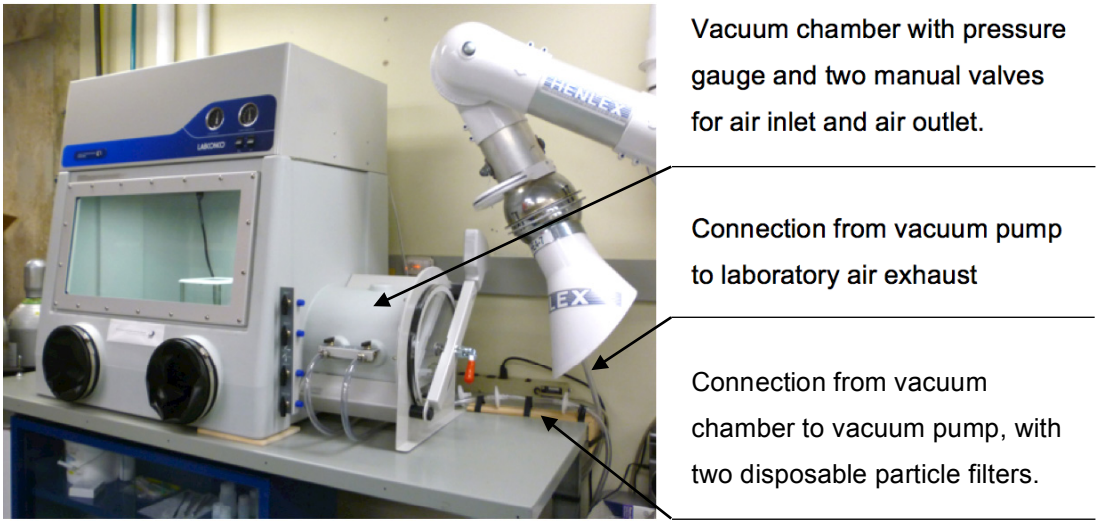

Figure A.1. Photograph and description of engineering control, i.e., glove box with attached vacuum chamber for material transport and air cleaning.

Work performed inside the glove box typically involves weighing of bulk CNTs and mixing of CNTs with a liquid (e.g. polymer or solvent). The two main roles of the engineering control are (i) to place a barrier between the worker and the dry CNTs in

order to minimize/eliminate both pulmonary and dermal exposure to CNTs, and (ii) to prevent a release of airborne CNTs into the laboratory environment in order to minimize/eliminate contamination of nearby workspace.

Although the above engineering control is the main exposure control, additional exposure control is provided by basic personal protective equipment, i.e., gloves, safety glasses, non-woven lab coat and P100 particulate respirator. Elements of the working practice that are key to exposure control are outlined in Table A.1.

Table A.1. Elements of the working practice that are key to exposure control, namely transfer of material sample out of glove box and air cleaning in vacuum chamber.

Initial situation	Material sample (e.g. container with CNT in liquid suspension, produced inside glove box) ready for transfer out of glove box. Exterior door of vacuum chamber closed; interior door of vacuum chamber open.
Step 1	Wet wipe cleaning of container surfaces.
Step 2	Positioning of open material sample (i.e., container with no lid) on vacuum chamber shelf. Closing of interior door of vacuum chamber.
Step 3	Evacuation of air from vacuum chamber for 4 minutes.
Step 4	Refilling of vacuum chamber with filtered air.
Step 5	Evacuation of air from vacuum chamber for 2 minutes. Repetition of Step 4.
Step 6	Opening of exterior door of vacuum chamber. Removal and closure of material sample. Wet wipe cleaning of container surfaces.

A.4. Experimental Details

Airborne particle number and respirable mass concentrations were measured with two direct-read instruments: an ultrafine condensation particle counter (CPC), and an optical particle counter (OPC). The CPC (P-TRAK® Ultrafine Particle Counter 8525, TSI Inc., MN, USA) was used to provide total particle number concentration (PNC) from 0 to

5×10^5 particles/cm^3, for particles that ranged in diameter from 0.02 to 1 μm. The OPC (DustTrakTM 8520 Aerosol Particulate Monitor, TSI Inc., MN, USA) was used to provide particle mass concentration (PMC) for particles ranging from 0.1 to 10 μm in diameter. The effectiveness of the exposure control measure was evaluated by transferring the CPC, initially positioned inside the glove box, out of glove box according to the working practice outlined in Table A.1, while simultaneously monitoring the PNC. For proof of concept, matches and candles were lightened inside the glove box in order to increase the concentration of airborne particles to above 5×10^5 particles/cm^3. In addition, the proneness of Baytubes C 150 P MWCNT to become airborne during material weighing and mixing was studied by measuring the concentration of airborne particles with both the CPC and the OPC located inside the glove box. Detailed information about the MWCNTs is given in Chapter 3.3.1.

A.5 Results and Discussion

A.5.1 Effectiveness of proposed exposure control measure

Figure A.2 shows the variation in particle number concentration during material sample transfer as outlined in Table A.1. The particle number concentration in the laboratory environment was measured to be around 7.5×10^3 particles/cm^3. Evacuation of air from the vacuum chamber leads to a decrease in particle number concentration with evacuation time, as can be seen in section (3) of Figure A.2. The constant particulate level at the beginning of section (3) indicates that the initial particle number produced by lightening matches and candles inside the glove box was well above 5×10^5 particles/cm^3.

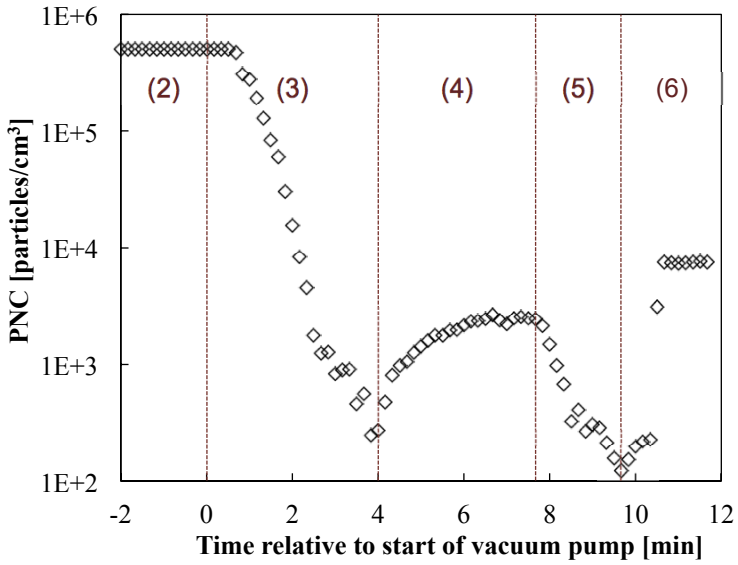

Figure A.2. Semi-logarithmic plot of variation in particle number concentration inside vacuum chamber during material sample transfer out of glove box; the labels indicate the step number of the corresponding working practice outlined in Table A.1

Four minutes of air evacuation decrease the particle number concentration inside the vacuum chamber to 250 particles/cm^3. Refilling the vacuum chamber with air leads to a re-increase in particulate level. For the presented analysis, air evacuation was stopped by switching off the vacuum pump, and not by closing the air-outlet valve of the vacuum chamber. In addition, the air-inlet valve of the vacuum chamber was opened only after air evacuation was stopped. It is therefore likely that some back-flow of air, and, hence, particles, took place prior to opening the vacuum chamber air-inlet valve, which may explain the re-increase in particle number concentration in section (4). Since the air-inlet valve is connected to a particulate filter, it is unlikely that the higher particle number concentration in the laboratory environment is the source for the observed re-increase in particulate level. Also, in the latter case one would expect the particulate level at the

beginning of section (5) to be the same as the one in the laboratory, which is not the case. Two minutes of additional air evacuation decreases the particle number concentration inside the vacuum chamber further, to around 100 particles/cm^3, i.e., to a particulate level more than three orders of magnitude lower than the initial one. As expected, in section (6), after completion of Step 6 outlined in Table A.1, around 7.5×10^3 particles/cm^3 are detected.

Although shown to be effective, the above working practice is meant to be an example. Stopping the evacuation processes after a certain time is a compromise between optimizing effectiveness on the one hand and a reasonable working time on the other hand. Evacuating air for a longer period of time would provide an even more efficient exposure control. Instead of applying a series of two low to medium vacuums, air cleaning could also be achieved by flushing the vacuum chamber environment by evacuating air while keeping the vacuum chamber air-inlet valve open. It should be noted though that preliminary experiments have shown that the latter approach is not more effective. The above working practice is not yet optimized and a higher effectiveness over working time ratio can be achieved. Also, the effectiveness analysis should be complement by morphological characterization of the airborne particles remaining in the vacuum chamber after air cleaning.

In view of practicality, an engineering control is likely to be used to minimize/eliminate exposure to different types of NPs; cross-contamination of material samples is therefore a major concern. Figure A.3 provides evidence that the proposed engineering control can be cleaned relatively easily. The variation in particle number

concentration with time of glove box air cleaning is plotted for a period of 25 minutes. Glove box air cleaning was achieved by evacuating air from the vacuum chamber while keeping the vacuum chamber interior door and the glove box air-inlet valve open. Within the given period of time the particle number concentration decreases from initially 2.5×10^5 particles/cm^3 to below the particulate level of the laboratory environment, i.e., below 7.5×10^3 particles/cm^3. Cross-contamination can be further minimized by wet wipe cleaning of the engineering control interior surfaces, and by running multiple air cleaning cycles.

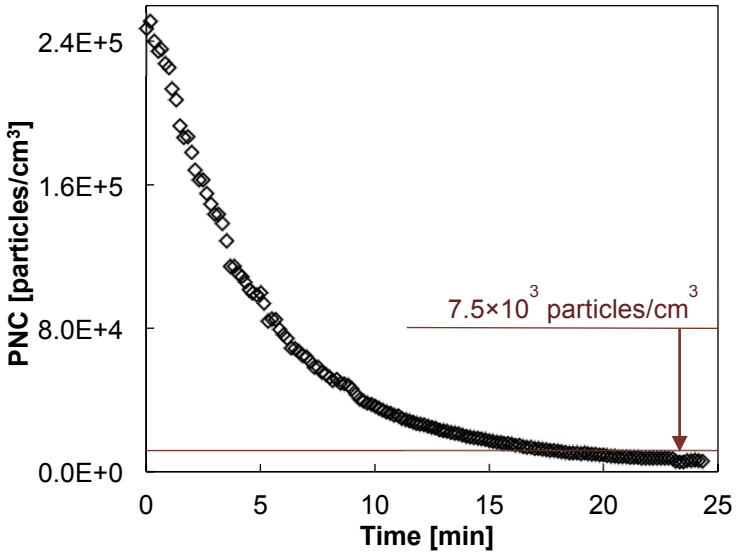

Figure A.3. Particle number concentration inside glove box and attached vacuum chamber as a function of time of air cleaning.

A.5.2 Concentration of airborne MWCNTs during material weighing

As can be seen in Figure A.4, the proneness for the MWCNTs to form airborne particles is rather low, even when the material is agitated. No airborne particles smaller

than 1 μm in diameter and only very few particles with diameters between 1 and 10 μm were detected. This is in line with both the fact that the MWCNTs were provided in powder form, with an average loose agglomerate size in the micrometer range, and results reported by Cena et al. [302], who, for a similar NP sample, found that weighing contributes little to the measured airborne particle number and particle mass concentrations.

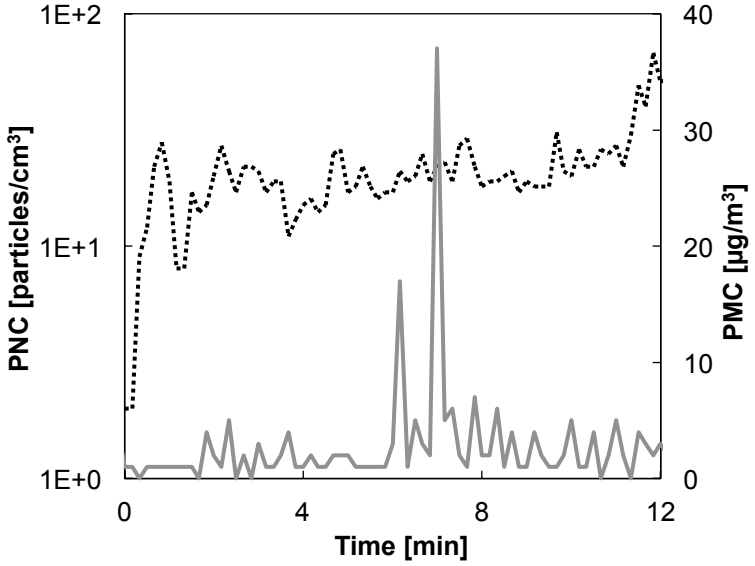

Figure A.4. Plot of airborne particle number concentration (dotted line) and particle mass concentration (full line) during weighing of dry Baytubes C 150 P MWCNTs inside glove box.

It is likely that the proneness for the MWCNTs to form airborne particles depends on the working environment; the particular environment inside the glove box, i.e., no or little air circulation over extend period of time, might be part of the reason for the low concentration of airborne particles. The average particle number concentration inside the

glove box was measured to be around 20 particles/cm^3, i.e., more than two orders of magnitude smaller than the average particle number concentration in the laboratory environment. No or little air circulation over an extended time period may lead to particle settling, particle agglomeration and settling, chemical reactions, and chemical reaction and settling. In view of cleanness of the work environment and cross-contamination this is certainly a advantageous.

A.6 Summary and Conclusions

This study addressed the need for additional data and information on the effectiveness of exposure control measures with respect to occupational exposure to potentially hazardous NPs. A new exposure control measure is proposed and its effectiveness is analyzed. Both the engineering control, i.e., glove box with attached vacuum chamber for material transport and air cleaning, and the corresponding working practice are described in detail. The engineering control was found to be highly effective in minimize potential health, safety, and environmental risks associated with pulmonary and dermal exposure to dry NPs. The working practice can be further optimized to obtain a higher ratio of effectiveness to working time, and the analysis might be complement by morphological characterization of airborne particles that remain in the vacuum chamber after air cleaning.

This study also analyzed to what extend handling of Baytubes C 150 P, the NPs used in this dissertation research, releases airborne MWCNTs and or MWCNT agglomerates, and found the proneness for Baytubes C 150 P MWCNTs to form airborne particles to be

very low when manipulating dry CNTs inside the glove box. However, due to the particular environment inside the glove box, i.e., no or little air circulation over extend period of time, this result does not allow for direct conclusions as regards the potential exposure to airborne CNTs when manipulating Baytubes C 150 P MWCNTs using another or no engineering control. All MWCNT in PDMS suspension produced during this dissertation research were obtained using the exposure control measure presented in this chapter.

Overall, the results provide new information that are believed to be helpful for both the selection and the use of an appropriate engineering control to minimize/eliminate exposure to airborne CNTs, and NPs in general.

APPENDIX B

Nomenclature

B.1 List of Symbols

α		Aspect ratio
γ	[s^{-1}]	Equilibrium shear strain
γ'	[s^{-1}]	Shear rate
ε		Strain
ε_0		Reference compressive strain
ε_c		Compressive strain
ε_r		Relative permittivity
η	[Pa.s]	Shear viscosity
η^*	[Pa.s]	Complex viscosity
$\theta(\alpha)$		Scale factor depending on α
λ	[μm]	Gap between parallel plates
$\mu(g)$	[S]	Mean value of the distribution of local conductances
$\xi(\varepsilon)$		Scale factor depending on ε
ρ	[Ω.m]	Electrical resistivity
σ	[$S.m^{-1}$]	Electrical conductivity
σ_{AC}	[S]	AC electrical conductivity
σ_{max}	[S]	Maximum electrical conductivity

σ_x	[$S.m^{-1}$]	Electrical percolation proportionality constant
τ	[s]	Hold time
ϕ	[V]	Mean potential barrier height
ϕ_0	[V]	Height of rectangular potential barrier
ψ_1	[$Pa.s^2$]	1st normal stress coefficient
ω	[$rad.s^{-1}$]	Angular frequency
Υ		Shear-thinning index
ΔV	[V]	Electric potential difference
ΔV_0	[V]	Reference electric potential difference
c_p		Scale factor depending on p and p_c
d_c	[mm]	Crosshead displacement
e	[C]	Elementary charge
f	[Hz]	AC frequency
f_0	[Hz]	Critical AC frequency
g	[S]	Local conductance
g_i	[S]	Local conductance of specific value
j		Imaginary unit
l	[µm]	Electrode spacing / Sample thickness
p		Particle mass fraction
p_c		Electrical percolation threshold
$p_c^{optimized}$		Optimized electrical percolation threshold
p_r		Rheological percolation threshold
p_v		Particle volume fraction
r		AC-exponent
s	[Å]	Thickness of insulating thin film
s_1, s_2	[Å]	Limits of potential barrier at the Fermi level

t		Conductivity exponent
t_0		Reference conductivity exponent
t_c		Compressive strain dependent conductivity exponent
$\tan\delta$		Loss factor
u		Elasticity exponent
A	$[m^2]$	Electrode area
A_c	$[m^2]$	Area onto which compressive force is applied
C	[F]	Capacitance
DI	[%]	Dispersion index
E	$[V.m^{-1}]$	Electric field
E_F	[eV]	Fermi level
F_c	[N]	Compressive force
G	[S]	Electrical conductance
G'	[Pa]	Storage modulus
G''	[Pa]	Loss modulus
G^*	[Pa]	Complex shear modulus
G'_x	[Pa]	Rheological percolation proportionality constant
GF		Piezoresistive strain coefficient
I	[A]	Electric current
I_0	[A]	Reference electric current
J	$[A/cm^2]$	Current density penetrating insulating thin film
N		Number of electron-conducting paths
P	[MPa]	Pressure
R	[Ω]	Electrical resistance
R_0	[Ω]	Reference electrical resistance
R_c	[Ω]	Compressive strain dependent electrical resistance

R_h	[Ω]	Electrical resistance at high voltage
R_l	[Ω]	Electrical resistance at low voltage
R_n	[Ω]	Electrical resistance of electron-conducting network
R_p	[Ω]	Electrical resistance of electron-conducting path
R_R		Resistance ratio
R^2		Coefficient of determination
T	[°C]	Temperature
U	[V]	Voltage across the insulating thin film
V_h	[V]	High voltage
V_l	[V]	Low voltage
V_{AV}	[V]	Alternating voltage
V_{OV}	[V]	Offset voltage
Var(g)	[S^2]	Variance of the distribution of local conductances
WPF		White pixel fraction
Y	[MPa]	Young's modulus
Y_{AC}	[S]	Admittance
Z_{AC}	[Ω]	Impedance

B.2 List of Acronyms

AC	Alternating current
CNT	Carbon nanotube
DC	Direct current
IV	Current-voltage
MWCNT	Multi-walled carbon nanotube
NP	Nanoparticle
NC	Nanocomposite

OM	Optical microscopy
PDMS	Polydimethylsiloxane
SWCNT	Single-walled carbon nanotube
SEM	Scanning electron microscopy
TEM	Transmission electron microscopy

REFERENCES

[1] Gordon RG. Criteria for choosing transparent conductors. Mrs Bulletin. 2000;25:52-7.

[2] Ginley D, Hosono H, Paine DC. Handbook of Transparent Conductors: Springer; 2010.

[3] Boukallel M, Yousef H, Godin C, Coutier C. Flexible Tactile Sensors for Multidigital Dexterous In-Hand Manipulation. Flexible Robotics: Wiley-ISTE; 2013. p. 181-242.

[4] Segev-Bar M, Haick H. Flexible Sensors Based on Nanoparticles. ACS Nano. 2013;7:8366-78.

[5] Chen Z, Cotterell B, Wang W. The fracture of brittle thin films on compliant substrates in flexible displays. Engineering Fracture Mechanics. 2002;69:597-603.

[6] Leterrier Y, Medico L, Demarco F, Manson JAE, Betz U, Escola MF, et al. Mechanical integrity of transparent conductive oxide films for flexible polymer-based displays. Thin Solid Films. 2004;460:156-66.

[7] Hecht DS, Hu LB, Irvin G. Emerging Transparent Electrodes Based on Thin Films of Carbon Nanotubes, Graphene, and Metallic Nanostructures. Advanced Materials. 2011;23:1482-513.

[8] Pang C, Lee C, Suh K-Y. Recent advances in flexible sensors for wearable and implantable devices. Journal of Applied Polymer Science. 2013;130:1429-41.

[9] Iijima S. Helical Microtubules of Graphitic Carbon. Nature. 1991;354:56-8.

[10] Shulaker MM, Hills G, Patil N, Wei H, Chen HY, PhilipWong HS, et al. Carbon nanotube computer. Nature. 2013;501:526-30.

[11] Kreupl F. Carbon-Nanotube Computer Has Arrived. Nature. 2013;501:495-6.

[12] Jung YC, Shimamoto D, Muramatsu H, Kim YA, Hayashi T, Terrones M, et al. Robust, Conducting, and Transparent Polymer Composites using Surface-Modified and Individualized Double-Walled Carbon Nanotubes. Advanced Materials. 2008;20:4509-12.

[13] Sierros KA, Hecht DS, Banerjee DA, Morris NJ, Hu L, Irvin GC, et al. Durable transparent carbon nanotube films for flexible device components. Thin Solid Films. 2010;518:6977-83.

[14] Scardaci V, Coull R, Lyons PE, Rickard D, Coleman JN. Spray deposition of highly transparent, low-resistance networks of silver nanowires over large areas. Small. 2011;7:2621-8.

[15] Ajayan PM, Stephan O, Colliex C, Trauth D. Aligned Carbon Nanotube Arrays Formed by Cutting a Polymer Resin-Nanotube Composite. Science. 1994;265:1212-4.

[16] Hamada N, Sawada S, Oshiyama A. New One-Dimensional Conductors - Graphitic Microtubules. Physical Review Letters. 1992;68:1579-81.

[17] Iijima S, Ichihashi T, Ando Y. Pentagons, Heptagons and Negative Curvature in Graphite Microtubule Growth. Nature. 1992;356:776-8.

[18] Saito R, Fujita M, Dresselhaus G, Dresselhaus MS. Electronic-Structure of Graphene Tubules Based on C-60. Physical Review B. 1992;46:1804-11.

[19] Hiura H, Ebbesen TW, Tanigaki K, Takahashi H. Raman Studies of Carbon Nanotubes. Chemical Physics Letters. 1993;202:509-12.

[20] Thostenson ET, Ren ZF, Chou TW. Advances in the science and technology of carbon nanotubes and their composites: a review. Composites Science and Technology. 2001;61:1899-912.

[21] Baughman RH, Zakhidov AA, de Heer WA. Carbon nanotubes - the route toward applications. Science. 2002;297:787-92.

[22] Thostenson ET, Li CY, Chou TW. Nanocomposites in context. Composites Science and Technology. 2005;65:491-516.

[23] Coleman JN, Khan U, Blau WJ, Gun'ko YK. Small but strong: A review of the mechanical properties of carbon nanotube-polymer composites. Carbon. 2006;44:1624-52.

[24] Fiedler B, Gojny FH, Wichmann MHG, Nolte MCM, Schulte K. Fundamental aspects of nano-reinforced composites. Composites Science and Technology. 2006;66:3115-25.

[25] Li C, Thostenson ET, Chou TW. Sensors and actuators based on carbon nanotubes and their composites: A review. Composites Science and Technology. 2008;68:1227-49.

[26] Bauhofer W, Kovacs JZ. A review and analysis of electrical percolation in carbon nanotube polymer composites. Composites Science and Technology. 2009;69:1486-98.

[27] Rahmat M, Hubert P. Carbon nanotube-polymer interactions in nanocomposites: A review. Composites Science and Technology. 2011;72:72-84.

[28] Pandey G, Thostenson ET. Carbon Nanotube-Based Multifunctional Polymer Nanocomposites. Polymer Reviews. 2012;52:355-416.

[29] Shima H. Buckling of Carbon Nanotubes: A State of the Art Review. Materials. 2012;5:47-84.

[30] De Volder MFL, Tawfick SH, Baughman RH, Hart AJ. Carbon Nanotubes: Present and Future Commercial Applications. Science. 2013;339:535-9.

[31] Harris PJF. Carbon Nanotube Science: Synthesis, Properties and Applications. 1st ed: Cambridge University Press; 2009.

[32] Grady BP. Carbon Nanotube-Polymer Composites: Manufacture, Properties, and Applications. 1st ed: Wiley; 2011.

[33] McNally T, Pötschke P. Polymer-Carbon Nanotube Composites: Preparation, Properties and Applications. 1st ed: Woodhead Publishing; 2011.

[34] Grossiord N, Hermant MC, Koning C. Polymer carbon nanotube composites: The polymer latex concept: Pan Stanford; 2012.

[35] Tasis D, Papagelis K. Carbon Nanotube-Filled Polymer Composites. Polymer Composites: Wiley-VCH Verlag GmbH & Co. KGaA; 2013. p. 219-47.

[36] Mittal V. Polymer Nanotubes Nanocomposites: Synthesis, Properties and Applications. 2nd ed: Wiley-Scrivener; 2014.

[37] Vigolo B, Penicaud A, Coulon C, Sauder C, Pailler R, Journet C, et al. Macroscopic fibers and ribbons of oriented carbon nanotubes. Science. 2000;290:1331-4.

[38] Wu ZC, Chen ZH, Du X, Logan JM, Sippel J, Nikolou M, et al. Transparent, conductive carbon nanotube films. Science. 2004;305:1273-6.

[39] Yamada T, Hayamizu Y, Yamamoto Y, Yomogida Y, Izadi-Najafabadi A, Futaba DN, et al. A stretchable carbon nanotube strain sensor for human-motion detection. Nature Nanotechnology. 2011;6:296-301.

[40] Behabtu N, Young CC, Tsentalovich DE, Kleinerman O, Wang X, Ma AWK, et al. Strong, Light, Multifunctional Fibers of Carbon Nanotubes with Ultrahigh Conductivity. Science. 2013;339:182-6.

[41] Niu ZQ, Dong HB, Zhu BW, Li JZ, Hng HH, Zhou WY, et al. Highly Stretchable, Integrated Supercapacitors Based on Single-Walled Carbon Nanotube Films with Continuous Reticulate Architecture. Advanced Materials. 2013;25:1058-64.

[42] Schonenberger C, Bachtold A, Strunk C, Salvetat JP, Forro L. Interference and Interaction in multi-wall carbon nanotubes. Applied Physics a-Materials Science & Processing. 1999;69:283-95.

[43] Wei BQ, Vajtai R, Ajayan PM. Reliability and current carrying capacity of carbon nanotubes. Applied Physics Letters. 2001;79:1172-4.

[44] Nirmalraj PN, Lyons PE, De S, Coleman JN, Boland JJ. Electrical connectivity in single-walled carbon nanotube networks. Nano Letters. 2009;9:3890-5.

[45] Kim P, Shi L, Majumdar A, McEuen PL. Thermal transport measurements of individual multiwalled nanotubes. Physical Review Letters. 2001;87.

[46] Peng B, Locascio M, Zapol P, Li SY, Mielke SL, Schatz GC, et al. Measurements of near-ultimate strength for multiwalled carbon nanotubes and irradiation-induced crosslinking improvements. Nature Nanotechnology. 2008;3:626-31.

[47] Boehm HP. The first observation of carbon nanotubes. Carbon. 1997;35:581-4.

[48] Monthioux M, Kuznetsov VL. Who should be given the credit for the discovery of carbon nanotubes? Carbon. 2006;44:1621-3.

[49] Radushkevich LV, Lukyanovich VM. O strukture ugleroda, obrazujucegosja pri termiceskom razlozenii okisi ugleroda na zeleznom kontakte (About the structure of carbon formed by thermal decomposition of carbon monoxide on iron substrate). Zurn Fisic Chim. 1952:88–95.

[50] Vilatela JJ, Eder D. Nanocarbon Composites and Hybrids in Sustainability: A Review. Chemsuschem. 2012;5:456-78.

[51] Kearns JC, Shambaugh RL. Polypropylene fibers reinforced with carbon nanotubes. Journal of Applied Polymer Science. 2002;86:2079-84.

[52] Coleman JN, Cadek M, Blake R, Nicolosi V, Ryan KP, Belton C, et al. High-performance nanotube-reinforced plastics: Understanding the mechanism of strength increase. Advanced Functional Materials. 2004;14:791-8.

[53] Putz KW, Mitchell CA, Krishnamoorti R, Green PF. Elastic modulus of single-walled carbon nanotube/poly(methyl methacrylate) nanocomposites. Journal of Polymer Science Part B-Polymer Physics. 2004;42:2286-93.

[54] Spitalsky Z, Tasis D, Papagelis K, Galiotis C. Carbon nanotube-polymer composites: Chemistry, processing, mechanical and electrical properties. Progress in Polymer Science. 2010;35:357-401.

[55] Chou TW, Gao LM, Thostenson ET, Zhang ZG, Byun JH. An assessment of the science and technology of carbon nanotube-based fibers and composites. Composites Science and Technology. 2010;70:1-19.

[56] Bokobza L. Mechanical, electrical and spectroscopic investigations of carbon nanotube-reinforced elastomers. Vibrational Spectroscopy. 2009;51:52-9.

[57] Dufresne A, Paillet M, Putaux JL, Canet R, Carmona F, Delhaes P, et al. Processing and characterization of carbon nanotube/poly(styrene-co-butyl acrylate) nanocomposites. Journal of Materials Science. 2002;37:3915-23.

[58] Gojny FH, Wichmann MHG, Köpke U, Fiedler B, Schulte K. Carbon nanotube-reinforced epoxy-composites: enhanced stiffness and fracture toughness at low nanotube content. Composites Science and Technology. 2004;64:2363-71.

[59] Martinez-Rubi Y, Ashrafi B, Guan JW, Kingston C, Johnston A, Simard B, et al. Toughening of Epoxy Matrices with Reduced Single-Walled Carbon Nanotubes. Acs Applied Materials & Interfaces. 2011;3:2309-17.

[60] Cadek M, Coleman JN, Barron V, Hedicke K, Blau WJ. Erratum: "Morphological and mechanical properties of carbon-nanotube-reinforced semicrystalline and amorphous polymer composites" (vol 81, pg 5123, 2002). Applied Physics Letters. 2003;83:2718.

[61] Cadek M, Coleman JN, Barron V, Hedicke K, Blau WJ. Morphological and mechanical properties of carbon-nanotube-reinforced semicrystalline and amorphous polymer composites. Applied Physics Letters. 2002;81:5123-5.

[62] Sahoo NG, Rana S, Cho JW, Li L, Chan SH. Polymer nanocomposites based on functionalized carbon nanotubes. Progress in Polymer Science. 2010;35:837-67.

[63] Martinez-Rubi Y, Gonzalez-Dominguez JM, Anson-Casaos A, Kingston CT, Daroszewska M, Barnes M, et al. Tailored SWCNT functionalization optimized for compatibility with epoxy matrices. Nanotechnology. 2012;23.

[64] Moniruzzaman M, Winey KI. Polymer nanocomposites containing carbon nanotubes. Macromolecules. 2006;39:5194-205.

[65] Hu M, Yu DM, Wei JB. Thermal conductivity determination of small polymer samples by differential scanning calorimetry. Polymer Testing. 2007;26:333-7.

[66] Han ZD, Fina A. Thermal conductivity of carbon nanotubes and their polymer nanocomposites: A review. Progress in Polymer Science. 2011;36:914-44.

[67] Hong WT, Tai NH. Investigations on the thermal conductivity of composites reinforced with carbon nanotubes. Diamond and Related Materials. 2008;17:1577-81.

[68] Yang DJ, Zhang Q, Chen G, Yoon SF, Ahn J, Wang SG, et al. Thermal conductivity of multiwalled carbon nanotubes. Physical Review B. 2002;66.

[69] Yi W, Lu L, Zhang DL, Pan ZW, Xie SS. Linear specific heat of carbon nanotubes. Physical Review B. 1999;59:R9015-R8.

[70] Jin Z, Sun X, Xu G, Goh SH, Ji W. Nonlinear optical properties of some polymer/multi-walled carbon nanotube composites. Chemical Physics Letters. 2000;318:505-10.

[71] Chen YC, Raravikar NR, Schadler LS, Ajayan PM, Zhao YP, Lu TM, et al. Ultrafast optical switching properties of single-wall carbon nanotube polymer composites at 1.55 μm. Applied Physics Letters. 2002;81:975-7.

[72] Wang J, Liao KS, Früchtl D, Tian Y, Gilchrist A, Alley NJ, et al. Nonlinear optical properties of carbon nanotube hybrids in polymer dispersions. Materials Chemistry and Physics. 2012;133:992-7.

[73] Dewaghe C, Lew CY, Claes M, Belgium SA, Dubois P. Fire-retardant applications of polymer-carbon nanotubes composites: Improved barrier effect and synergism. Polymer-Carbon Nanotube Composites: Preparation, Properties and Applications. 1st ed: Woodhead Publishing; 2011. p. 718-45.

[74] Chen WX, Li F, Han G, Xia JB, Wang LY, Tu JP, et al. Tribological behavior of carbon-nanotube-filled PTFE composites. Tribology Letters. 2003;15:275-8.

[75] Liu H, Wang T, Wang Q. Synthesis and Tribological Properties of Thermosetting Polyimide and Its Carbon Nanotube-Containing Composites. Polymer - Plastics Technology and Engineering. 2012;51:1-5.

[76] Bakshi SR, Lahiri D, Agarwal A. Carbon nanotube reinforced metal matrix composites - a review. International Materials Reviews. 2010;55:41-64.

[77] Cho J, Boccaccini AR, Shaffer MSP. Ceramic matrix composites containing carbon nanotubes. Journal of Materials Science. 2009;44:1934-51.

[78] Chen SJ, Collins FG, Macleod AJN, Pan Z, Duan WH, Wang CM. Carbon nanotube–cement composites: A retrospect. The IES Journal Part A: Civil & Structural Engineering. 2011;4:254-65.

[79] Yanagi K, Moriya R, Yomogida Y, Takenobu T, Naitoh Y, Ishida T, et al. Electrochromic carbon electrodes: Controllable visible color changes in metallic single-wall carbon nanotubes. Advanced Materials. 2011;23:2811-4.

[80] Yan J, Jeong YG. Multiwalled carbon nanotube/polydimethylsiloxane composite films as high performance flexible electric heating elements. Applied Physics Letters. 2014;105.

[81] Cui S, Canet R, Derre A, Couzi M, Delhaes P. Characterization of multiwall carbon nanotubes and influence of surfactant in the nanocomposite processing. Carbon. 2003;41:797-809.

[82] Sandler JKW, Kirk JE, Kinloch IA, Shaffer MSP, Windle AH. Ultra-low electrical percolation threshold in carbon-nanotube-epoxy composites. Polymer. 2003;44:5893-9.

[83] Potschke P, Fornes TD, Paul DR. Rheological behavior of multiwalled carbon nanotube/polycarbonate composites. Polymer. 2002;43:3247-55.

[84] Potschke P, Abdel-Goad M, Alig I, Dudkin S, Lellinger D. Rheological and dielectrical characterization of melt mixed polycarbonate-multiwalled carbon nanotube composites. Polymer. 2004;45:8863-70.

[85] Lin B, Sundararaj U, Potschke P. Melt mixing of polycarbonate with multi-walled carbon nanotubes in miniature mixers. Macromolecular Materials and Engineering. 2006;291:227-38.

[86] Abbasi S, Carreau PJ, Derdouri A, Moan M. Rheological properties and percolation in suspensions of multiwalled carbon nanotubes in polycarbonate. Rheologica Acta. 2009;48:943-59.

[87] Hu CH, Liu CH, Chen LZ, Peng YC, Fan SS. Resistance-pressure sensitivity and a mechanism study of multiwall carbon nanotube networks/poly(dimethylsiloxane) composites. Applied Physics Letters. 2008;93.

[88] Kwon SY, Park YK, Kim MS. Piezoresistive properties of multi-walled carbon nanotubepoly(dimethylsiloxane) composites for low-pressure-sensing applications. Nano. 2012;7.

[89] Rizvi R, Cochrane B, Biddiss E, Naguib H. Piezoresistance characterization of poly(dimethyl-siloxane) and poly(ethylene) carbon nanotube composites. Smart Materials and Structures. 2011;20.

[90] Coleman JN, Curran S, Dalton AB, Davey AP, McCarthy B, Blau W, et al. Percolation-dominated conductivity in a conjugated-polymer-carbon-nanotube composite. Physical Review B. 1998;58:R7492-R5.

[91] Andrews R, Jacques D, Minot M, Rantell T. Fabrication of carbon multiwall nanotube/polymer composites by shear mixing. Macromolecular Materials and Engineering. 2002;287:395-403.

[92] Mitchell CA, Bahr JL, Arepalli S, Tour JM, Krishnamoorti R. Dispersion of functionalized carbon nanotubes in polystyrene. Macromolecules. 2002;35:8825-30.

[93] Poa CH, Silva SRP, Watts PCP, Hsu WK, Kroto HW, Walton DRM. Field emission from nonaligned carbon nanotubes embedded in a polystyrene matrix. Applied Physics Letters. 2002;80:3189-91.

[94] Ramasubramaniam R, Chen J, Liu H. Homogeneous carbon nanotube/polymer composites for electrical applications. Applied Physics Letters. 2003;83:2928-30.

[95] Du FM, Scogna RC, Zhou W, Brand S, Fischer JE, Winey KI. Nanotube networks in polymer nanocomposites: Rheology and electrical conductivity. Macromolecules. 2004;37:9048-55.

[96] Kharchenko SB, Douglas JF, Obrzut J, Grulke EA, Migler KB. Flow-induced properties of nanotube-filled polymer materials. Nature Materials. 2004;3:564-8.

[97] Regev O, ElKati PNB, Loos J, Koning CE. Preparation of conductive nanotube-polymer composites using latex technology. Advanced Materials. 2004;16:248-51.

[98] Seo MK, Park SJ. Electrical resistivity and rheological behaviors of carbon nanotubes-filled polypropylene composites. Chemical Physics Letters. 2004;395:44-8.

[99] McNally T, Pötschke P, Halley P, Murphy M, Martin D, Bell SEJ, et al. Polyethylene multiwalled carbon nanotube composites. Polymer. 2005;46:8222-32.

[100] Dettlaff-Weglikowska U, Kaempgen M, Hornbostel B, Skakalova V, Wang J, Liang J, et al. Conducting and transparent SWNT/polymer composites. Physica Status Solidi (B) Basic Research. 2006;243:3440-4.

[101] Hornbostel B, Pötschke P, Kotz J, Roth S. Single-walled carbon nanotubes/polycarbonate composites: Basic electrical and mechanical properties. Physica Status Solidi (B) Basic Research. 2006;243:3445-51.

[102] Hu GJ, Zhao CG, Zhang SM, Yang MS, Wang ZG. Low percolation thresholds of electrical conductivity and rheology in poly(ethylene terephthalate) through the networks of multi-walled carbon nanotubes. Polymer. 2006;47:480-8.

[103] Zhang Q, Rastogi S, Chen D, Lippits D, Lemstra PJ. Low percolation threshold in single-walled carbon nanotube/high density polyethylene composites prepared by melt processing technique. Carbon. 2006;44:778-85.

[104] Antonucci V, Faiella G, Giordano M, Nicolais L, Pepe G. Electrical properties of single walled carbon nanotube reinforced polystyrene composites. Macromolecular Symposia. 2007;247:172-81.

[105] Chen H, Muthuraman H, Stokes P, Zou J, Liu X, Wang J, et al. Dispersion of carbon nanotubes and polymer nanocomposite fabrication using trifluoroacetic acid as a co-solvent. Nanotechnology. 2007;18.

[106] Dalmas F, Cavaillé JY, Gauthier C, Chazeau L, Dendievel R. Viscoelastic behavior and electrical properties of flexible nanofiber filled polymer nanocomposites. Influence of processing conditions. Composites Science and Technology. 2007;67:829-39.

[107] Gorrasi G, Romeo V, Sannino D, Sarno M, Ciambelli P, Vittoria V, et al. Carbon nanotube induced structural and physical property transitions of syndiotactic polypropylene. Nanotechnology. 2007;18.

[108] Kota AK, Cipriano BH, Duesterberg MK, Gershon AL, Powell D, Raghavan SR, et al. Electrical and rheological percolation in polystyrene/MWCNT nanocomposites. Macromolecules. 2007;40:7400-6.

[109] Schmidt RH, Kinloch IA, Burgess AN, Windle AH. The effect of aggregation on the electrical conductivity of spin-coated polymer/carbon nanotube composite films. Langmuir. 2007;23:5707-12.

[110] Tjong SC, Liang GD, Bao SP. Electrical behavior of polypropylene/multiwalled carbon nanotube nanocomposites with low percolation threshold. Scripta Materialia. 2007;57:461-4.

[111] Bose S, Bhattacharyya AR, Bondre AP, Kulkarni AR, Potschke P. Rheology, electrical conductivity, and the phase behavior of cocontinuous PA6/ABS blends with MWNT: Correlating the aspect ratio of MWNT with the percolation threshold. Journal of Polymer Science Part B-Polymer Physics. 2008;46:1619-31.

[112] Grossiord N, Kivit PJJ, Loos J, Meuldijk J, Kyrylyuk AV, van der Schoot P, et al. On the influence of the processing conditions on the performance of electrically conductive carbon nanotube/polymer nanocomposites. Polymer. 2008;49:2866-72.

[113] Mathur RB, Pande S, Singh BP, Dhami TL. Electrical and mechanical properties of multi-walled carbon nanotubes reinforced PMMA and PS composites. Polymer Composites. 2008;29:717-27.

[114] Bangarusampath DS, Ruckdaschel H, Altstadt V, Sandler JKW, Garray D, Shaffer MSP. Rheological and electrical percolation in melt-processed poly(ether ether ketone)/multi-wall carbon nanotube composites. Chemical Physics Letters. 2009;482:105-9.

[115] Han MS, Lee YK, Lee HS, Yun CH, Kim WN. Electrical, morphological and rheological properties of carbon nanotube composites with polyethylene and poly(phenylene sulfide) by melt mixing. Chemical Engineering Science. 2009;64:4649-56.

[116] Huang Y-L, Yuen S-M, Ma C-CM, Chuang C-Y, Yu K-C, Teng C-C, et al. Morphological, electrical, electromagnetic interference (EMI) shielding, and tribological properties of functionalized multi-walled carbon nanotube/poly methyl methacrylate (PMMA) composites. Composites Science and Technology. 2009;69:1991-6.

[117] Li YJ, Shimizu H. Toward a Stretchable, Elastic, and Electrically Conductive Nanocomposite: Morphology and Properties of Poly[styrene-b-(ethylene-co-butylene)-b-styrene]/Multiwalled Carbon Nanotube Composites Fabricated by High-Shear Processing. Macromolecules. 2009;42:2587-93.

[118] Zhang C, Zhu J, Ouyang M, Ma CA, Sumita M. Conductive Network Formation and Electrical Properties of Poly(vinylidene fluoride)/Multiwalled Carbon Nanotube Composites: Percolation and Dynamic Percolation. Journal of Applied Polymer Science. 2009;114:1405-11.

[119] Dubnikova I, Kuvardina E, Krasheninnikov V, Lomakin S, Tchmutin I, Kuznetsov S. The Effect of Multiwalled Carbon Nanotube Dimensions on the Morphology, Mechanical, and Electrical Properties of Melt Mixed Polypropylene-Based Composites. Journal of Applied Polymer Science. 2010;117:259-72.

[120] Grossiord N, Wouters MEL, Miltner HE, Lu KB, Loos J, Van Mele B, et al. Isotactic polypropylene/carbon nanotube composites prepared by latex technology: Electrical conductivity study. European Polymer Journal. 2010;46:1833-43.

[121] Yakuphanoglu F, Yahia IS, Barim G, Senkal BF. Double-walled carbon nanotube/polymer nanocomposites: Electrical properties under dc and ac fields. Synthetic Metals. 2010;160:1718-26.

[122] Huang CL, Wang C. Rheological and conductive percolation laws for syndiotactic polystyrene composites filled with carbon nanocapsules and carbon nanotubes. Carbon. 2011;49:2334-44.

[123] McClory C, Potschke P, McNally T. Influence of Screw Speed on Electrical and Rheological Percolation of Melt-Mixed High-Impact Polystyrene/MWCNT Nanocomposites. Macromolecular Materials and Engineering. 2011;296:59-69.

[124] Mohiuddin M, Van Hoa S. Electrical resistance of CNT-PEEK composites under compression at different temperatures. Nanoscale Research Letters. 2011;6:1-5.

[125] Oliva-Aviles AI, Aviles F, Sosa V. Electrical and piezoresistive properties of multi-walled carbon nanotube/polymer composite films aligned by an electric field. Carbon. 2011;49:2989-97.

[126] Penu C, Hu GH, Fernandez A, Marchal P, Choplin L. Rheological and electrical percolation thresholds of carbon nanotube/polymer nanocomposites. Polymer Engineering and Science. 2012;52:2173-81.

[127] Pan YZ, Li L. Percolation and gel-like behavior of multiwalled carbon nanotube/polypropylene composites influenced by nanotube aspect ratio. Polymer. 2013;54:1218-26.

[128] Jouni M, Faure-Vincent J, Fedorko P, Djurado D, Boiteux G, Massardier V. Charge carrier transport and low electrical percolation threshold in multiwalled carbon nanotube polymer nanocomposites. Carbon. 2014;76:10-8.

[129] Sandler J, Shaffer MSP, Prasse T, Bauhofer W, Schulte K, Windle AH. Development of a dispersion process for carbon nanotubes in an epoxy matrix and the resulting electrical properties. Polymer. 1999;40:5967-71.

[130] Allaoui A, Bai S, Cheng HM, Bai JB. Mechanical and electrical properties of a MWNT/epoxy composite. Composites Science and Technology. 2002;62:1993-8.

[131] Bai JB, Allaoui A. Effect of the length and the aggregate size of MWNTs on the improvement efficiency of the mechanical and electrical properties of nanocomposites - Experimental investigation. Composites Part A: Applied Science and Manufacturing. 2003;34:689-94.

[132] Barrau S, Demont P, Peigney A, Laurent C, Lacabanne C. Dc and ac conductivity of carbon nanotubes-polyepoxy composites. Macromolecules. 2003;36:5187-94.

[133] Kim B, Lee J, Yu I. Electrical properties of single-wall carbon nanotube and epoxy composites. Journal of Applied Physics. 2003;94:6724-8.

[134] Martin CA, Sandler JKW, Shaffer MSP, Schwarz MK, Bauhofer W, Schulte K, et al. Formation of percolating networks in multi-wall carbon-nanotube-epoxy composites. Composites Science and Technology. 2004;64:2309-16.

[135] Pécastaings G, Delhaès P, Derré A, Saadaoui H, Carmona F, Cui S. Role of interfacial effects in carbon nanotube/epoxy nanocomposite behavior. Journal of Nanoscience and Nanotechnology. 2004;4:838-43.

[136] Barrau S, Demont P, Maraval C, Bernes A, Lacabanne C. Glass transition temperature depression at the percolation threshold in carbon nanotube-epoxy resin and polypyrrole-epoxy resin composites. Macromolecular Rapid Communications. 2005;26:390-4.

[137] Brown JM, Anderson DP, Justice RS, Lafdi K, Belfor M, Strong KL, et al. Hierarchical morphology of carbon single-walled nanotubes during sonication in an aliphatic diamine. Polymer. 2005;46:10854-65.

[138] Bryning MB, Islam MF, Kikkawa JM, Yodh AG. Very low conductivity threshold in bulk isotropic single-walled carbon nanotube-epoxy composites. Advanced Materials. 2005;17:1186-91.

[139] Kim YJ, Shin TS, Choi HD, Kwon JH, Chung YC, Yoon HG. Electrical conductivity of chemically modified multiwalled carbon nanotube/epoxy composites. Carbon. 2005;43:23-30.

[140] Du F, Guthy C, Kashiwagi T, Fischer JE, Winey KI. An infiltration method for preparing single-wall nanotube/ epoxy composites with improved thermal conductivity. Journal of Polymer Science, Part B: Polymer Physics. 2006;44:1513-9.

[141] Gojny FH, Wichmann MHG, Fiedler B, Kinloch IA, Bauhofer W, Windle AH, et al. Evaluation and identification of electrical and thermal conduction mechanisms in carbon nanotube/epoxy composites. Polymer. 2006;47:2036-45.

[142] Moisala A, Li Q, Kinloch IA, Windle AH. Thermal and electrical conductivity of single- and multi-walled carbon nanotube-epoxy composites. Composites Science and Technology. 2006;66:1285-8.

[143] Wichmann MHG, Sumfleth J, Fiedler B, Gojny FH, Schulte K. Multiwall carbon nanotube/epoxy composites produced by a masterbatch process. Mechanics of Composite Materials. 2006;42:395-406.

[144] Yu A, Itkis ME, Bekyarova E, Haddon RC. Effect of single-walled carbon nanotube purity on the thermal conductivity of carbon nanotube-based composites. Applied Physics Letters. 2006;89.

[145] Kovacs JZ, Velagala BS, Schulte K, Bauhofer W. Two percolation thresholds in carbon nanotube epoxy composites. Composites Science and Technology. 2007;67:922-8.

[146] Li C, Thostenson ET, Chou TW. Dominant role of tunneling resistance in the electrical conductivity of carbon nanotube-based composites. Applied Physics Letters. 2007;91.

[147] Li J, Ma PC, Chow WS, To CK, Tang BZ, Kim JK. Correlations between percolation threshold, dispersion state, and aspect ratio of carbon nanotubes. Advanced Functional Materials. 2007;17:3207-15.

[148] Liu L, Matitsine S, Gan YB, Chen LF, Kong LB, Rozanov KN. Frequency dependence of effective permittivity of carbon nanotube composites. Journal of Applied Physics. 2007;101.

[149] Simsek Y, Ozyuzer L, Seyhan A, Tanoglu M, Schulte K. Temperature dependence of electrical conductivity in double-wall and multi-wall carbon nanotube/polyester nanocomposites. Journal of Materials Science. 2007;42:9689-95.

[150] Yuen SM, Chen-Chi M, Wu HH, Kuan HC, Chen WJ, Liao SH, et al. Preparation and thermal, electrical, and morphological properties of multiwalled carbon nanotube and epoxy composites. Journal of Applied Polymer Science. 2007;103:1272-8.

[151] Kovacs JZ, Mandjarov RE, Blisnjuk T, Prehn K, Sussiek M, Muller J, et al. On the influence of nanotube properties, processing conditions and shear forces on the electrical conductivity of carbon nanotube epoxy composites. Nanotechnology. 2009;20.

[152] Thostenson ET, Ziaee S, Chou TW. Processing and electrical properties of carbon nanotube/vinyl ester nanocomposites. Composites Science and Technology. 2009;69:801-4.

[153] Allaoui A, El Bounia N. Rheological and Electrical Transitions in Carbon Nanotube/Epoxy Suspensions. Current Nanoscience. 2010;6:158-62.

[154] Chapartegui M, Markaide N, Florez S, Elizetxea C, Fernandez M, Santamaria A. Specific rheological and electrical features of carbon nanotube dispersions in an epoxy matrix. Composites Science and Technology. 2010;70:879-84.

[155] Sumfleth J, Buschhorn ST, Schulte K. Comparison of rheological and electrical percolation phenomena in carbon black and carbon nanotube filled epoxy polymers. Journal of Materials Science. 2011;46:659-69.

[156] Chen GX, Kim HS, Park BH, Yoon JS. Highly insulating silicone composites with a high carbon nanotube content. Carbon. 2006;44:3373-5.

[157] Hu CH, Liu CH, Chen LZ, Fan SS. Semiconductor behaviors of low loading multiwall carbon nanotube/poly(dimethylsiloxane) composites. Applied Physics Letters. 2009;95.

[158] Khosla A, Gray BL. Preparation, characterization and micromolding of multi-walled carbon nanotube polydimethylsiloxane conducting nanocomposite polymer. Materials Letters. 2009;63:1203-6.

[159] Hwang J, Jang J, Hong K, Kim KN, Han JH, Shin K, et al. Poly(3-hexylthiophene) wrapped carbon nanotube/poly(dimethylsiloxane) composites for use in finger-sensing piezoresistive pressure sensors. Carbon. 2011;49:106-10.

[160] Lee JB, Khang DY. Electrical and mechanical characterization of stretchable multi-walled carbon nanotubes/polydimethylsiloxane elastomeric composite conductors. Composites Science and Technology. 2012;72:1257-63.

[161] Norkhairunnisa M, Azizan A, Mariatti M, Ismail H, Sim LC. Thermal stability and electrical behavior of polydimethylsiloxane nanocomposites with carbon nanotubes and carbon black fillers. Journal of Composite Materials. 2012;46:903-10.

[162] Allaoui A, Hoa SV, Evesque P, Bai JB. Electronic transport in carbon nanotube tangles under compression: The role of contact resistance. Scripta Materialia. 2009;61:628-31.

[163] Chapartegui M, Barcena J, Irastorza X, Elizetxea C, Fernandez M, Santamaria A. Analysis of the conditions to manufacture a MWCNT buckypaper/benzoxazine nanocomposite. Composites Science and Technology. 2012;72:489-97.

[164] Xing YJ, Zhang XH, Chen HY, Chen MJ, Li QW. Enhancing buckypaper conductivity through co-deposition with copper nanowires. Carbon. 2013;61:501-6.

[165] Lyons PE, De S, Blighe F, Nicolosi V, Pereira LFC, Ferreira MS, et al. The relationship between network morphology and conductivity in nanotube films. Journal of Applied Physics. 2008;104.

[166] Stauffer D, Aharony A. Introduction to percolation theory: Taylor & Francis; 1992.

[167] Sahimi M. Applications of percolation theory: Taylor & Francis; 1994.

[168] Balberg I. Percolation Theory and Its Application in Electrically Conducting Materials. Semiconducting Polymer Composites: Principles, Morphologies, Properties and Applications2013. p. 145-69.

[169] Balberg I, Anderson CH, Alexander S, Wagner N. Excluded volume and its relation to the onset of percolation. Physical Review B. 1984;30:3933-43.

[170] Vionnet-Menot S, Grimaldi C, Maeder T, Strässler S, Ryser P. Tunneling-percolation origin of nonuniversality: Theory and experiments. Physical Review B - Condensed Matter and Materials Physics. 2005;71.

[171] Simmons JG. Generalized Formula for Electric Tunnel Effect between Similar Electrodes Separated by a Thin Insulating Film. Journal of Applied Physics. 1963;34:1793-803.

[172] Ounaies Z, Park C, Wise KE, Siochi EJ, Harrison JS. Electrical properties of single wall carbon nanotube reinforced polyimide composites. Composites Science and Technology. 2003;63:1637-46.

[173] Balberg I. Tunneling and Nonuniversal Conductivity in Composite-Materials. Physical Review Letters. 1987;59:1305-8.

[174] Kilbride BE, Coleman JN, Fraysse J, Fournet P, Cadek M, Drury A, et al. Experimental observation of scaling laws for alternating current and direct current conductivity in polymer-carbon nanotube composite thin films. Journal of Applied Physics. 2002;92:4024-30.

[175] Kohlmeyer RR, Javadi A, Pradhan B, Pilla S, Setyowati K, Chen J, et al. Electrical and Dielectric Properties of Hydroxylated Carbon Nanotube-Elastomer Composites. Journal of Physical Chemistry C. 2009;113:17626-9.

[176] Huang YY, Terentjev EM. Tailoring the Electrical Properties of Carbon Nanotube-Polymer Composites. Advanced Functional Materials. 2010;20:4062-8.

[177] Oh K, Lee JY, Lee SS, Park M, Kim D, Kim H. Highly stretchable dielectric nanocomposites based on single-walled carbon nanotube/ionic liquid gels. Composites Science and Technology. 2013;83:40-6.

[178] Dyre JC. The Random Free-Energy Barrier Model for Ac Conduction in Disordered Solids. Journal of Applied Physics. 1988;64:2456-68.

[179] Venet C, Pearson C, Jombert AS, Mabrook MF, Zeze DA, Petty MC. The morphology and electrical conductivity of single-wall carbon nanotube thin films prepared by the Langmuir-Blodgett technique. Colloids and Surfaces a-Physicochemical and Engineering Aspects. 2010;354:113-7.

[180] Thostenson ET, Chou TW. Carbon nanotube networks: Sensing of distributed strain and damage for life prediction and self healing. Advanced Materials. 2006;18:2837-41.

[181] Knite M, Tupureina V, Fuith A, Zavickis J, Teteris V. Polyisoprene-multi-wall carbon nanotube composites for sensing strain. Materials Science & Engineering C-Biomimetic and Supramolecular Systems. 2007;27:1125-8.

[182] Zhang R, Baxendale M, Peijs T. Universal resistivity-strain dependence of carbon nanotube/polymer composites. Physical Review B. 2007;76.

[183] Park M, Kim H, Youngblood JP. Strain-dependent electrical resistance of multi-walled carbon nanotube/polymer composite films. Nanotechnology. 2008;19.

[184] Pham GT, Park YB, Liang Z, Zhang C, Wang B. Processing and modeling of conductive thermoplastic/carbon nanotube films for strain sensing. Composites Part B-Engineering. 2008;39:209-16.

[185] Kang JH, Park C, Scholl JA, Brazin AH, Holloway NM, High JW, et al. Piezoresistive Characteristics of Single Wall Carbon Nanotube/Polyimide Nanocomposites. Journal of Polymer Science Part B-Polymer Physics. 2009;47:994-1003.

[186] Wichmann MHG, Buschhorn ST, Gehrmann J, Schulte K. Piezoresistive response of epoxy composites with carbon nanoparticles under tensile load. Physical Review B. 2009;80.

[187] de la Vega A, Sumfleth J, Wittich H, Schulte K. Time and temperature dependent piezoresistance of carbon nanofiller/polymer composites under dynamic load. Journal of Materials Science. 2012;47:2648-57.

[188] Nanni F, Mayoral BL, Madau F, Montesperelli G, McNally T. Effect of MWCNT alignment on mechanical and self-monitoring properties of extruded PET-MWCNT nanocomposites. Composites Science and Technology. 2012;72:1140-6.

[189] Zhao JH, Dai K, Liu CG, Zheng GQ, Wang B, Liu CT, et al. A comparison between strain sensing behaviors of carbon black/polypropylene and carbon nanotubes/polypropylene electrically conductive composites. Composites Part a-Applied Science and Manufacturing. 2013;48:129-900.

[190] Jiang MJ, Dang ZM, Xu HP. Significant temperature and pressure sensitivities of electrical properties in chemically modified multiwall carbon nanotube/methylvinyl silicone rubber nanocomposites. Applied Physics Letters. 2006;89.

[191] Jiang MJ, Dang ZM, Xu HP, Yao SH, Bai J. Effect of aspect ratio of multiwall carbon nanotubes on resistance-pressure sensitivity of rubber nanocomposites. Applied Physics Letters. 2007;91.

[192] Dang ZM, Jiang MJ, Xie D, Yao SH, Zhang LQ, Bai J. Supersensitive linear piezoresistive property in carbon nanotubes silicone rubber nanocomposites. Journal of Applied Physics. 2008;104.

[193] Wichmann MHG, Buschhorn ST, Böger L, Adelung R, Schulte K. Direction sensitive bending sensors based on multi-wall carbon nanotube/epoxy nanocomposites. Nanotechnology. 2008;19.

[194] Gau C, Ko HS, Chen HT. Piezoresistive characteristics of MWNT nanocomposites and fabrication as a polymer pressure sensor. Nanotechnology. 2009;20.

[195] de la Vega A, Kinloch IA, Young RJ, Bauhofer W, Schulte K. Simultaneous global and local strain sensing in SWCNT-epoxy composites by Raman and impedance spectroscopy. Composites Science and Technology. 2011;71:160-6.

[196] Amini A, Bahreyni B. Behavioral model for electrical response and strain sensitivity of nanotube-based nanocomposite materials. Journal of Vacuum Science and Technology B: Microelectronics and Nanometer Structures. 2012;30.

[197] Ferrreira A, Rocha JG, Anson-Casaos A, Martinez MT, Vaz F, Lanceros-Mendez S. Electromechanical performance of poly(vinylidene fluoride)/carbon nanotube composites for strain sensor applications. Sensors and Actuators a-Physical. 2012;178:10-6.

[198] Window AL. Strain gauge technology: Elsevier Applied Science; 1992.

[199] Lu NS, Wang X, Suo ZG, Vlassak J. Metal films on polymer substrates stretched beyond 50%. Applied Physics Letters. 2007;91.

[200] Smith CS. Piezoresistance Effect in Germanium and Silicon. Physical Review. 1954;94:42-9.

[201] Sze SM. Semiconductor sensors: Wiley; 1994.

[202] Oliva-Aviles AI, Aviles F, Seidel GD, Sosa V. On the contribution of carbon nanotube deformation to piezoresistivity of carbon nanotube/polymer composites. Composites Part B-Engineering. 2013;47:200-6.

[203] Aneli JN, Zaikov GE, Khananashvili LM. Effects of mechanical deformations on the structurization and electric conductivity of electric conducting polymer composites. Journal of Applied Polymer Science. 1999;74:601-21.

[204] Chen L, Chen GH, Lu L. Piezoresistive behavior study on finger-sensing silicone rubber/graphite nanosheet nanocomposites. Advanced Functional Materials. 2007;17:898-904.

[205] Hou Y, Wang D, Zhang XM, Zhao H, Zha JW, Dang ZM. Positive piezoresistive behavior of electrically conductive alkyl-functionalized graphene/polydimethylsilicone nanocomposites. Journal of Materials Chemistry C. 2013;1:515-21.

[206] Kim YS, Wright JB, Grunlan JC. Influence of polymer modulus on the percolation threshold of latex-based composites. Polymer. 2008;49:570-8.

[207] Bao YB, Wang JB, Xue PF, Li QY, Guo WH, Wu CF. Lowering the percolation threshold of polymer matrix composite by using raspberry-like carbon black/polystyrene composite particles. Journal of Materials Science. 2012;47:1289-95.

[208] Zhang XW, Pan Y, Zheng Q, Yi XS. Time dependence of piezoresistance for the conductor-filled polymer composites. Journal of Polymer Science Part B-Polymer Physics. 2000;38:2739-49.

[209] Hussain M, Choa YH, Niihara K. Fabrication process and electrical behavior of novel pressure-sensitive composites. Composites - Part A: Applied Science and Manufacturing. 2001;32:1689-96.

[210] Zhang XW, Pan Y, Zheng Q, Yi XS. Piezoresistance of conductor filled insulator composites. Polymer International. 2001;50:229-36.

[211] Zhou JF, Sony YH, Zheng Q, Wu Q, Zhang MQ. Percolation transition and hydrostatic piezoresistance for carbon black filled poly(methylvinylsilioxane) vulcanizates. Carbon. 2008;46:679-91.

[212] Negri RM, Rodriguez SD, Bernik DL, Molina FV, Pilosof A, Perez O. A model for the dependence of the electrical conductance with the applied stress in insulating-conducting composites. Journal of Applied Physics. 2010;107.

[213] Park C, Ounaies Z, Watson KA, Crooks RE, Smith J, Lowther SE, et al. Dispersion of single wall carbon nanotubes by in situ polymerization under sonication. Chemical Physics Letters. 2002;364:303-8.

[214] Knite M, Teteris V, Kiploka A, Kaupuzs J. Polyisoprene-carbon black nanocomposites as tensile strain and pressure sensor materials. Sensors and Actuators a-Physical. 2004;110:142-9.

[215] Song XH, Liu S, Gan ZY, Lv Q, Cao H, Yan H. Controllable fabrication of carbon nanotube-polymer hybrid thin film for strain sensing. Microelectronic Engineering. 2009;86:2330-3.

[216] Loh KJ, Lynch JP, Shim BS, Kotov NA. Tailoring piezoresistive sensitivity of multilayer carbon nanotube composite strain sensors. Journal of Intelligent Material Systems and Structures. 2008;19:747-64.

[217] Baltopoulos A, Athanasopoulos N, Fotiou I, Vavouliotis A, Kostopoulos V. Sensing strain and damage in polyurethane-MWCNT nano-composite foams using electrical measurements. Express Polymer Letters. 2013;7:40-54.

[218] Liu CX, Choi JW. Strain-Dependent Resistance of PDMS and Carbon Nanotubes Composite Microstructures. Ieee Transactions on Nanotechnology. 2010;9:590-5.

[219] Beeby S. MEMS mechanical sensors: Artech House; 2004.

[220] Kang TK. Evidence for giant piezoresistance effect in n-type silicon nanowire field-effect transistors. Applied Physics Letters. 2012;100.

[221] Yoshikawa S, Ota T, Newnham R, Amin A. Piezoresistivity in Polymer-Ceramic Composites. Journal of the American Ceramic Society. 1990;73:263-7.

[222] Das NC, Chaki TK, Khastgir D. Effect of processing parameters, applied pressure and temperature on the electrical resistivity of rubber-based conductive composites. Carbon. 2002;40:807-16.

[223] Sichel EK, Sheng P, Gittleman JI, Bozowski S. Observation of Fluctuation Modulation of Tunnel-Junctions by Applied Ac Stress in Carbon Polyvinylchloride Composites. Physical Review B. 1981;24:6131-4.

[224] Balberg I. Limits on the continuum-percolation transport exponents. Physical Review B. 1998;57:13351-4.

[225] Grimaldi C, Balberg I. Tunneling and nonuniversality in continuum percolation systems. Physical Review Letters. 2006;96.

[226] Johner N, Ryser P, Grimaldi C, Balberg I. Piezoresistivity and tunneling-percolation transport in apparently nonuniversal systems. Physical Review B. 2007;75.

[227] Johner N, Grimaldi C, Balberg I, Ryser P. Transport exponent in a three-dimensional continuum tunneling-percolation model. Physical Review B. 2008;77.

[228] Tonpheng B, Yu J, Andersson BM, Andersson O. Tensile Strength and Young's Modulus of Polyisoprene/Single-Wall Carbon Nanotube Composites Increased by High Pressure Cross-linking. Macromolecules. 2010;43:7680-8.

[229] Onsager L. The Effects of Shape on the Interaction of Colloidal Particles. Annals of the New York Academy of Sciences. 1949;51:627-59.

[230] Celzard A, McRae E, Deleuze C, Dufort M, Furdin G, Mareche JF. Critical concentration in percolating systems containing a high-aspect-ratio filler. Physical Review B. 1996;53:6209-14.

[231] Zhao D, Lei Q, Qin C, Bai X. Melt process and performance of multi-walled carbon nanotubes reinforced LDPE composites. Pigment & Resin Technology. 2006;35:341-5.

[232] White SI, Mutiso RM, Vora PM, Jahnke D, Hsu S, Kikkawa JM, et al. Electrical Percolation Behavior in Silver Nanowire-Polystyrene Composites: Simulation and Experiment. Advanced Functional Materials. 2010;20:2709-16.

[233] Singh BP, Saini K, Choudhary V, Teotia S, Pande S, Saini P, et al. Effect of length of carbon nanotubes on electromagnetic interference shielding and mechanical properties of their reinforced epoxy composites. Journal of Nanoparticle Research. 2013;16.

[234] Zha JW, Shehzad K, Li WK, Dang ZM. The effect of aspect ratio on the piezoresistive behavior of the multiwalled carbon nanotubes/thermoplastic elastomer nanocomposites. Journal of Applied Physics. 2013;113.

[235] Ha MLP, Grady BP, Lolli G, Resasco DE, Ford WT. Composites of single-walled carbon nanotubes and styrene-isoprene copolymer latices. Macromolecular Chemistry and Physics. 2007;208:446-56.

[236] Balberg I, Azulay D, Toker D, Millo O. Percolation and tunneling in composite materials. International Journal of Modern Physics B. 2004;18:2091-121.

[237] Abbasi S, Carreau PJ, Derdouri A. Flow induced orientation of multiwalled carbon nanotubes in polycarbonate nanocomposites: Rheology, conductivity and mechanical properties. Polymer. 2010;51:922-35.

[238] Liu X, Krückel J, Zheng G, Schubert DW. Mapping the electrical conductivity of poly(methyl methacrylate)/carbon black composites prior to and after shear. ACS Applied Materials and Interfaces. 2013;5:8857-60.

[239] Prasse T, Flandin L, Schulte K, Bauhofer W. In situ observation of electric field induced agglomeration of carbon black in epoxy resin. Applied Physics Letters. 1998;72:2903-5.

[240] Koerner H, Jacobs D, Tomlin DW, Busbee JD, Vaia RD. Tuning polymer nanocomposite morphology: AC electric field manipulation of epoxy-montmorillonite (clay) suspensions. Advanced Materials. 2004;16:297-302.

[241] Martin CA, Sandler JKW, Windle AH, Schwarz MK, Bauhofer W, Schulte K, et al. Electric field-induced aligned multi-wall carbon nanotube networks in epoxy composites. Polymer. 2005;46:877-86.

[242] Park C, Wilkinson J, Banda S, Ounaies Z, Wise KE, Sauti G, et al. Aligned single-wall carbon nanotube polymer composites using an electric field. Journal of Polymer Science, Part B: Polymer Physics. 2006;44:1751-62.

[243] Ma C, Zhang W, Zhu YF, Ji LJ, Zhang RP, Koratkar N, et al. Alignment and dispersion of functionalized carbon nanotubes in polymer composites induced by an electric field. Carbon. 2008;46:706-10.

[244] Wang MW, Hsu TC, Weng CH. Alignment of MWCNTs in polymer composites by dielectrophoresis. European Physical Journal-Applied Physics. 2008;42:241-6.

[245] Zhang C, Zhu J, Ouyang M, Ma CA. Electric field controlled formation and dissociation of multiwalled carbon nanotube conductive pathways in a polymer melt. Applied Physics Letters. 2009;94.

[246] Zhu YF, Ma C, Zhang W, Zhang RP, Koratkar N, Liang J. Alignment of multiwalled carbon nanotubes in bulk epoxy composites via electric field. Journal of Applied Physics. 2009;105.

[247] Domingues D, Logakis E, Skordos AA. The use of an electric field in the preparation of glass fibre/epoxy composites containing carbon nanotubes. Carbon. 2012;50:2493-503.

[248] Ren D, Zheng S, Wu F, Yang W, Liu Z, Yang M. Formation and evolution of the carbon black network in polyethylene/carbon black composites: Rheology and conductivity properties. Journal of Applied Polymer Science. 2014;131.

[249] Camponeschi E, Vance R, Al-Haik M, Garmestani H, Tannenbaum R. Properties of carbon nanotube-polymer composites aligned in a magnetic field. Carbon. 2007;45:2037-46.

[250] Steinert BW, Dean DR. Magnetic field alignment and electrical properties of solution cast PET-carbon nanotube composite films. Polymer. 2009;50:898-904.

[251] Erb RM, Libanori R, Rothfuchs N, Studart AR. Composites Reinforced in Three Dimensions by Using Low Magnetic Fields. Science. 2012;335:199-204.

[252] Mezger TG. The Rheology Handbook: For Users of Rotational and Oscillatory Rheometers: Vincentz Network; 2006.

[253] Wu GZ, Asai S, Zhang C, Miura T, Sumita M. A delay of percolation time in carbon-black-filled conductive polymer composites. Journal of Applied Physics. 2000;88:1480-7.

[254] Liu C, Zhang J, He J, Hu G. Gelation in carbon nanotube/polymer composites. Polymer. 2003;44:7529-32.

[255] Tai XY, Wu GZ, Tominaga Y, Asai S, Sumita M. An approach to one-dimensional conductive polymer composites. Journal of Polymer Science Part B-Polymer Physics. 2005;43:184-9.

[256] Zhang QH, Rastogi S, Chen DJ, Lippits D, Lemstra PJ. Low percolation threshold in single-walled carbon nanotube/high density polyethylene composites prepared by melt processing technique. Carbon. 2006;44:778-85.

[257] Alig I, Lellinger D, Dudkin SM, Potschke P. Conductivity spectroscopy on melt processed polypropylene-multiwalled carbon nanotube composites: Recovery after shear and crystallization. Polymer. 2007;48:1020-9.

[258] Alig I, Skipa T, Engel M, Lellinger D, Pegel S, Pötschke P. Electrical conductivity recovery in carbon nanotube-polymer composites after transient shear. Physica Status Solidi (B) Basic Research. 2007;244:4223-6.

[259] Lin B, Gelves GA, Haber JA, Sundararaj U. Electrical, rheological, and mechanical properties of polystyrene/copper nanowire nanocomposites. Industrial & Engineering Chemistry Research. 2007;46:2481-7.

[260] Obrzut J, Douglas JF, Kharchenko SB, Migler KB. Shear-induced conductor-insulator transition in melt-mixed polypropylene-carbon nanotube dispersions. Physical Review B - Condensed Matter and Materials Physics. 2007;76.

[261] Alig I, Skipa T, Lellinger D, Bierdel M, Meyer H. Dynamic percolation of carbon nanotube agglomerates in a polymer matrix: Comparison of different model approaches. Physica Status Solidi (B) Basic Research. 2008;245:2264-7.

[262] Alig I, Skipa T, Lellinger D, Pötschke P. Destruction and formation of a carbon nanotube network in polymer melts: Rheology and conductivity spectroscopy. Polymer. 2008;49:3524-32.

[263] Gelves GA, Lin B, Sundararaj U, Haber JA. Electrical and rheological percolation of polymer nanocomposites prepared with functionalized copper nanowires. Nanotechnology. 2008;19.

[264] Park SD, Han DH, Teng D, Kwon Y. Rheological properties and dispersion of multi-walled carbon nanotube (MWCNT) in polystyrene matrix. Current Applied Physics. 2008;8:482-5.

[265] Deng H, Skipa T, Zhang R, Lellinger D, Bilotti E, Alig I, et al. Effect of melting and crystallization on the conductive network in conductive polymer composites. Polymer. 2009;50:3747-54.

[266] Kayatin MJ, Davis VA. Viscoelasticity and Shear Stability of Single-Walled Carbon Nanotube/Unsaturated Polyester Resin Dispersions. Macromolecules. 2009;42:6624-32.

[267] Zhang R, Dowden A, Deng H, Baxendale M, Peijs T. Conductive network formation in the melt of carbon nanotube/thermoplastic polyurethane composite. Composites Science and Technology. 2009;69:1499-504.

[268] Skipa T, Lellinger D, Bohm W, Saphiannikova M, Alig I. Influence of shear deformation on carbon nanotube networks in polycarbonate melts: Interplay between build-up and destruction of agglomerates. Polymer. 2010;51:201-10.

[269] Garate H, Fascio ML, Mondragon I, D'Accorso NB, Goyanes S. Surfactant-aided dispersion of polystyrene-functionalized carbon nanotubes in a nanostructured poly(styrene-b-isoprene-b-styrene) block copolymer. Polymer. 2011;52:2214-20.

[270] Huang SL, Liu ZY, Yin CL, Wang Y, Gao YJ, Chen C, et al. Dynamic Electrical and Rheological Percolation in Isotactic Poly(propylene)/Carbon Black Composites. Macromolecular Materials and Engineering. 2012;297:51-9.

[271] Hilarius K, Lellinger D, Alig I, Villmow T, Pegel S, Potschke P. Influence of shear deformation on the electrical and rheological properties of combined filler networks in polymer melts: Carbon nanotubes and carbon black in polycarbonate. Polymer. 2013;54:5865-74.

[272] Liebscher M, Tzounis L, Pötschke P, Heinrich G. Influence of the viscosity ratio in PC/SAN blends filled with MWCNTs on the morphological, electrical, and melt rheological properties. Polymer (United Kingdom). 2013;54:6801-8.

[273] Mizuno C, John B, Okamoto M. Percolated Network Structure Formation and Rheological Properties in Nylon 6/Clay Nanocomposites. Macromolecular Materials and Engineering. 2013;298:400-11.

[274] Monemian S, Jafari SH, Khonakdar HA, Goodarzi V, Reuter U, Potschke P. MWNT-filled PC/ABS blends: Correlation of morphology with rheological and electrical response. Journal of Applied Polymer Science. 2013;130:739-48.

[275] Park DH, Kan TG, Lee YK, Kim WN. Effect of multi-walled carbon nanotube dispersion on the electrical and rheological properties of poly(propylene carbonate)/poly(lactic acid)/multi-walled carbon nanotube composites. Journal of Materials Science. 2013;48:481-8.

[276] Zhang K, Choi HJ. Smart Polymer/Carbon Nanotube Nanocomposites and Their Electrorheological Response. Materials. 2014;7:3399-414.

[277] Michels MAJ, Brokkenzijp JCM, Groenewoud WM, Knoester A. Systematic Study of Percolative Network Formation and Effective Electric-Response in Low-Concentration-Carbon-Black Polymer Composites. Physica A. 1989;157:529-34.

[278] Seyhan AT, Gojny FH, Tanoglu M, Schulte K. Rheological and dynamic-mechanical behavior of carbon nanotube/vinyl ester-polyester suspensions and their nanocomposites. European Polymer Journal. 2007;43:2836-47.

[279] de la Vega A, Kovacs JZ, Bauhofer W, Schulte K. Combined Raman and dielectric spectroscopy on the curing behaviour and stress build up of carbon nanotube-epoxy composites. Composites Science and Technology. 2009;69:1540-6.

[280] Faiella G, Piscitelli F, Lavorgna M, Antonucci V, Giordano M. Tuning the insulator to conductor transition in a multiwalled carbon nanotubes/epoxy composite at substatistical percolation threshold. Applied Physics Letters. 2009;95.

[281] Hubert P, Ashrafi B, Adhikari K, Meredith J, Vengallatore S, Guan JW, et al. Synthesis and characterization of carbon nanotube-reinforced epoxy: Correlation between viscosity and elastic modulus. Composites Science and Technology. 2009;69:2274-80.

[282] Thuau D, Koutsos V, Cheung R. Electrical and mechanical properties of carbon nanotube-polyimide composites. Journal of Vacuum Science and Technology B: Microelectronics and Nanometer Structures. 2009;27:3139-44.

[283] Bokobza L. Multiwall carbon nanotube elastomeric composites: A review. Polymer. 2007;48:4907-20.

[284] Wichiansee W, Sirivat A. Electrorheological properties of poly(dimethylsiloxane) and poly(3,4-ethylenedioxy thiophene)/poly(stylene sulfonic acid)/ethylene glycol blends. Materials Science and Engineering C. 2009;29:78-84.

[285] Bokobza L. Multiwall carbon nanotube-filled natural rubber: Electrical and mechanical properties. Express Polymer Letters. 2012;6:213-23.

[286] Hong J, Park DW, Shim SE. Electrical, thermal, and rheological properties of carbon black and carbon nanotube dual filler-incorporated poly(dimethylsiloxane) nanocomposites. Macromolecular Research. 2012;20:465-72.

[287] Romasanta LJ, Lopez-Manchado MA, Verdejo R. The role of carbon nanotubes in both physical and chemical liquid-solid transition of polydimethylsiloxane. European Polymer Journal. 2013;49:1373-80.

[288] Farage TFF, Reinhardt J, Brader JM. Normal-stress coefficients and rod climbing in colloidal dispersions. Physical Review E. 2013;88.

[289] Buschhorn ST, Wichmann MHG, Sumfleth J, Schulte K, Pegel S, Kasaliwal GR, et al. Charakterisierung der Dispersionsgüte von Carbon Nanotubes in Polymer-Nanokompositen - Characterization of the state of dispersion of carbon nanotubes in polymer nanocomposites. Chemie Ingenieur Technik. 2011;83:767-81.

[290] Higgins JS, Dodgson K, Semlyen JA. Studies of Cyclic and Linear Poly(Dimethyl Siloxanes) .3. Neutron-Scattering Measurements of the Dimensions of Ring and Chain Polymers. Polymer. 1979;20:553-8.

[291] Yourdkhani M, Hubert P. Quantitative Dispersion Analysis of Inclusions in Polymer Composites. Acs Applied Materials & Interfaces. 2013;5:35-41.

[292] Schueler R, Petermann J, Schulte K, Wentzel HP. Agglomeration and electrical percolation behavior of carbon black dispersed in epoxy resin. Journal of Applied Polymer Science. 1997;63:1741-6.

[293] Cattin C, Hubert P. Network Formation and Electrical Conduction in Carbon Nanotube Modified Polydimethylsiloxane. 2011 MRS Fall Meeting. 2011;1410.

[294] Poland CA, Duffin R, Kinloch I, Maynard A, Wallace WAH, Seaton A, et al. Carbon nanotubes introduced into the abdominal cavity of mice show asbestos-like pathogenicity in a pilot study. Nature Nanotechnology. 2008;3:423-8.

[295] Donaldson K, Aitken R, Tran L, Stone V, Duffin R, Forrest G, et al. Carbon nanotubes: A review of their properties in relation to pulmonary toxicology and workplace safety. Toxicological Sciences. 2006;92:5-22.

[296] Aschberger K, Johnston HJ, Stone V, Aitken RJ, Hankin SM, Peters SAK, et al. Review of carbon nanotubes toxicity and exposure-Appraisal of human health risk assessment based on open literature. Critical Reviews in Toxicology. 2010;40:759-90.

[297] Johnston HJ, Hutchison GR, Christensen FM, Peters S, Hankin S, Aschberger K, et al. A critical review of the biological mechanisms underlying the in vivo and in vitro toxicity of carbon nanotubes: The contribution of physico-chemical characteristics. Nanotoxicology. 2010;4:207-46.

[298] The Institut de recherche Robert-Sauvé en santé et en sécurité du travail (Occupational Health and Safety Research Institute). Montreal QC Canada.

[299] The National Institute for Occupational Safety and Health. Centers for Disease Control and Prevention. Atlanta GA USA.

[300] Ostiguy C, Debia M, Roberge B, Dufresne A. Nanomatériaux – Guide de bonnes pratiques favorisant la gestion des risques en milieu de travail, 2e édition. IRSST Études et recherches / Rapport R-840. Montreal QC Canada. 2014.

[301] NIOSH Current Intelligence Bulletin 65. Occupational Exposure to Carbon Nanotubes and Nanofibers. DHHS (NIOSH) Publication No 2013-145. Atlanta GA USA. 2013.

[302] Cena LG, Peters TM. Characterization and Control of Airborne Particles Emitted During Production of Epoxy/Carbon Nanotube Nanocomposites. Journal of Occupational and Environmental Hygiene. 2011;8:86-92.

[303] Tsai SJ, Ada E, Isaacs JA, Ellenbecker MJ. Airborne nanoparticle exposures associated with the manual handling of nanoalumina and nanosilver in fume hoods. Journal of Nanoparticle Research. 2009;11:147-61.

[304] Tsai SJ, Huang RF, Ellenbecker MJ. Airborne nanoparticle exposures while using constant-flow, constant-velocity, and air-curtain-isolated fume hoods. Annals of Occupational Hygiene. 2010;54:78-87.